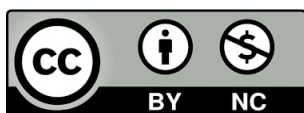Borhan Asadi

Multifaceted Analysis of Neuro-Muscular Data in Stroke Patients Using EEG and Ultrasound Imaging for Indicators Identification and Functional Pattern Recognition

Director/es

Herrero Gallego, Pablo

Universidad Zaragoza
1542

Tesis Doctoral

MULTIFACETED ANALYSIS OF NEURO-MUSCULAR DATA IN STROKE PATIENTS USING EEG AND ULTRASOUND IMAGING FOR INDICATORS IDENTIFICATION AND FUNCTIONAL PATTERN RECOGNITION

Autor

Borhan Asadi

Director/es

Herrero Gallego, Pablo

UNIVERSIDAD DE ZARAGOZA
Escuela de Doctorado

2025

Tesis Doctoral

Multifaceted Analysis of Neuro-Muscular Data in Stroke Patients Using EEG and Ultrasound Imaging for Indicators Identification and Functional Pattern Recognition

Autor

Borhan Asadi

Director/es

Pablo Herrero Gallego

UNIVERSIDAD DE ZARAGOZA Escuela de Doctorado

Programa de Doctorado en Ciencias de la Salud y del Deporte

2025

Professor Pablo Herrero Gallego

CERTIFIES:

That the work entitled "Multifaceted Analysis of Neuro-Muscular Data in Stroke Patients Using EEG and Ultrasound Imaging for Indicators Identification and Functional Pattern Recognition", presented by Mr. Borhan Asadi, graduate in Information Technology engineering, has been carried out under my supervision and guidance in the Department of Physiatry and Nursing. In my opinion, it possesses sufficient originality and academic content to be submitted to the corresponding Committee and to be considered for the degree of Doctor at the University of Zaragoza.

For the record and for all relevant purposes, this certificate is issued in Zaragoza on April Xth, 2025.

Signed: Pablo Herrero Gallego

Mr. Borhan Asadi requests the submission of his doctoral thesis as a compendium of publications with a thematic unity on "Multifaceted Analysis of Neuro-Muscular Data in Stroke Patients Using EEG and Ultrasound Imaging for Indicators Identification and Functional Pattern Recognition"

To that end, he provides the full references of the articles that constitute the body of the thesis.

1. **Asadi B**, Fard KR, Ansari NN, Marco Á, Calvo S, Herrero P. The Effect of dry Needling in Chronic Stroke with a complex Network Approach: A Case Study. Clinical EEG and Neuroscience. 2022;54(2):179-188. doi:10.1177/15500594221120136.
    - 5-year Impact factor 1.9; Third Quartile
    - First Author
2. **Asadi, B.**; Cuenca-Zaldivar, J.N.; Nakhostin Ansari, N.; Ibáñez, J.; Herrero, P.; Calvo, S. Brain Analysis with a Complex Network Approach in Stroke Patients Based on Electroencephalography: A Systematic Review and Meta-Analysis. *Healthcare* **2023**, *11*,666. doi:10.3390/healthcare11050666.
    - 5-year Impact factor 2.5; Second Quartile
    - First Author
3. **Asadi, B.**; Pujol-Fuentes, C.; Carcasona-Otal, A.; Calvo, S.; Herrero, P.; Lapuente-Hernández, D. Characterizing Muscle Tissue Quality Post-Stroke: Echovariation as a Clinical Indicator. *J. Clin. Med.* **2024**, *13*, 7800. doi:10.3390/jcm13247800.
    - 5-year Impact factor 3.4; First Quartile
    - First Author
4. **Asadi, B**.; Cuenca-Zaldívar, J.N.; Carcasona-Otal, A.; Herrero, P.; Lapuente-Hernández, D. Improving the Reliability of Muscle Tissue Characterization Post-Stroke: A Secondary Statistical Analysis of Echotexture Features. *J. Clin. Med.* **2025**, *14*, 2902. doi:10.3390/jcm14092902.
    - 5-year Impact factor 3.4, First Quartile
    - First Author
5. **Asadi, B.**; Abdi, S.; Pérez-Espallargas, L.; Nakhostin Ansari, N.; Lapuente-Hernández, D. A Complementary Patch-Based Histogram Analysis for Quantifying Muscle Tissue in Ultrasound Imaging. *Invasive Physiother Musculoskelet Med* **2025**, *1*. doi:10.63360/ipmm.v1.e10.
    - No indexed
    - First Author

Abbreviation

DN: Dry Needling

EEG: Electroencephalography

ROI: Region of Interest

Echovariation: EV

Echointensity: EI

Content

Abstract

This PhD dissertation focuses on the investigation and analysis of neuro-muscular function in stroke patients through the integration of electroencephalography (EEG) data and muscle ultrasound imaging. The primary aim of this research was to understand how stroke impacts both the brain's structural connectivity and the condition of muscle tissue, and to identify reliable biomarkers that can support clinical evaluation and rehabilitation strategies.

The research was carried out in five interconnected studies. The first study was a case study designed to explore the effects of dry needling on brain network structure in a stroke patient. Using EEG recordings and complex network analysis techniques, the study demonstrated that dry needling could induce significant changes in the brain's network architecture. This suggested a potential neuroplastic response triggered by the intervention, highlighting the brain's capacity for structural reorganization even in chronic stroke phases.

The second study was a systematic review aimed at synthesizing existing literature on brain network organization in stroke patients. By analyzing studies that used EEG and functional connectivity metrics, this review revealed that brain network topology can vary significantly among stroke survivors. These variations were influenced by factors such as lesion location, severity of the stroke, and time since onset. The study underscored the importance of individualized network analysis for understanding post-stroke brain dynamics.

In the third study, the focus shifted from the brain to the muscle system, specifically the gastrocnemius muscle, using B-mode ultrasound images. The goal was to identify a potential biomarker within these images that could reflect the degree of muscle involvement due to stroke. The study introduced and validated "Echovariation"—a measure of pixel intensity variability, as a promising quantitative biomarker. A strong correlation was found between Echovariation and the Heckmatt scale, a clinical grading system for muscle tissue changes. This indicated that Echovariation could serve as an objective, image-based indicator of neuromuscular impairment in stroke patients.

Building on these findings, the fourth study aimed to refine and validate predictive models developed from the third study. Two models were constructed based on Echovariation and Echointensity, respectively. Both models demonstrated strong performance in estimating muscle damage, but the Echovariation-based model showed superior accuracy and correlation with clinical assessments. This reinforced the role of Echovariation as a reliable tool for muscle evaluation.

The fifth and final study introduced an innovative image analysis approach based on patch-based segmentation. This method involved dividing ultrasound images into smaller, consistent patches for separate analysis. The findings revealed that patch-based analysis could detect significant local variations in Echovariation, thereby enhancing sensitivity to subtle muscle changes. Interestingly, this technique did not produce meaningful changes in Echointensity, suggesting that Echovariation is more responsive to localized structural alterations.

In conclusion, this thesis presents a comprehensive approach to understanding stroke-induced changes in both brain and muscle systems. Through the integration of EEG-based network analysis and advanced ultrasound imaging techniques, it introduces novel, quantitative methods for assessing neuro-muscular dysfunction. These findings contribute to the growing field of neurorehabilitation by offering new tools for diagnosis, monitoring, and treatment planning in stroke recovery.

RESUMEN

Esta tesis doctoral se centra en la investigación y análisis de la función neuromuscular en pacientes con accidente cerebrovascular mediante la integración de datos de electroencefalografía (EEG) y de imágenes de ultrasonido muscular. El objetivo principal de esta investigación fue comprender cómo el accidente cerebrovascular afecta tanto la conectividad estructural del cerebro como el estado del tejido muscular, e identificar biomarcadores confiables que puedan apoyar la evaluación clínica y las estrategias de rehabilitación.

La investigación se llevó a cabo en cinco estudios interrelacionados. El primer estudio fue un estudio de caso diseñado para explorar los efectos de la punción seca en la estructura de la red cerebral de un paciente con accidente cerebrovascular. Utilizando registros de EEG y técnicas de análisis de redes complejas, el estudio demostró que la punción seca puede inducir cambios significativos en la arquitectura de la red cerebral. Esto sugiere una posible respuesta neuroplástica desencadenada por la intervención, lo que destaca la capacidad del cerebro para reorganizarse estructuralmente incluso en fases crónicas del ictus.

El segundo estudio fue una revisión sistemática cuyo objetivo fue sintetizar la literatura existente sobre la organización de las redes cerebrales en pacientes con accidente cerebrovascular. Al analizar estudios que utilizaron EEG y métricas de conectividad funcional, esta revisión reveló que la topología de las redes cerebrales puede variar considerablemente entre los sobrevivientes de un accidente cerebrovascular. Estas variaciones estaban influenciadas por factores como la localización de la lesión, la gravedad del accidente cerebrovascular y el tiempo transcurrido desde el evento. El estudio subrayó la importancia del análisis de redes individualizado para comprender la dinámica cerebral post-ictus.

En el tercer estudio, el enfoque se desplazó del cerebro al sistema muscular, específicamente al músculo gastrocnemio, utilizando imágenes de ultrasonido en modo B. El objetivo fue identificar un posible biomarcador dentro de estas imágenes que pudiera reflejar el grado de afectación muscular debido al accidente cerebrovascular. El estudio introdujo y validó la "Ecovariación"—una medida de la variabilidad de la intensidad de los píxeles—como un prometedor biomarcador cuantitativo. Se encontró una fuerte correlación entre la Ecovariación y la escala de Heckmatt, un sistema clínico de evaluación del cambio en el tejido muscular. Esto indicó que la Ecovariación podría servir como un indicador objetivo basado en imágenes de la disfunción neuromuscular en pacientes con accidente cerebrovascular.

Sobre la base de estos hallazgos, el cuarto estudio tuvo como objetivo refinar y validar los modelos predictivos desarrollados en el tercer estudio. Se construyeron dos modelos, uno basado en la Ecovariación y otro en la Ecointensidad. Ambos modelos mostraron un buen rendimiento en la estimación del daño muscular, aunque el modelo basado en la Ecovariación demostró mayor precisión y correlación con las evaluaciones clínicas, reforzando el valor de la Ecovariación como herramienta confiable para la evaluación muscular.

El quinto y último estudio introdujo un enfoque innovador de análisis de imágenes basado en la segmentación por parches. Este método consistió en dividir las imágenes de ultrasonido en parches pequeños y consistentes para su análisis por separado. Los resultados mostraron que este análisis por parches podía detectar variaciones locales significativas en la Ecovariación, aumentando así la sensibilidad a cambios sutiles en el músculo. Curiosamente, esta técnica no mostró cambios significativos en la Ecointensidad, lo que sugiere que la Ecovariación es más sensible a alteraciones estructurales localizadas.

En conclusión, esta tesis presenta un enfoque integral para comprender los cambios inducidos por el accidente cerebrovascular tanto en el cerebro como en los sistemas musculares. A través de la integración del análisis de redes basado en EEG y de técnicas avanzadas de imagen por ultrasonido, se introducen métodos cuantitativos novedosos para la evaluación de la disfunción neuromuscular. Estos hallazgos contribuyen al campo en expansión de la neurorrehabilitación, ofreciendo nuevas herramientas para el diagnóstico, monitoreo y planificación del tratamiento en la recuperación post-ictus.

Introduction

Stroke remains a major public health challenge and is consistently reported among the leading causes of long-term disability across the globe (1-3). It is estimated that approximately 13.7 million individuals experience a stroke annually, a figure that is expected to rise due to global population aging and increased life expectancy (4, 5). Notably, up to 70% of stroke survivors endure moderate to severe post-stroke impairments, contributing to a substantial physical, emotional, and socioeconomic burden for patients, caregivers, and healthcare systems alike (1). These impairments often include persistent motor, sensory, and cognitive deficits that compromise functional independence, limit participation in daily activities, and reduce overall quality of life.

Given the chronic and often progressive nature of stroke-related dysfunction, coupled with the economic demands of long-term care, there is a critical and growing need for cost-effective, evidence-based rehabilitation strategies that can be implemented across diverse clinical settings. The urgency of this need is underscored by the increasing incidence of stroke in low- and middle-income countries, where access to specialized rehabilitation services may be limited and healthcare resources are often constrained (3, 5).

Early intervention during the subacute and chronic phases of stroke recovery has been shown to play a pivotal role in facilitating neuroplasticity, promoting functional gains, and mitigating the risk of secondary complications such as spasticity, contractures, and deconditioning (1). Moreover, the integration of structured rehabilitation programs can significantly reduce long-term disability and dependence, thereby alleviating the overall burden on caregivers and health systems. In this context, timely and targeted rehabilitation enhances individual outcomes and contributes to broader public health goals by improving reintegration into the community and reducing rehospitalization rates.

Implementing objective, reliable, and clinically feasible assessment tools is essential to achieve these goals. Such tools serve multiple purposes: they enable clinicians to accurately monitor patient progress, inform data-driven decision-making, and tailor interventions to meet individual recovery trajectories. Furthermore, objective assessment methods enhance the reproducibility and comparability of research findings, supporting the development of standardized rehabilitation protocols and advancing evidence-based practice.

As stroke continues to be a significant global health burden, both in terms of its clinical outcomes and its socioeconomic ramifications, it remains imperative to invest in scalable and scientifically grounded

approaches to rehabilitation (3, 4). This includes the integration of modern technologies such as neuroimaging, wearable sensors, and machine learning-based analytics, which hold promise for refining diagnostic precision and optimizing treatment efficacy. Ultimately, the strategic application of comprehensive, patient-centered rehabilitation supported by accurate and objective assessment can transform stroke care, reduce disparities in health outcomes, and improve the lives of millions affected by this debilitating condition.

Rehabilitation in stroke survivors typically involves multifaceted, interdisciplinary protocols designed to address both neural and musculoskeletal impairments resulting from central nervous system injury. These protocols often combine a variety of physiotherapeutic interventions such as motor retraining, task-specific practice, stretching, and strengthening exercises with pharmacological treatments aimed at reducing spasticity and enhancing functional independence. Common pharmacologic strategies include administering oral antispastic agents, such as baclofen or tizanidine, and localized botulinum toxin type A (BTX-A) injections. BTX-A, in particular, has gained widespread clinical use for its ability to temporarily block neuromuscular transmission, thereby reducing hypertonicity and facilitating improved voluntary movement patterns.

Despite their benefits, pharmacologic treatments may be limited by systemic side effects, cost, and the need for repeated administration. Consequently, there has been growing interest in exploring non-pharmacological interventions that can complement or, in some cases, substitute traditional approaches. Among these, DN has emerged as a promising technique for the management of spasticity and sensorimotor dysfunction in individuals with chronic stroke (6).

DN involves inserting thin, solid needles into myofascial trigger points to improve tissue extensibility and modulate neuromuscular activity. Beyond its peripheral mechanical effects, evidence suggests that DN may also exert central neurophysiological effects through mechanisms involving altered cortical excitability, spinal reflex modulation, and enhanced sensorimotor integration (7-9). These findings imply that DN contributes to muscle relaxation and pain reduction and may also facilitate neuroplastic changes essential for functional recovery after stroke.

Moreover, DN has been recognized as a cost-effective intervention, especially when integrated into multidisciplinary rehabilitation programs (10). Its relative safety, simplicity of application, and minimal risk of adverse effects further underscore its potential as a valuable adjunctive tool in modern neurorehabilitation frameworks.

Neurophysiological assessment of stroke

EEG has emerged as a valuable neurophysiological tool for investigating the functional status of the central nervous system (CNS) in stroke patients, particularly in response to therapeutic interventions (11-14). As a non-invasive, real-time, and cost-effective method, EEG allows for continuous monitoring of cerebral activity with high temporal resolution, uniquely evaluating spontaneous and stimulus-induced brain dynamics. This technique offers critical insights into the pathophysiological alterations that occur following cerebrovascular events, such as ischemic or hemorrhagic strokes, and contributes to a deeper understanding of neuroplasticity during recovery.

Post-stroke brain regions, particularly those affected by the lesion, frequently demonstrate a slowing of oscillatory activity, which can be quantified by examining the spectral composition of the EEG signal. A standard method involves calculating the power ratio between low-frequency bands (e.g., delta: 0.5–4 Hz) and high-frequency bands (e.g., alpha: 8–12 Hz, beta: 13–30 Hz, gamma: >30 Hz) (15). An increase in delta power relative to alpha or beta activity in the lesioned hemisphere often reflects impaired cortical function, disrupted neural synchronization, or compromised thalamo-cortical connectivity.

EEG-based spectral and connectivity metrics are promising biomarkers for assessing stroke severity, evaluating treatment efficacy, and tracking functional recovery over time. These markers can be particularly useful during the early, pre-treatment phases, providing clinicians with objective data to inform short-term clinical decisions and long-term prognostic assessments. Furthermore, by capturing dynamic changes in cortical excitability and inter-hemispheric communication, EEG may also serve as a guide for tailoring neurorehabilitation strategies and optimizing patient-specific interventions to enhance neuroplasticity and functional outcomes (15).

The study of brain network organization has significantly advanced over the past two decades, particularly through applying quantitative approaches rooted in graph theory. This mathematical framework allows modeling the brain as a complex system composed of interconnected regions, offering a robust methodology for evaluating its structural and functional architecture (16). Brain networks, representing the physical and functional interactions among neural regions, are inherently dynamic and subject to significant disruption following neurological injury, such as stroke. Indeed, lesions caused by stroke frequently induce widespread alterations in the organization and efficiency of these networks, often affecting not only the injured hemisphere but also the intact contralesional side.

Stroke may damage local neural structures and disrupt large-scale brain networks, affecting structural and functional connectivity. Stroke-induced lesions can impair the integrity of major networks such as the default mode network (DMN) and the cortico-thalamic circuits, resulting in reduced global efficiency and altered modular organization of the brain. These disruptions compromise the brain's capacity to coordinate activity across widespread regions, particularly between the two hemispheres, vital for complex motor and cognitive functions. Impaired connectivity within the DMN has been linked to deficits in attention, memory, and self-referential thinking, while damage to cortico-thalamic pathways affects sensory integration and motor execution. Furthermore, the resulting imbalance between hemispheres may trigger maladaptive plasticity or excessive compensatory activity in contralesional areas, further complicating recovery. Such network-level dysfunctions can hinder neuroplasticity, reduce the brain's adaptability, and limit the effectiveness of rehabilitation. Understanding these widespread effects underscores the importance of targeting brain network reorganization through personalized interventions and neuromodulation techniques to support functional recovery following stroke (17).

In clinical neuroscience, graph theoretical analysis provides a robust tool for mapping and quantifying these post-lesional changes in brain connectivity. Network analysis contributes to the clinical characterization of stroke patients by offering objective metrics that describe the integrity and efficiency of information processing within the brain (18). One of this field's most widely utilized concepts is the small-world (SW) index, which captures the balance between local specialization and global integration in brain networks (19). A network with high SW characteristics typically combines short path lengths (global integration) with high clustering coefficients (local segregation), features thought to support efficient information transmission and processing.

Graph analysis enables researchers to explore the temporal and frequency-specific dynamics of brain reorganization following stroke when applied to EEG data. For example, studies have demonstrated that ischemic stroke is associated with a frequency-dependent reconfiguration of interhemispheric information flow, often manifested as decreased efficiency in long-range connections and altered synchronization across cortical regions (20). These insights underscore the utility of EEG-based graph metrics for tracking post-stroke changes in brain connectivity with high temporal resolution.

Its rapidly expanding body of literature reflects the field's growing relevance. Since 1985, the number of publications indexed under the term "brain network" has increased dramatically, with a notable rise from 8,387 articles in 2016 to over 14,256 in 2021 (PubMed database), indicating a surging interest in network neuroscience and its applications in clinical research.

From a topological perspective, stroke leads to functional reorganization of brain networks, as evidenced by changes in spontaneous connectivity patterns and information flow dynamics (21, 22). These alterations reflect compensatory mechanisms triggered by ischemic lesions, aiming to restore lost functionality by recruiting alternative pathways and reweighted connections [18]. Graph theory conceptualizes brain networks as sets of nodes (i.e., brain regions) and edges (i.e., functional or structural connections), which can be analyzed using various parameters to describe the overall architecture and performance of the system (23).

Among the most informative metrics used in network analysis are:

- Clustering Coefficient (CC): This parameter assesses the tendency of nodes to form local clusters, reflecting segregated processing within specialized brain regions. The local CC calculates the interconnectedness of a node's immediate neighbors, while the global CC summarizes this behavior across the entire network (24).
- Path Length (PL): Defined as the average number of steps required to connect any two nodes in the network, PL is a measure of global integration, indicating how efficiently information is transmitted across distant brain regions (19, 21-23, 25).
- Small-World Index (SW): This composite measure is calculated as the ratio of CC to PL (26, 27). A network with SW > 1 exhibits small-world properties, which are thought to support specialized processing and distributed communication hallmarks of healthy brain function.

Deviations from normal small-world configurations often correlate with impaired cognitive or motor function in post-stroke individuals, emphasizing the relevance of network topology as a biomarker for clinical outcomes. Understanding how these network parameters shift after stroke and how they may be modulated through rehabilitation offers a promising avenue for precision medicine in neurorehabilitation.

In EEG research, functional connectivity refers to the statistical interdependence or coordination of neural activity between distinct brain regions over time. Among various methods used to quantify this interdependence, EEG coherence has emerged as a widely accepted and robust metric for assessing general synchronization between two EEG signals (16, 28). Coherence reflects the consistency of phase and amplitude relationships across frequencies, thus offering insights into the degree to which distant cortical areas engage in coordinated oscillatory activity.

An increase in EEG coherence is typically interpreted as an indication of functional coupling between two anatomically or functionally distinct brain regions (29). Such coupling implies that the regions work in

concert either directly via structural connections or indirectly through shared neural networks to support a cognitive, sensory, or motor process. Importantly, coherence can be assessed within specific frequency bands (e.g., delta, theta, alpha, beta, gamma), allowing researchers to track frequency-specific network interactions that underlie different aspects of brain function and dysfunction.

Beyond its role in assessing connectivity, EEG coherence serves as a valuable tool for investigating the "binding problem," the longstanding neuroscientific question of how the brain integrates information from distributed areas into a unified perceptual or behavioral output (30). In this context, coherence is viewed as a neural signature of synchrony, potentially reflecting the mechanism by which temporally aligned activity across brain areas leads to the integration of spatially distinct signals (31).

This aspect of coherence analysis is particularly relevant in clinical populations such as stroke survivors, where disrupted communication between brain regions, especially between hemispheres, is a common consequence of cortical or subcortical damage. Monitoring coherence patterns provides critical information about neurophysiological disruptions, compensatory mechanisms, and the efficacy of rehabilitative interventions to restore functional network connectivity.

Overall, EEG coherence allows researchers and clinicians to quantify functional connectivity with high temporal resolution and provides a theoretical and practical framework for understanding how distributed neural circuits synchronize to produce coherent behavior, perception, and cognition.

Musculoskeletal assessment with Ultrasound

Medical imaging technologies have become indispensable tools in modern healthcare, serving as a cornerstone not only for the accurate diagnosis and localization of pathological changes but also for the detailed quantification of tissue properties, longitudinal monitoring of disease progression, and objective evaluation of treatment efficacy across a wide range of medical conditions (32). The integration of imaging modalities into routine clinical workflows has significantly enhanced the ability of clinicians to detect early pathological alterations that may not be evident through traditional examination methods. In recent years, rapid and transformative advances in digital image processing, computational modeling, and artificial intelligence, particularly through the use of machine learning algorithms, have further amplified the utility of medical imaging by enabling the extraction of high-dimensional, clinically relevant information from complex datasets with unprecedented levels of precision and consistency (33-35). These developments have opened new frontiers in predictive diagnostics, personalized medicine, and automated decision support systems, transforming healthcare delivery. Importantly, such innovations

hold particular promise in rehabilitation sciences, where detailed and quantitative analysis of soft tissue architecture, such as muscle echogenicity, echotexture, and deformation patterns, can yield valuable insights into the underlying biological processes associated with injury, degeneration, or recovery. This, in turn, supports more informed prognosis, facilitates targeted therapeutic interventions, and enhances the overall quality of clinical decision-making and patient outcomes in rehabilitation settings.

Among the various imaging modalities available, ultrasound has emerged as a particularly attractive and versatile tool for musculoskeletal assessment, especially in populations with neurological disorders such as stroke patients. Its non-invasive nature, real-time imaging capability, and relatively low operational cost make it highly suitable for routine clinical practice and advanced research settings (36-38). Unlike other imaging techniques requiring ionizing radiation, contrast agents, or costly infrastructure, ultrasound provides a portable and accessible alternative that allows dynamic evaluation of soft tissue structures, including muscles, tendons, and fascia, during functional tasks or therapeutic interventions. This dynamic capability is particularly valuable in stroke rehabilitation, where clinicians and researchers seek to monitor muscle architecture, tone, and quality changes over time to guide individualized treatment plans. Furthermore, the method's high temporal resolution and responsiveness to subtle physiological changes facilitate immediate feedback during assessment and training sessions, enhancing its utility in neurorehabilitation protocols. Ultrasound imaging carries minimal biological risk, as it uses low-intensity acoustic waves rather than ionizing radiation, rendering it safe for repeated and longitudinal use, even in vulnerable populations such as older adults or individuals with impaired neurological function (39). This safety profile and its practicality and diagnostic value position ultrasound as a critical component in developing objective, scalable, and patient-centered assessment frameworks for musculoskeletal and neurorehabilitation care.

Ultrasound has been extensively utilized to evaluate the structural and functional properties of skeletal muscle in a variety of health conditions, including but not limited to stroke, amyotrophic lateral sclerosis, chronic low back pain, myofascial pain syndrome, breast cancer-related musculoskeletal complications, and muscle-tendon injuries (39-43). Its ability to capture macrostructural features (such as muscle thickness, pennation angle, and fascicle length) and microstructural echotexture patterns makes it a valuable tool for understanding the impact of neuromuscular disorders on tissue integrity and function.

In the case of stroke-related muscle pathology, ultrasound imaging holds particular promise for assessing muscle changes associated with disuse atrophy, spasticity, and fibro-adipose tissue replacement. These

changes are often subtle and progressive, necessitating imaging modalities that can detect and quantify such alterations with precision and repeatability qualities that US imaging inherently offers.

Texture analysis is a well-established computational technique used to quantify pixel intensities' spatial distribution within an image's defined region of interest (ROI) (44, 45). Initially developed for applications in computer vision and digital image processing, this method has found significant utility in medical imaging for the quantitative characterization of tissue structure. Texture analysis is particularly valuable when visual assessment alone cannot detect subtle structural variations. In clinical settings, especially within ultrasound imaging, texture analysis has been adapted to evaluate the microstructural integrity of soft tissues through a process known as echotexture analysis (40, 46, 47).

Echotexture analysis focuses on ultrasound-specific texture features that describe how the grayscale intensity values are distributed and related spatially across the muscle image. These features can be categorized into several classes of statistical descriptors:

First-order statistics constitute a fundamental category of intensity-based image features that are commonly extracted from grayscale histograms in ultrasound imaging. These features are calculated without considering spatial relationships between pixels and are widely used to quantify tissue properties based on the overall distribution of pixel intensities within a ROI. A range of descriptors can be obtained through histogram-based analysis, including measures related to central tendency, dispersion, asymmetry, peakedness, uniformity, and randomness. This class of features typically includes echointensity, variance, standard deviation, skewness, kurtosis, energy, and entropy (40, 48-55). Such metrics are applicable at both the ROI and patch levels and are essential tools for quantitatively assessing muscle tissue quality in post-stroke ultrasound evaluations. Table 1 briefly shows the first-order parameters.

Table 1. Histogram-based parameters with their formula are shown.

Statistical approach	Feature	Brief Description	Formula
Histogram-based (first-order) features	Echogenicity, also called Echointensity	The ability of tissues to reflect ultrasound waves. Specifies the average brightness of the ultrasound image.	$mean(ROI)$

	Variance	Measures the dispersion of pixel intensity values.	$\frac{1}{N}\sum_{i=1}^{N}(x_i - \mu)^2$
	Standard Deviation	The square root of variance.	$\sqrt{var(image)}$
	Echovariation, also called the Coefficient of variation	Variation in echo intensities in an ultrasound image.	$\frac{std(image) * 100}{mean(image)}$
	Skew	Measures the asymmetry of the distribution of pixel intensity values.	$\frac{\sum_{i=1}^{N}(x_i - \mu)^3}{(N-1)\sigma^3}$
	Kurtosis	Measures the "tailedness" of the distribution of pixel intensity values.	$\frac{\sum_{i=1}^{N}(x_i - \mu)^4}{(N-1)\sigma^4}$

Second-order statistical features, most notably derived from the GLCM, provide a quantitative framework for analyzing the spatial relationship between pairs of pixels in an image. Unlike first-order statistics, which focus solely on the distribution of individual pixel intensities, second-order features capture how intensity levels co-occur at a given offset and orientation, offering deeper insights into texture organization and local spatial patterns.

Among the most widely used second-order features are the Haralick descriptors, introduced by Haralick et al. in 1973. These descriptors include contrast, correlation, homogeneity, energy, and others (56). These features are especially valuable in medical imaging, where subtle changes in tissue architecture, such as fibrosis, atrophy, or infiltration, may not significantly affect average intensity values but do alter spatial texture patterns. Some of these second-order parameters are:

- Contrast: it measures the local intensity variation, emphasizing differences between neighboring pixel values. High contrast indicates greater texture heterogeneity, often seen in disorganized or pathological tissue.
- Correlation reflects the linear dependency of gray levels across the image, offering insights into structural alignment within the tissue.

- Homogeneity (also known as inverse difference moment): it evaluates the closeness of the distribution of elements in the GLCM to the GLCM diagonal, with higher values indicating more uniform textures.
- Energy: it represents textural uniformity and is derived from the sum of squared GLCM elements. Higher values denote repetitive or highly ordered patterns (57).

These features are particularly useful in musculoskeletal ultrasound and neuroimaging, where GLCM-based analysis has been employed to detect microstructural abnormalities, quantify muscle degeneration, or differentiate healthy versus pathological tissues.

As briefly outlined in Table 2, the selected GLCM features used in this study capture diverse aspects of image texture and contribute to a more objective and reproducible evaluation of tissue quality beyond visual interpretation.

Table 2. Grey Level Co-occurrence Matrix (GLCM) parameters with their formula are shown

Statistical approach	Feature	Brief Description	Formula
Grey Level Co-occurrence Matrix (GLCM)	Correlation	Measures the statistical correlation between neighboring pixels.	$\dfrac{\sum_{i,j} (i - \mu_i)(j - \mu_j)P(i,j)}{\sigma_i \sigma_j}$
	Dissimilarity	Measures the mean absolute difference between neighboring pixel values.	$\sum_{i,j} |i - j|P(i,j)$
	Contrast	Measures the intensity contrast between a pixel and its neighbor over the whole image.	$\sum_{i,j} (i - j)^2 P(i,j)$
	Homogeneity	Measures the closeness of the distribution of elements in the GLCM to the GLCM diagonal.	$\sum_{i,j} \dfrac{P(i,j)}{1 + |i - j|}$
	Angular Second Moment	Similar to energy, it measures the uniformity of the GLCM.	$\sum_{i,j} P(i,j)^2$
	Energy	The sum of squared elements in the GLCM represents texture uniformity.	$\sqrt{\sum_{i,j} P(i,j)^2}$

	Max Probability	The highest value in the GLCM.	$max\ (P(i,j))$
	Entropy	Measures the randomness or complexity of the texture	$-\sum_{i,j} P(i,j)log\ (P(i,j))$
	Cluster Shade	Measures the skewness of the distribution of the GLCM.	$\sum_{i,j} \left(i+j-\mu_x-\mu_y\right)^3 P(i,j)$
	Cluster Prominence	Measures the peakedness of the distribution of the GLCM.	$\sum_{i,j} \left(i+j-\mu_x-\mu_y\right)^4 P(i,j)$

Run-length statistics, derived from the Gray-Level Run-Length Matrix (GLRLM), offer a valuable method for analyzing the directional and linear texture properties within medical images. GLRLM quantifies the number of consecutive pixels (runs) that share the same gray-level intensity in specific directions, effectively capturing repetitive structural patterns such as muscle fiber alignment or tissue organization (58).

Each element (i,j) of the GLRLM represents the count of runs with gray level i and run length j, from this matrix, several texture descriptors are calculated, which provide insights into the texture granularity, linearity, and uniformity of the region of interest.

Some key GLRLM-based features include:

- Short Run Emphasis (SRE): This emphasizes the prevalence of short, homogeneous pixel runs, which indicate fine textures or granular tissue patterns.
- Long Run Emphasis (LRE): it emphasizes the presence of long, continuous runs, typical of coarser, more uniform textures.
- Gray-Level Uniformity (GLU): Measures the consistency of gray levels across all runs. Higher GLU values reflect a uniform intensity distribution, suggesting homogeneous tissue composition or less textural complexity.
- Run-Length Uniformity (RLU): Quantifies the uniformity of run lengths across the image. A high RLU indicates that runs tend to be of similar lengths, which may imply orderly or repetitive tissue structure. At the same time, low RLU suggests greater variation and possibly disorganized or pathological textures.

- Run Percentage (RP): This measure reflects the density of runs relative to the size of the ROI, providing an estimate of overall textural activity.

These features are particularly effective in distinguishing normal from abnormal muscle tissue, as seen in conditions like stroke, ALS, or muscular dystrophy. For instance, lower GLU and RLU values might indicate heterogeneous textures or fiber disarray, which is common in muscle atrophy or neurogenic damage.

As presented in Table 3, the extracted GLRLM parameters contribute to a quantitative, objective muscle and tissue quality assessment, offering complementary information to first-order statistics and GLCM-based analyses. Their inclusion strengthens diagnostic precision and enhances disease progression or rehabilitation outcomes monitoring.

Table 3. Gray Level Run Length Matrix (GLRLM) parameters with their formula is shown

Statistical approach	Feature	Brief Description	Formula
Gray Level Run Length Matrix (GLRLM)	Short Run Emphasis	Measures the distribution of short runs.	$\dfrac{1}{N}\sum_{i,j}\dfrac{P(i,j)}{j^2}$
	Long Run Emphasis	Measures the distribution of long runs.	$\dfrac{1}{N}\sum_{i,j}P(i,j)j^2$
	Gray Level Uniformity	Measures the uniformity of gray levels.	$\sum_{i,j}P(i,j)^2$
	Run Length Uniformity	Measures the uniformity of run lengths.	$\sum_{j}\left(\sum_{i}P(i,j)\right)^2$
	Run Percentage	The ratio of the number of runs to the number of pixels.	$\dfrac{Number\ of\ Runs}{Number\ of\ Pixel}$

Advanced computational approaches include Fast Fourier Transform (FFT) for frequency domain analysis, machine learning algorithms, and, more recently, patch-based echotexture analysis, which divides the ROI into multiple subregions to extract localized texture patterns (59).

While these echotexture descriptors have shown promising potential for identifying pathological changes in muscle tissue, especially in conditions like stroke and neuromuscular disorders, several limitations often hinder their clinical translation. Chief among these are challenges related to reproducibility and standardization, which stem from variability in ultrasound machine settings, operator technique, probe

orientation, and patient-specific anatomical factors (49, 60-63). These sources of variation can significantly influence the extracted texture features, limiting the comparability of results across studies and impeding their integration into routine clinical workflows.

To overcome these limitations, recent research efforts have emphasized the need for protocol standardization, robust statistical validation, and multi-center collaboration to ensure the development of reliable echotexture-based biomarkers. As a result, texture analysis is increasingly recognized not merely as a research tool but as a viable quantitative imaging biomarker in rehabilitation and diagnostic medicine.

EI is the most extensively studied and widely applied feature among the various echotexture parameters investigated in post-stroke populations. EI represents the average grayscale intensity within the muscle fascia, and elevated EI values are generally interpreted as indicators of pathological changes such as muscle atrophy, fibrosis, and fibro-adipose tissue infiltration (40, 64-68).

EI can be evaluated through both qualitative and quantitative approaches. The qualitative method is typically based on the Heckmatt scale, in its original or modified version, which classifies muscle echogenicity into four levels of impairment using visual inspection (69, 70). Although widely used in clinical settings, this approach is inherently subjective and dependent on the examiner's experience. On the other hand, quantitative EI assessment employs image processing software to extract pixel intensity values directly from ultrasound images, offering greater precision and repeatability. Nevertheless, this method has limitations, as it remains highly sensitive to factors such as ultrasound system settings, probe orientation, and the delineation of the region of interest (49, 62, 63).

In recent years, an alternative parameter known as EV, defined as the degree of grayscale intensity variation within the ROI, has gained increasing attention as a potentially more sensitive and informative measure of muscle tissue heterogeneity (71-73). Unlike EI, which only captures the central tendency of pixel values, EV provides additional insight into the internal texture fluctuations that may better reflect the microstructural integrity of the muscle.

Notably, studies in stroke patients have reported a strong correlation between EV and the modified Heckmatt scale, suggesting that EV may serve as a quantitative surrogate marker for muscle quality, particularly in populations with upper motor neuron lesions (73). However, much of the existing evidence has been derived from relatively small and selective image sets, often based on expert-chosen subsets of extreme cases. This introduces a risk of selection bias and limits the generalizability of findings. As such,

further research involving larger datasets, standardized acquisition protocols, and rigorous statistical validation is needed to fully establish the clinical utility of EV in post-stroke muscle assessment.

Following a stroke, the nervous system undergoes a range of changes that directly affect the structure and function of skeletal muscles. One of the most prominent neuromuscular consequences is the progressive infiltration of fatty and fibrous tissue into previously healthy, contractile muscle fibers (68, 74). These changes are primarily the result of reduced voluntary activation, muscle disuse, and neurogenic atrophy, all of which are common in individuals with upper motor neuron lesions, such as those caused by stroke.

These pathological muscle transformations can be visualized and quantified using ultrasound imaging through direct structural measurements and echotexture analysis. Structurally, stroke-induced muscle degeneration may appear as reductions in muscle thickness, shortening of fascicle length, and alterations in pennation angle, which are typically evaluated to assess the macroscopic architecture of muscle tissue (75-78).

However, structural measurements alone may not fully capture the underlying tissue quality. Therefore, echotexture-based features, particularly EI and EV, have become essential tools in characterizing the microstructural changes that occur post-stroke (79, 80).

EI reflects the muscle's average grayscale brightness, which increases with the accumulation of fibrous and fatty tissue. On the other hand, EV represents the variation or dispersion of grayscale values within the muscle, offering insight into tissue heterogeneity and internal texture irregularities.

While EI is useful for detecting general increases in echogenicity due to degeneration, it may overlook localized variations within the muscle. In contrast, EV provides complementary information by highlighting inconsistencies and disruptions in the tissue structure that EI alone may not detect (73). This makes EV particularly valuable in capturing the complex and uneven nature of muscle remodeling in stroke survivors.

Together, these parameters offer a comprehensive and non-invasive means of evaluating stroke-related muscle alterations, supporting more accurate diagnosis, monitoring, and personalized rehabilitation planning.

One of the most important and sometimes most difficult steps in echotexture analysis is deciding which part of the muscle image should be analyzed; this area is called the ROI. In some studies, researchers

select the entire muscle area between the superficial and deep fascia as one large ROI (73). In other studies, however, this area is divided into multiple smaller regions, or "patches", to allow for more detailed analysis (39, 41, 43, 81, 82), new methodologies, such as patch-based analysis, are proposed to address this limitation. The idea behind patch-based analysis is to reduce measurement errors and improve accuracy by: 1) Dividing the large ROI into smaller, more uniform regions; 2)Extracting multiple measurements across these patches instead of relying on a single average value; 3)Detecting local differences in muscle texture that may not be visible when analyzing the whole area as one unit.

Even though this method seems promising, many unanswered questions remain about how the size of the patches or how they are selected affects the values of important features like EI and EV. Because of this, researchers are still concerned about how standardized and reproducible these measurements are when using patch-based techniques. More research is needed to understand how these choices influence the final results and to develop clear guidelines that ensure consistency across different studies and clinical applications.

Objectives

Study 1: The Effect of Dry Needling in Chronic Stroke with a Complex Network Approach: A Case Study

Despite the increasing clinical adoption of DN as a non-pharmacological intervention in post-stroke rehabilitation, particularly for managing muscle spasticity and improving motor function, the underlying neurophysiological mechanisms, especially those involving CNS activity, remain poorly elucidated. While a growing body of evidence supports the peripheral effects of DN on muscle tone, trigger point modulation, and nociceptive pathways, far less is known about its influence on central neural processes, including cortical excitability and functional brain connectivity. Several studies have documented improvements in clinical outcomes such as spasticity reduction, enhanced voluntary motor control, and improved gait dynamics in patients with chronic stroke following DN treatment. However, no systematic investigation has explored how DN may affect large-scale brain network organization, particularly through EEG-based complex network analysis. This presents a critical gap in the literature, especially given the increasing recognition of functional brain network plasticity as a key mechanism underlying motor recovery and behavioral gains after stroke. EEG, as a non-invasive and temporally precise method of measuring brain activity, provides valuable insights into the dynamic functional architecture of the brain. When coupled with graph theoretical approaches, which enable quantitative modeling of connectivity

patterns through indices such as clustering coefficient, characteristic path length, global efficiency, and small-worldness, this method offers a robust framework for assessing network-level changes in brain organization. The integration of these tools allows researchers to move beyond regional activation patterns and instead determine how distributed brain networks may reorganize in response to therapeutic interventions such as DN.

Based on the information above, the objective of this study was to evaluate whether DN induces measurable alterations in EEG-derived brain network topology in a chronic stroke patient. The study seeks to determine whether DN can facilitate functional reorganization of cortical connectivity by applying graph theoretical metrics to resting-state EEG data before and after DN. This neuroplastic process may contribute to the observed clinical benefits in motor recovery. The findings from this exploratory analysis could provide foundational insights for future controlled trials and contribute to a more mechanistic understanding of DN's role within neurorehabilitation paradigms.

Study 2: Brain Analysis with a Complex Network Approach in Stroke Patients Based on Electroencephalography: A Systematic Review and Meta-Analysis

Stroke results in a broad spectrum of clinical manifestations, ranging from mild motor deficits to severe and persistent impairments in cognition, perception, and sensory integration, often depending on the location, extent, and type of cerebrovascular insult. This clinical heterogeneity presents a significant challenge in research and clinical practice, as it is further compounded by the inconsistent use of assessment methods and measurement tools across studies, many of which suffer from limited psychometric validation, poor reproducibility, or context-specific applicability (31, 32).

As a result, the lack of methodological standardization limits the comparability of findings across different research settings. It impedes the development of tailored, evidence-based interventions designed to address the nuanced needs of diverse stroke phenotypes. Among the many domains of post-stroke research, one remarkably underexplored yet up-and-coming area is the quantitative analysis of functional brain network reorganization using EEG-derived connectivity metrics.

While several neuroimaging studies employing MRI, PET, and fNIRS have examined structural, perfusional, and metabolic alterations in regions such as the Broca's area, cerebellum, thalamus, and areas supplied by the middle cerebral artery, there remains a relative paucity of research that systematically investigates the dynamics of EEG-based functional connectivity, especially using advanced analytical frameworks such as graph theory across different stages of stroke recovery (i.e., acute, subacute, and chronic).

Furthermore, despite the increasing popularity of EEG as a non-invasive, cost-effective, and temporally sensitive modality for tracking neural activity, there is currently no universally accepted framework or consensus for applying complex network analysis to EEG data in stroke populations.

Our objective in this study was to systematically review research that has examined brain networks in stroke patients and to identify potential biomarkers within these networks. We sought to find specific indicators or parameters that show higher or lower values in individuals who have experienced a stroke. Identifying such biomarkers could significantly contribute to the advancement of neurorehabilitation.

Study 3: Characterizing Muscle Tissue Quality Post-Stroke: Echovariation as a Clinical Indicator

As discussed in the introduction, there is currently no standardized or universally accepted framework for classifying the extent of muscle involvement in individuals affected by stroke using ultrasound-derived quantitative metrics. This gap presents a major limitation in musculoskeletal ultrasound's clinical utility and research reproducibility, especially in neurorehabilitation. A critical challenge observed in prior studies lies in the inconsistent selection and application of echotexture features, such as grayscale histograms, entropy, contrast, and echogenicity, which often leads to divergent findings, suboptimal diagnostic accuracy, and limited comparability across studies. These methodological inconsistencies hinder the establishment of normative reference values and compromise efforts to develop reliable imaging-based biomarkers for muscle integrity assessment.

Given these limitations, the primary objective of the study presented in study 3 is to systematically investigate and identify the most informative echotexture features extracted from B-mode ultrasound images of the gastrocnemius medialis muscle in individuals with chronic stroke. The focus is particularly placed on evaluating the potential of EV. This quantitative measure captures textural heterogeneity within muscle tissue as a robust and sensitive biomarker capable of distinguishing varying degrees of muscle degeneration and structural disorganization. By quantifying EV across different levels of impairment, this study aims to determine its discriminative power in classifying muscle condition and to examine its correlation with established clinical grading tools, such as the Heckmatt Scale, through blinded expert assessments. The study seeks to bridge the gap between quantitative imaging science and real-world clinical decision-making by combining objective image-based analysis with subjective clinical judgment. The findings are anticipated to contribute toward standardizing ultrasound-based muscle evaluation protocols and enhance the diagnostic and prognostic value of sonographic imaging in post-stroke rehabilitation contexts.

Study 4: Improving the Reliability of Muscle Tissue Characterization Post-Stroke: A Secondary Statistical Analysis of Echotexture Features

In Study 3, we identified and initially validated specific echotexture features, most notably EV and EI, as promising objective indicators of muscle tissue deterioration in individuals with stroke. These parameters, derived from B-mode ultrasound images, demonstrated strong potential for reflecting pathological changes in muscle architecture and were found to correlate meaningfully with established clinical scales used to assess muscle quality. However, while these initial findings are encouraging, the clinical implementation of EV and EI as standardized biomarkers remains contingent upon further methodological refinement and validation. Despite yielding significant associations, the original analysis was constrained by several limitations, including the potential for selection bias and a degree of reliance on subjective expert interpretation for clinical scale ratings, which may affect reproducibility and generalizability.

To address these shortcomings, the primary objective of the follow-up investigation presented in Study 3 is to perform a rigorous secondary statistical analysis designed to enhance objectivity and methodological robustness. This is accomplished using advanced statistical approaches, such as correlation modeling, ROC curve analysis, and inter-rater reliability assessment, to evaluate the diagnostic accuracy and consistency of the echotexture features across different severity levels of muscle impairment.

The objective of this study was to explore the strength and nature of the relationship between quantitative ultrasound-derived measures and categorical clinical muscle classifications, such as those provided by the Heckmatt Scale, in a more systematic and unbiased manner. By minimizing the influence of subjective interpretation and improving the analytical framework, this research aspires to establish a stronger scientific foundation for integrating EV, EI, and potentially other echotexture parameters into routine clinical assessment protocols for post-stroke muscle evaluation. Ultimately, this could pave the way for more precise, accessible, and objective diagnostic tools in stroke rehabilitation settings.

Study 5: A Complementary Patch-Based Histogram Analysis for Quantifying Muscle Tissue in Ultrasound Imaging

Building on previous investigations that typically analyzed the entire muscle region as a single ROI, the current study introduces a novel and complementary methodological approach to enhance the granularity and accuracy of ultrasound-based muscle analysis. Specifically, Study 5 explores the effects of subdividing the global ROI into multiple smaller patches of varying sizes to assess the distribution and variability of key echotexture features, namely EV and EI. Rather than relying on a single averaged value

that may obscure important localized variations, this study employs a patch-wise histogram-based analysis to evaluate how these echotexture parameters fluctuate across different regions within the muscle.

The objective of this study is to determine whether finer spatial resolution improves sensitivity in detecting subtle or heterogeneous patterns of muscle degeneration in stroke patients by systematically altering the size and number of analyzed patches. Such spatial heterogeneity is often masked in global analyses but may hold clinical significance. This methodological framework also allows for a more nuanced understanding of muscle tissue organization and the potential to detect region-specific abnormalities not apparent in traditional assessments.

Ultimately, the overarching objective of this study is to assess the methodological implications and diagnostic value of localized versus global echotexture quantification. By capturing intra-muscular variability more accurately, this approach can improve ultrasound-based biomarkers' reliability, sensitivity, and clinical relevance in evaluating and monitoring post-stroke muscle alterations. If validated, this technique could serve as a foundation for more individualized and spatially-informed rehabilitation strategies, advancing the role of quantitative ultrasound in neurorehabilitation research and practice.

Methodology

Study 1

The Effect of dry Needling in Chronic Stroke with a complex Network Approach: A Case Study

This is a single-case quasi-experimental study using a pre- and post-intervention design.

Participant

A 62-year-old male with chronic ischemic stroke and right hemiplegia in Brunnstrom Stage 3 participated. Written informed consent was obtained.

EEG Assessment

Resting-state EEG was recorded for 5 minutes with eyes closed before and during dry needling (DN), and compared to a healthy age-matched control (61 years old). EEG data were collected using 18 electrodes (10-20 system) and sampled at 256 Hz.

Intervention

DN was applied for 60 seconds at the motor point of the brachialis muscle using a sterile 50×0.3 mm needle, using a fast in–fast-out technique at ~ a 1 Hz frequency.

Data Processing

EEG data were exported in EDF format, preprocessed in MATLAB using EEGLAB, and further analyzed in Python using NetworkX and SciPy. Artifacts such as blinks and EMG noise were removed.

Network Construction

A functional brain network was created using the electrodes as graph nodes and edges defined by generalized partial directed coherence (GPDC). Weighted coherence matrices were binarized using a 0.15 threshold.

Frequency Bands

2700 directed binary matrices were generated across five frequency bands: delta (<4 Hz), theta (4–8 Hz), alpha (8–13 Hz), beta (13–30 Hz), and gamma (30–45 Hz).

Graph Metrics

Network analysis included five key topological metrics: Density, Average shortest path length, Clustering coefficient, Betweenness centrality, and Small-worldness; these metrics were used to assess functional network changes before and after DN in the stroke patient.

Study 2

Brain Analysis with a Complex Network Approach in Stroke Patients Based on Electroencephalography: A Systematic Review and Meta-Analysis

This systematic review and meta-analysis was conducted following PRISMA guidelines and registered in PROSPERO (CRD42021285761).

Databases

PubMed, Cochrane, and ScienceDirect were searched up to October 2021 using a PICO-based strategy: Population: adults with stroke; Intervention: EEG assessment; Comparison: healthy controls; Outcome: brain network parameters.

Study Selection

Two independent reviewers screened titles, abstracts, and full texts based on the inclusion criteria: studies on stroke patients using EEG for brain connectivity analysis published in English. Exclusion criteria: interventional studies (e.g., rehabilitation trials).

Data Extraction

The data included the study design, sample characteristics, EEG and connectivity methods, outcome metrics, and main findings. Quality was assessed using the Newcastle–Ottawa Scale.

Data Analysis

Statistical analyses were performed in R. Mean and SD values were calculated or estimated from medians using standard methods. When unavailable, data were extracted from plots using WebPlotDigitizer.

Meta-analysis focused on the Small-World Index (SW) using a random-effects model. Heterogeneity was assessed using τ^2, Q, and I^2 statistics. Subgroup analyses were based on SW calculation methods. Publication bias was evaluated via funnel plots, Egger's and Begg's tests, and the trim-and-fill method.

Study 3

Characterizing Muscle Tissue Quality Post-Stroke: Echovariation as a Clinical Indicator

This observational study followed STROBE guidelines and the principles of the Declaration of Helsinki. Participants were recruited between February and April 2024 and provided written informed consent. Ethical approval was obtained (ID: PI24/030), and the study was registered at ClinicalTrials.gov (NCT06411587).

Participants and Data Collection

Post-stroke individuals were enrolled based on predefined inclusion and exclusion criteria at Hospital Clínico Universitario Lozano Blesa. Ultrasound (US) images of the gastrocnemius medialis were captured using a Butterfly iQ+ device under standardized settings. Each participant underwent image acquisition focused on whole-muscle ROIs, performed by experienced physiotherapists.

Echotexture Feature Extraction

First-order histogram-based features, gray-level co-occurrence matrix (GLCM) features, and gray-level run-length matrix (GLRLM) features were extracted from the selected ROIs without prior image preprocessing. GLRLM features were averaged across five different directions to ensure rotational invariance.

Ultrasound Imaging Assessment

An initial exploratory analysis identified features with the greatest potential to characterize muscle impairment. Three independent physiotherapists, blinded to participant information, rated muscle tissue quality and assessed the images with the modified Heckmatt scale scores. Inter-rater reliability was assessed, and relationships between extracted features and Heckmatt grades were examined.

Statistical Analysis

Data processing was performed in Python (v3.11.5), and statistical analyses were conducted using RStudio (v2024.09.0). Pearson's correlation was used to explore associations between features and Heckmatt scores. Differences among Heckmatt grades were analyzed using ANOVA or Kruskal–Wallis tests, followed by post hoc comparisons when appropriate. Statistical significance was set at $p < 0.05$.

Study 4

Improving the Reliability of Muscle Tissue Characterization Post-Stroke: A Secondary Statistical Analysis of Echotexture Features

The secondary analysis was based on the same dataset as the original study but employed a more refined and conservative image selection strategy. While the initial study included 420 regions of interest (ROIs), specifically, 20 ROIs per each of the 21 texture features selected based on their top and bottom values, the secondary analysis used a reduced and independent subset of 44 ROIs, choosing only one representative whole-muscle ultrasound image per limb for each patient. This approach was intended to eliminate redundancy and minimize potential bias from including multiple ROIs per individual.

Two expert physiotherapists conducted the initial feature selection and image classification in the original study. In contrast, the secondary analysis involved three physiotherapists, who independently assessed muscle tissue impairment (low and high) and modified Heckmatt scale scores. To ensure methodological rigor, inter-examiner reliability was reassessed, and the correlation between visual muscle impairment ratings and the Heckmatt scale was re-evaluated for the 44-image dataset.

Statistical Analysis

All analyses were performed in R (v4.1.3), with significance set at $p < 0.05$. Inter-examiner reliability was assessed using Cohen's and Light's kappa. Correlations were analyzed with polychoric correlation. Mann–Whitney U tests and Fisher's exact tests were used to explore group differences. Binary logistic regression models were developed using backward stepwise selection, optimizing the Akaike Information Criterion (AIC), and predictive performance was evaluated with ROC curve analysis.

Study 5

A complementary patch-based histogram analysis for quantifying muscle tissue in ultrasound imaging

In this follow-up study based on the original dataset, a novel patch-based analysis approach was introduced to enhance the assessment of muscle tissue. Unlike the initial study, which treated each ROI as a single, undivided unit, this analysis involved segmenting each ROI, already encompassing the entire muscle region, into multiple smaller patches of varying sizes. As a result, instead of extracting a single value per feature from each ROI, multiple feature values were obtained from individual patches within the same ROI. This granular representation allowed for a more detailed and localized evaluation of muscle tissue characteristics, thereby improving the sensitivity and precision of muscle impairment assessment.

Data Analysis

The grayscale ROI was divided into patches of varying sizes (10×10, 20×20, 30×30, 40×40, and 50×50 pixels). The echogenicity index (EI; mean pixel brightness) and echovariation (EV; standard deviation divided by mean intensity) were calculated for each patch. Descriptive statistics (mean, SD, median, IQR, skewness) characterized the distribution of EI and EV. Distribution shape was classified based on skewness. Normality was assessed visually through histograms; normally distributed features used mean/SD, while skewed distributions used median/IQR.

Kendall's tau coefficient was employed to analyze the correlation between feature intensity and dispersion. The extracted EI and EV values were compared graphically against the original ROI values. Furthermore, EV values were mapped onto a stroke-specific EV function derived from the primary research, illustrating the relationship between EV levels and muscle tissue quality. No equivalent functional mapping was available for EI.

Results

Study 1

Significant differences were observed between the stroke patient and the healthy control in the delta, theta, and alpha bands. During DN treatment, the patient's values moved closer to normal. Beta and gamma bands showed minor differences. Stroke patients exhibited smaller variations than controls, notably in the delta, theta, and alpha bands. DN application shifted the patient's values towards normal. Although no initial differences existed in beta and gamma bands, DN increased the parameter values. Significant differences were found in delta, theta, and alpha bands, with DN making the patient's brain network structure more similar to that of the healthy control. Patterns were similar to those observed for network density. Stroke patients had lower values across all bands compared to controls. DN treatment consistently moved the patient's measures toward normal, with the most pronounced differences in the delta, theta, and alpha bands. Significant alterations were noted in delta, theta, and alpha bands, with DN inducing a normalization effect. There were no differences in beta and gamma bands, although DN still promoted structural brain changes. Overall, DN treatment shifted the patient's brain network metrics towards patterns typical of healthy individuals, particularly in lower-frequency EEG bands.

The results of the EEG analysis using complex dynamic networks are presented in Figures 1 to 5, which show the variations of the metrics for each of the EEG bands. Each figure presents three curves showing the changes in the network metrics considered from their maximum value to their minimum value. The green and blue lines show the changes in the network parameter considered for the patient before and during the DN treatment, respectively, and the red line shows the parameter for the healthy subject as a control.
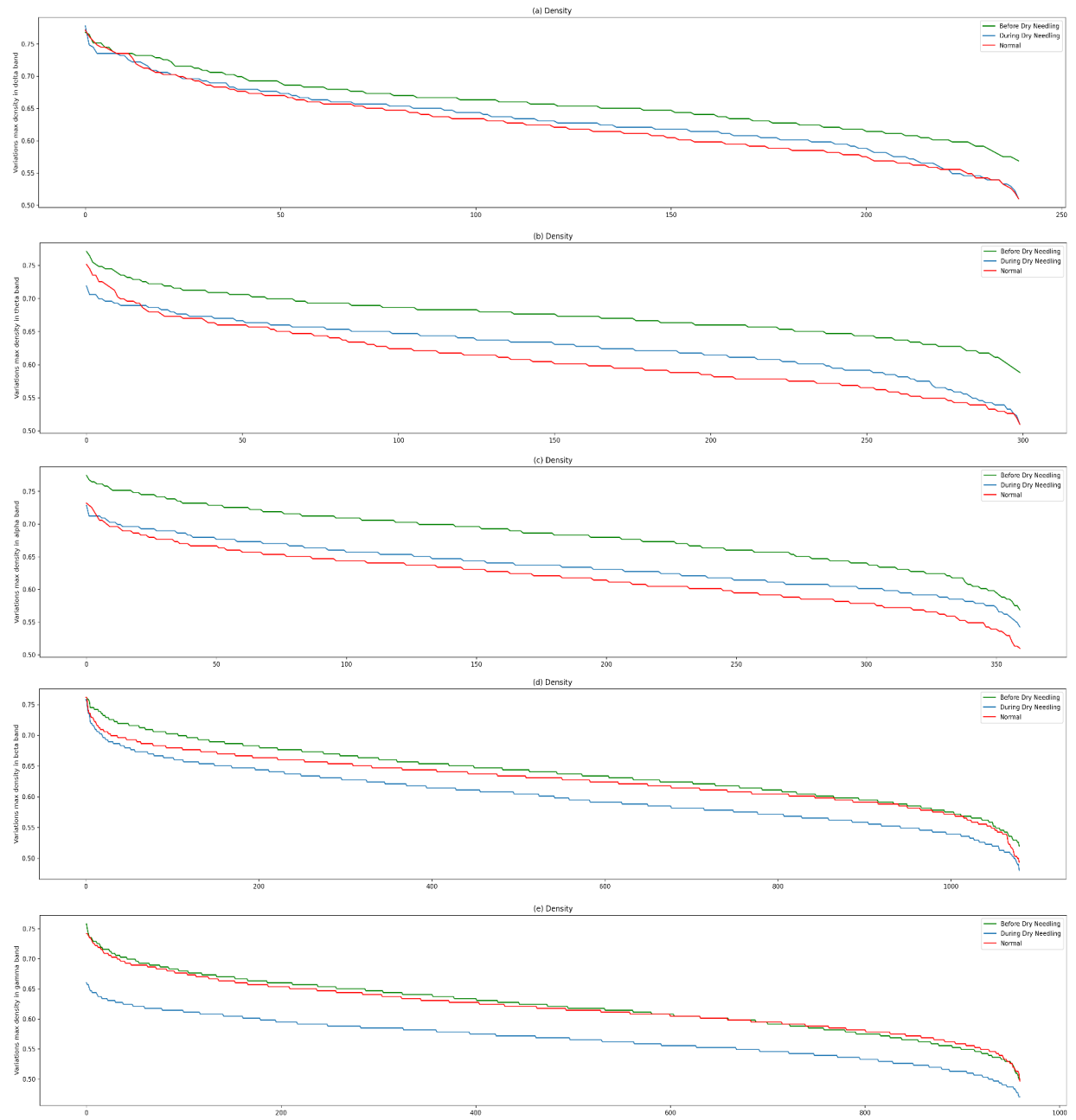
Figure 1. Variations in network density show delta (a), theta (b), and alpha (c) bands that becoming more similar to those of the healthy control during DN application. The beta (d) and gamma (e) bands show no significant differences between the stroke case and the healthy control.
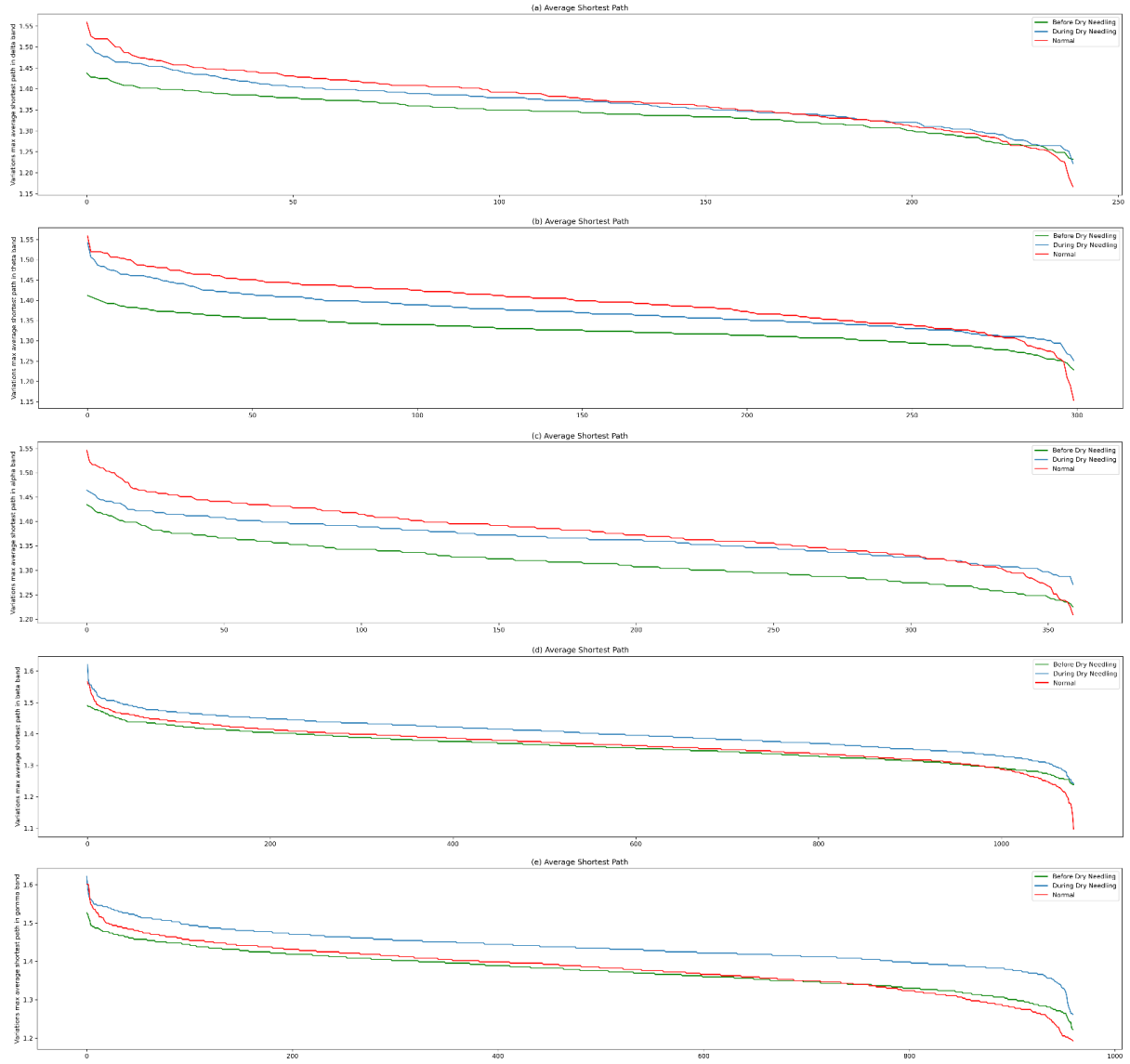
Figure 2. Variations in average shortest path show delta (a), theta (b), and alpha (c) bands becoming more similar to the healthy control during DN application. The beta (d) and gamma (e) bands show no significant differences between the stroke case and the healthy control.
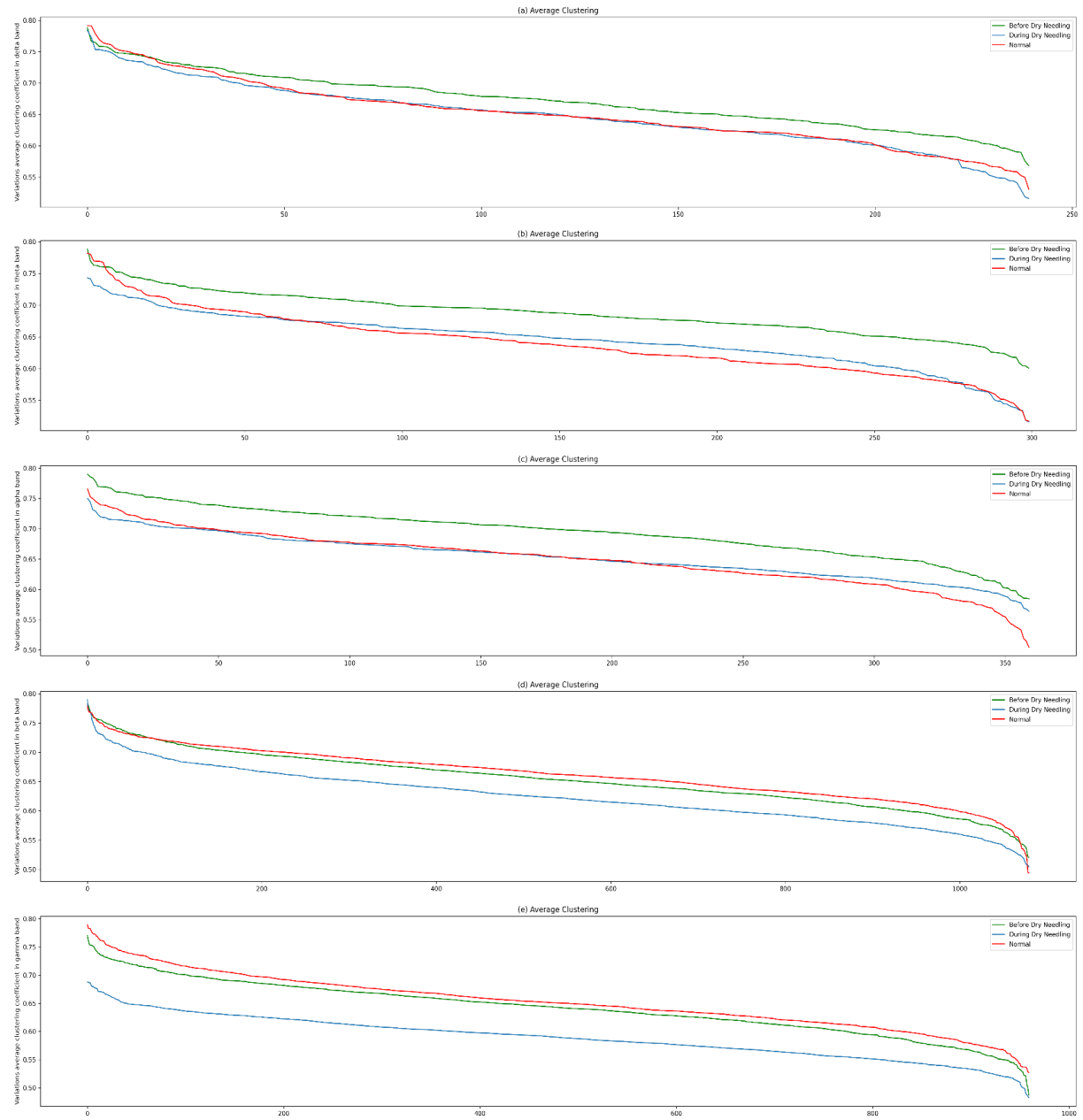
Figure 3. Variations in global clustering coefficient show delta (a), theta (b), and alpha (c) bands becoming more similar to the healthy control during DN application. The beta (d) and gamma (e) bands show no significant differences between the stroke case and the healthy control.
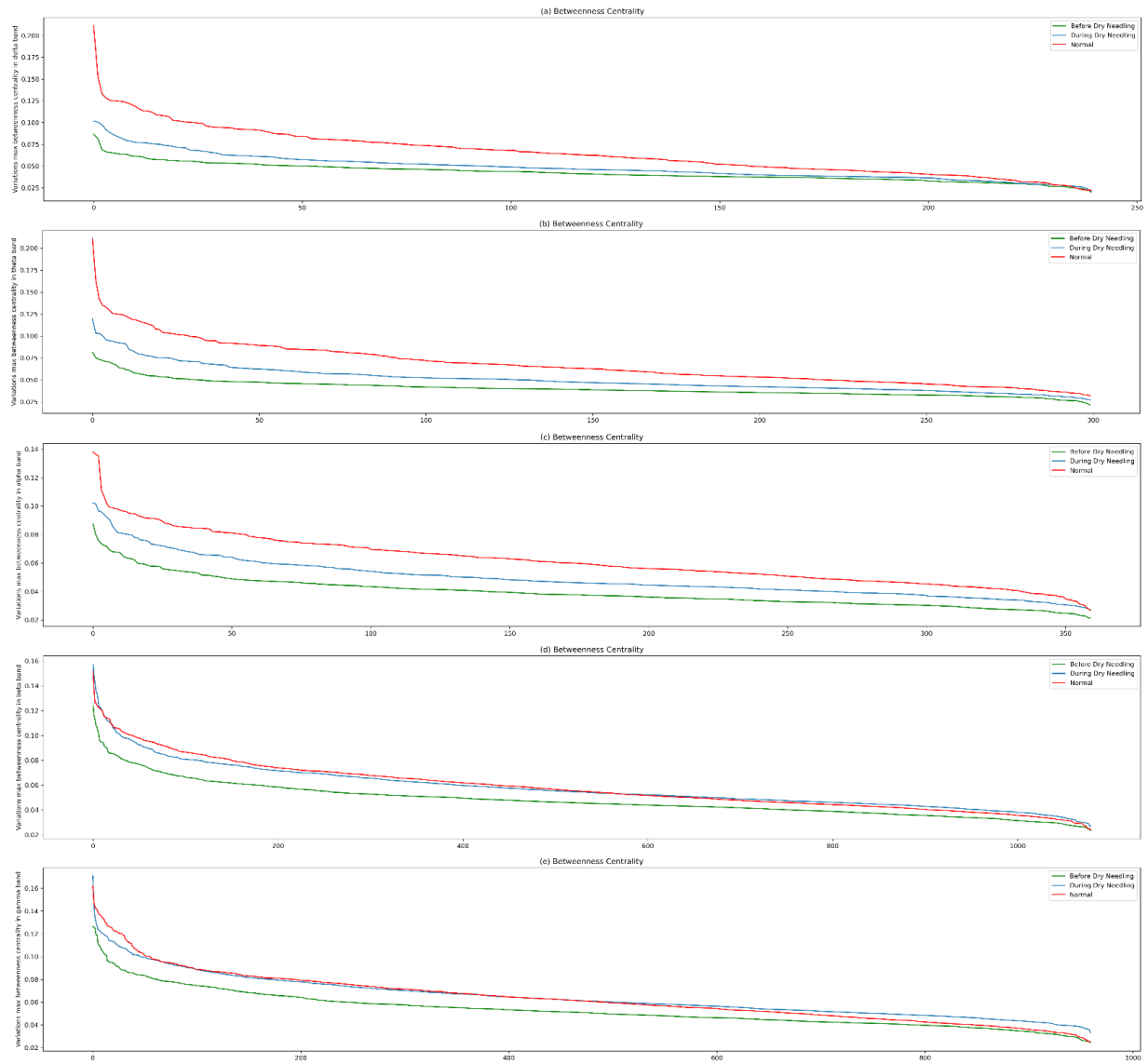
Figure 4. Variations in betweenness centrality show delta (a), theta (b), alpha (c), beta (d), and gamma (e) bands becoming more similar to the healthy control during DN application.
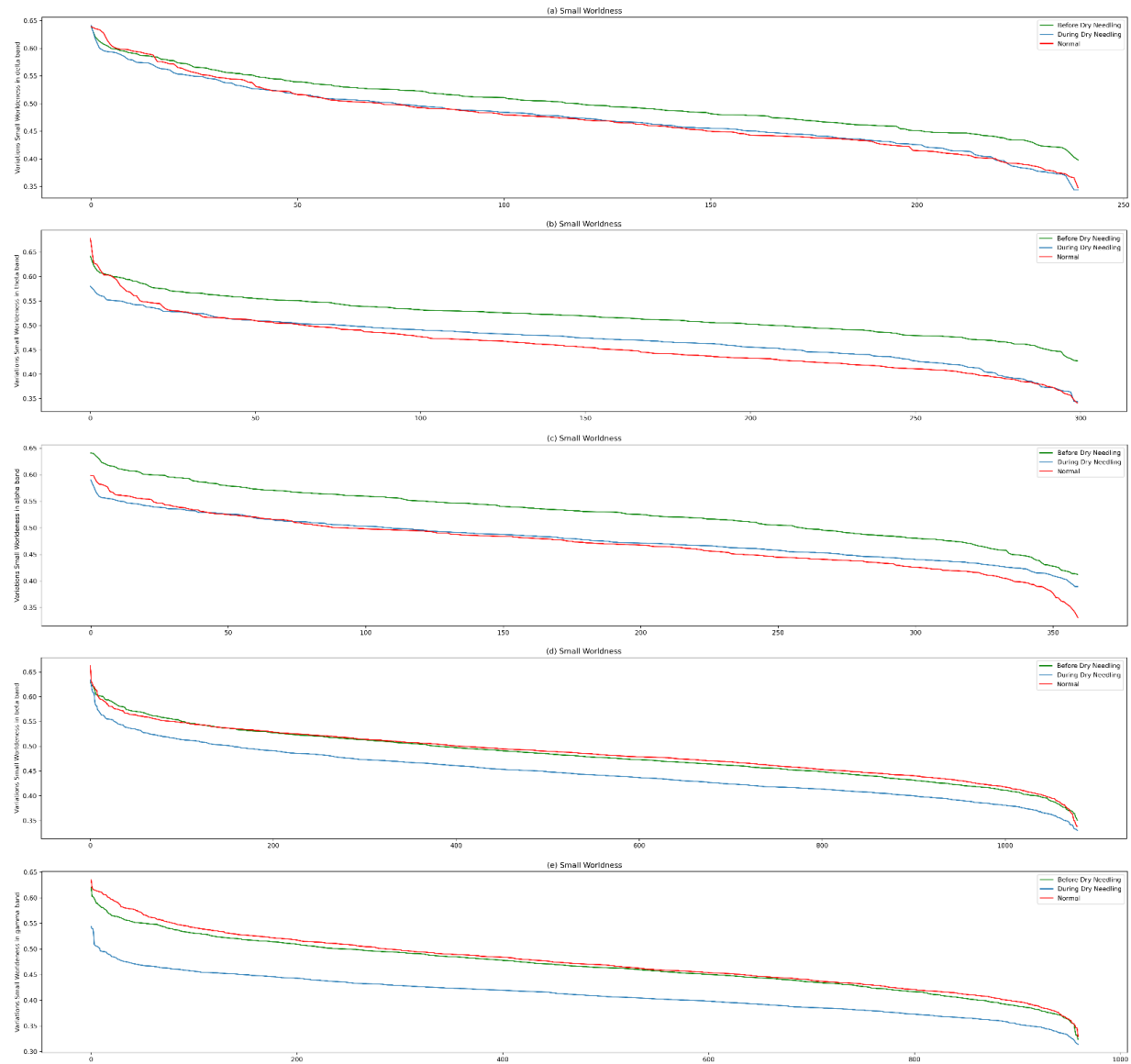
Figure 5. Variations in small-worldness show delta (a), theta (b), and alpha (c) bands becoming more similar to the healthy control during DN application. The beta (d) and gamma (e) bands show no significant differences between the stroke case and the healthy control.

Study 2

The electronic search initially identified 64 articles, with two additional records included from other sources. After removing duplicates and screening, 10 studies were ultimately selected (9 cohort studies and one cross-sectional study). All studies investigated changes in brain networks in stroke patients, consistently observing brain lesions that led to network alterations.

In network analysis, various parameters such as PL, CC, SW, cohesion, and FC were used, although there was no full consistency across studies. The risk of bias assessment showed that six studies had a low risk of bias, while three presented a moderate risk. There was considerable heterogeneity ($I^2 = 60\%$), and the overall effect size (Hedges' g = 0.189) was small and not statistically significant in favor of healthy controls (p = 0.592). Sensitivity analyses revealed that the study by Fanciullacci had the greatest influence on the meta-analysis results. Heterogeneity varied depending on the method used to calculate the small-worldness index. However, none of the subgroup analyses revealed a significant effect size. Tests for publication bias (Begg's and Egger's tests) indicated no evidence of publication bias.

Study 3

A total of 130 ROIs were extracted from ultrasound images of the gastrocnemius medialis muscles of 22 stroke patients (16 men and 6 women, mean age 64.32 ± 13.25 years). Most participants had ischemic strokes, and only one was on spasticity medication during the study. ROIs were analyzed to identify features most relevant to muscle impairment, with three features (Echovariation (EV), Echointensity (EI), and kurtosis) selected as the most informative.

Lower values of EV and kurtosis were associated with greater muscle damage, while higher EI values were linked to worse tissue quality. A strong, significant correlation was found between EV and the modified Heckmatt scale (r = −0.81) and between EI and the scale (r = 0.87), but not for kurtosis.

A mathematical model ($y = a * e^{b*x} + c * e^{d*x} + C$) was used to fit the EV distribution, achieving high accuracy ($R^2 = 0.993$). The graph showed that lower EV values corresponded to more severely impaired muscle tissue. Figure 6 illustrates the curve fitting applied to the EV values extracted from ultrasound images of stroke patients.
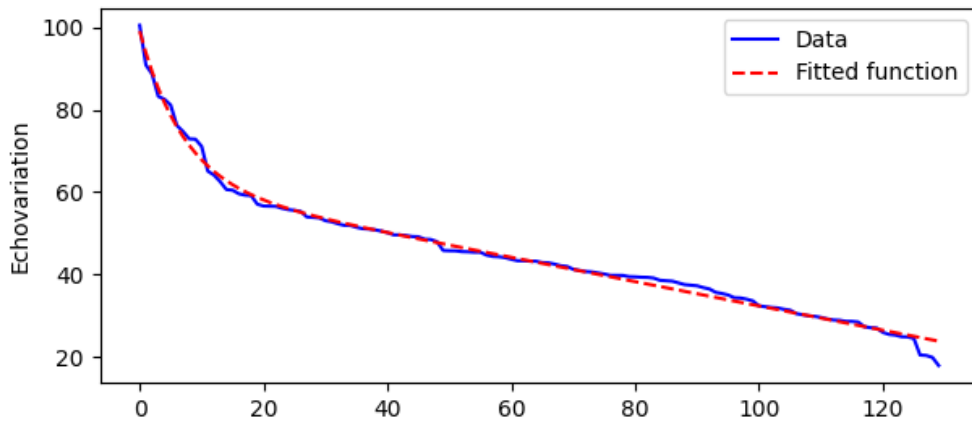
Figure 6. Fitted function on the distribution of the echovariation (EV) in the 130 ROIs extracted from the US images. The scale on the X-axis shows the number of the US image, while the Y-axis shows the echovariation (EV) values.

The EV and EI also showed a very strong inverse correlation (r = −0.90), indicating that as EI increased, EV decreased (Figure 7). Analysis of EV values across the four Heckmatt scale grades revealed significant differences (p < 0.001) between all groups, confirmed through post hoc Bonferroni-corrected comparisons (Figure 8). Mean and standard deviation values for each Heckmatt grade were visually presented, showing a clear trend of decreasing EV with worsening muscle quality.
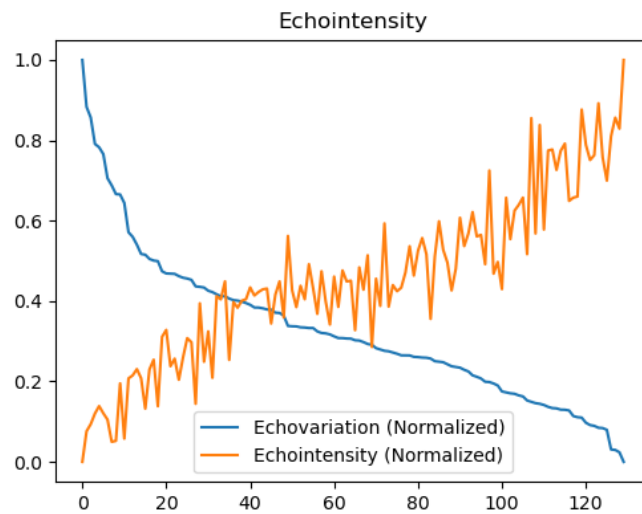
Figure 7. Graphical representation of the correlation between echovariation (EV) and echointensity (EI), the only one that has shown a Pearson's correlation coefficient >0.80. The scale on the X-axis shows the number of the US image, while the Y-axis shows the echovariation (EV) and echointensity (EI) values normalized on a scale from 0 to 1.
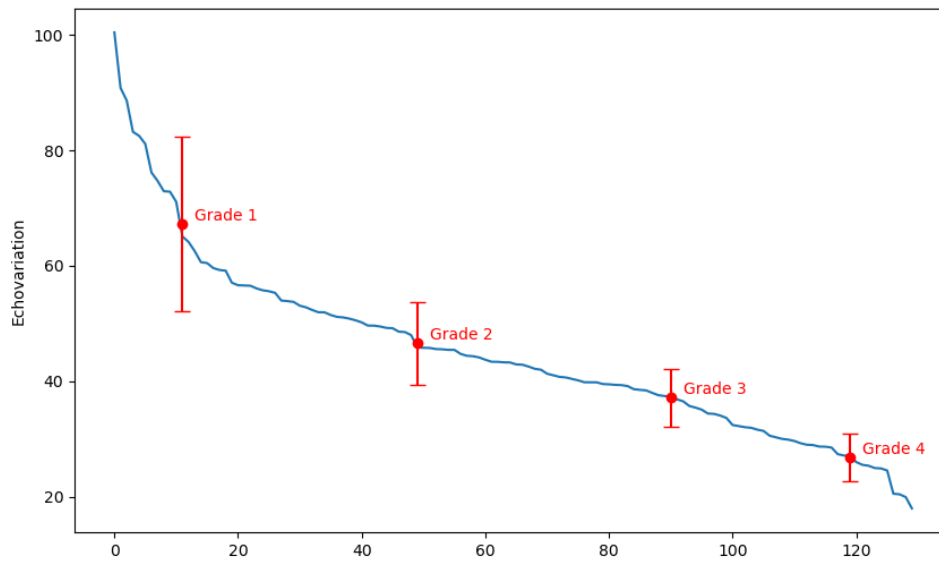
Figure 8. Distribution of the four grades of the modified Heckmatt scale along echovariation (EV) values, with mean and standard error bars for each grade. The scale on the X-axis shows the number of the US image, while the Y-axis shows the echovariation (EV) values.

Study 4

The study included 22 participants (16 males, 6 females) with a mean age of 64.32 ± 13.25 years. Inter-examiner reliability was excellent and significant for EI, EV, dissimilarity, entropy, GLU, homogeneity, kurtosis, RLU, and RPC. Agreement among examiners regarding the level of muscle impairment was very strong (Kappa = 0.85, $p < 0.001$), and their classification correlated highly with the modified Heckmatt scale ($r \approx 0.98–1.00$).

Among the 44 selected ROIs, 21 were classified as low impairment and 23 as high impairment. Significant differences were observed between groups for EV, EI, dissimilarity, energy, contrast, maximum probability, skewness, and the Heckmatt scale ($p < 0.05$) (Table 4).

Table 4. Descriptive statistics and comparison of echotexture features between ROIs classified as low and high impairment after the secondary analysis.

		Overall	Low impairment	High impairment	[a]p value
N		44	21	23	NA
Main outcomes					
Echovariation		46.26±16.69	56.84±16.52	36.60±9.58	<0.001*
Echointensity		82.89±23.60	66.56±17.92	97.80±17.58	<0.001*
Secondary outcomes					
Heckmatt scale, n (%)	Grade 1	3 (6.8)	3 (14.3)	0 (0.0)	<0.001*
	Grade 2	21 (47.7)	18 (85.7)	3 (13.0)	NA
	Grade 3	12 (27.3)	0 (0.0)	12 (52.2)	NA
	Grade 4	8 (18.2)	0 (0.0)	8 (34.8)	NA
Variance		1237.73±324.37	1267.46±301.08	1210.59±348.76	0.568
Standard Deviation		34.87±4.71	35.34±4.42	34.45±5.02	0.536
Skewness		0.50±0.34	0.65±0.32	0.37±0.31	0.005*
Kurtosis		0.03±0.65	0.22±0.81	-0.15±0.40	0.056
Correlation		0.97±0.01	0.97±0.01	0.98±0.01	0.103
Dissimilarity		5.97±0.74	6.21±0.81	5.75±0.60	0.037*
Energy		0.02±0.01	0.03±0.02	0.02±0.00	0.042*
Contrast		62.00±14.82	68.20±15.69	56.35±11.65	0.007*
Homogeneity		0.17±0.03	0.18±0.04	0.17±0.02	0.444
Angular Second Moment		0.00±0.00	0.00±0.00	0.00±0.00	0.058
Maximum Probability		0.01±0.02	0.01±0.02	0.00±0.00	0.013*
Entropy		7.04±0.22	7.00±0.24	7.07±0.20	0.275
Cluster Shade		8.03±0.23	7.99±0.25	8.07±0.20	0.234

Cluster Prominence	10.87±0.36	10.81±0.42	10.92±0.28	0.294
Short Run Emphasis	0.73±0.08	0.73±0.07	0.72±0.08	0.49
Long Run Emphasis	440.64±134.70	447.98±173.53	433.94±89.38	0.734
Gray Level Uniformity	10957.52±2970.64	10237.13±2319.04	11615.27±3378.09	0.126
Run Length Uniformity	17268.72±4566.54	17109.75±2938.33	17413.87±5732.68	0.828
Run Percentage	15.27±3.28	15.37±2.45	15.17±3.95	0.837

Data expressed with mean±standard deviation or with absolute and relative values (%). a significant if p<0.05 (marked with an asterisk).

All features (except EI) were higher in the low-impairment group, while EI was significantly higher in the high-impairment group. Following logistic regression analysis, after eliminating variables with a high VIF, dissimilarity, entropy, EV, GLU, and EI emerged as the main predictors of muscle impairment. Both models (based on EV or EI) demonstrated good model fit (lower AIC, non-significant Hosmer–Lemeshow test) and high explanatory power (Nagelkerke's R^2 around 0.74–0.76) (Table 5).

In the EV model:

- Each unit increase in EV and dissimilarity increased the odds of low impairment by 1.28 and 17.86 times, respectively.
- Entropy was negatively associated with low impairment (<0.001 times).

In the EI model:

- Each unit increase in EI decreased the probability of low impairment by 0.86 times.
- Dissimilarity increased the probability of low impairment by 15.65 times.

Table 5. Final model summary.

	Odds ratio (95%CI)	Coefficient (SE)	95%CI	Z value (·p value)	Variable importance
Echovariation main outcome model					
(Intercept)	7.77e+31 (111740.12, 1.63e+73)	73.43 (SE=38.61)	11.62, 168.57	0.057	
Echovariation	1.275 (1.1, 1.62)	0.24 (SE=0.09)	0.09, 0.48	0.012*	2.52
Dissimilarity	17.856 (2.61, 360)	2.88 (SE=1.19)	0.96, 5.88	0.016*	2.4
Entropy	<0.001 (0.001, 0.01)	-13.75 (SE=6.31)	-29.66, -3.98	0.029*	2.17
Gray Level Uniformity	1 (0.99, 1)	0 (SE=0)	-0.001, 0	0.154	1.42

Echointensity main outcome model

(Intercept)	3.64e+20 (0, 5.00e+54)	47.34 (SE=32.57)	-8.6, 125.95	0.146	
Echointensity	0.86 (0.74, 0.93)	-0.14 (SE=0.05)	-0.29, -0.06	0.009*	2.62
Dissimilarity	15.65 (2.33, 287.63)	2.75 (SE=1.17)	0.84, 5.66	0.019*	2.33
Entropy	0.001 (0, 5.02)	-6.69 (SE=4.87)	-18.43, 1.61	0.170	1.37
Gray Level Uniformity	1 (0.99, 1)	0 (SE=0)	-0.001, 0	0.142	1.46

95%CI: 95% confidence interval; SE: Standard Error. ᵃsignificant if p<0.05 (marked with an asterisk).

Both models achieved high sensitivity (90.48%). The ROC curve analysis showed an AUC of 94.20% for the EV model and 95.45% for the EI model. Classification accuracy was higher for the EI model (84.09%) compared to the EV model (22.73%) (Figure 9).
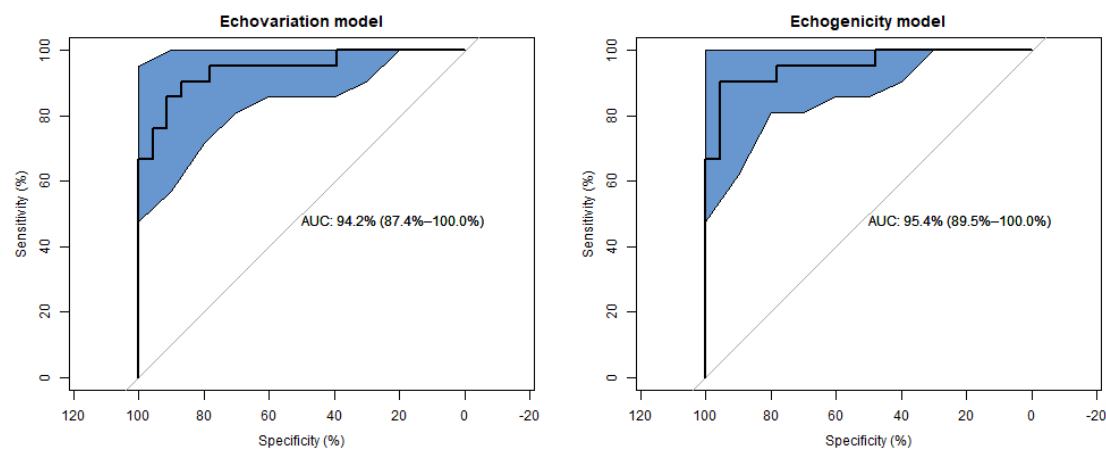
Figure 9. Model receiver operating characteristic (ROC) curves.

Study 5

In this study, the distribution characteristics and descriptive statistics of echointensity (EI) and echovariation (EV) were analyzed across five different patch sizes (10×10 to 50×50 pixels) extracted from the original ROI of the medial gastrocnemius muscle.

The EI feature demonstrated a normal distribution at all patch sizes, which allowed the use of mean and standard deviation for data description. Both parameters remained relatively stable across the different patch sizes, with values consistently approximating the original ROI mean of 81.89. Kendall's correlation coefficient between mean EI and standard deviation was -0.4, suggesting no significant relationship

between these two metrics. These findings indicate that EI measurements were robust and unaffected by patch size variations (Figure 10).
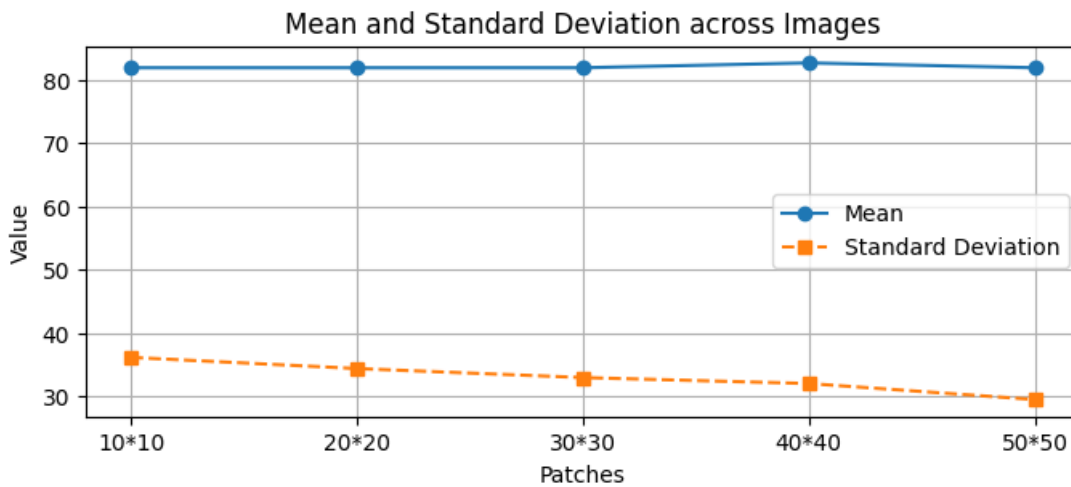

Figure 10. Line graph illustrating the mean and standard deviation values of echointensity for each patch size. The X-axis represents the patch sizes, while the Y-axis indicates the corresponding values of the mean and standard deviation of echointensity. The blue line represents the mean and the orange line the standard deviation.

In contrast, the EV feature exhibited a right-skewed, non-normal distribution. Consequently, the median and interquartile range (IQR) were used for its description. A perfect positive correlation (Kendall's tau = 1) was observed between median EV and IQR, highlighting a strong dependency between central tendency and dispersion. As the patch size increased, the median EV and IQR values rose steadily, approaching but remaining below the original ROI EV value of 45.54. The largest patch size (50×50 pixels) produced the highest median EV (26.48). Notably, smaller patch sizes were associated with lower variability, while larger patches reflected greater dispersion (Figure 11).
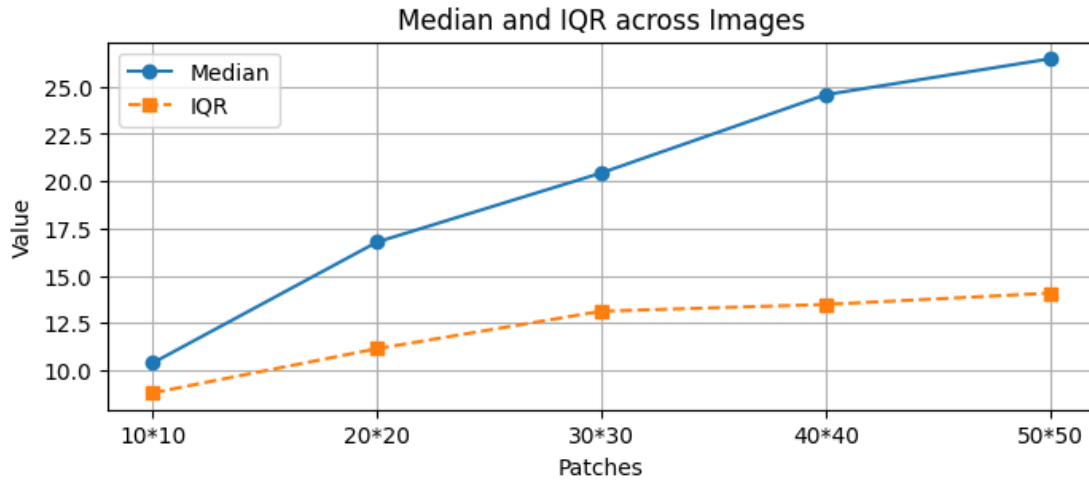
Figure 11. Line graph illustrating the median and interquartile range (IQR) values of echovariation for each patch size. The X-axis represents the patch sizes, while the Y-axis indicates the corresponding values of the median and IQR of echovariation. The blue line represents the median and the orange line the IQR.

When median EV values were plotted against the function derived from Study 3, a clear trend emerged: smaller patch sizes shifted the median EV toward values indicative of more affected tissue regions, whereas larger patch sizes led the median EV to converge towards the original ROI's value. This relationship suggests that patch size is critical in characterizing muscle tissue status in ultrasound images.

Discussion

This doctoral thesis presents a comprehensive investigation into neuro-muscular alterations following stroke, utilizing EEG and ultrasound imaging modalities for biomarker identification and functional pattern recognition. The research was structured around five studies; initially, a clinical case study showed that dry needling intervention can induce measurable changes in EEG network structures in a post-stroke patient. However, a cause-and-effect relationship cannot be established due to the study design. Building upon this, a systematic review and meta-analysis provided robust evidence that stroke significantly disrupts brain network architecture, analyzed through a complex network approach applied to EEG data. Extending the scope to the muscular system, three subsequent studies focused on characterizing muscle tissue quality post-stroke. These studies systematically explored echovariation and echotexture features as potential clinical indicators, emphasizing the need for improved reliability and proposing novel methodological advancements such as a complementary patch-based histogram analysis. Together, these investigations offer a multifaceted perspective on the neuro-muscular sequelae of stroke, laying the foundation for future developments in diagnostic biomarker discovery and functional recovery assessment.

Study 1 provides valuable evidence reinforcing the conceptualization of stroke not merely as a focal neurological event, but as a disorder that disrupts large-scale brain network connectivity, a perspective increasingly supported in contemporary neuroscience literature (83). The findings demonstrate that network-based metrics such as network density, global clustering coefficient, and small-worldness were markedly elevated in the stroke patient relative to a healthy control across multiple EEG frequency bands, specifically delta, theta, and alpha. These alterations suggest a compensatory or maladaptive network reconfiguration, reflecting the brain's attempt to reorganize following injury. Interestingly, following the application of DN, these indices showed a trend toward normalization, indicating that DN may facilitate partial restoration of brain network architecture.

However, specific graph-theoretical parameters, particularly betweenness centrality and average shortest path length, remained consistently impaired in the stroke patient. Betweenness centrality, which reflects the extent to which a given node acts as a critical connector or hub in network communication, was especially disrupted, with abnormalities noted across all frequency bands. This finding suggests that while DN may promote generalized improvements in network topology, certain high-order integrative functions may require more targeted or prolonged interventions to recover.

The neurophysiological impact of DN on brain activity, as captured through EEG, aligns well with previous findings from both EEG studies (84) and functional MRI investigations (9), which collectively indicate that DN can modulate regional brain activation, especially in areas associated with pain modulation and motor control. Nevertheless, the lack of significant reorganization in the beta and gamma bands observed in this study is consistent with the growing body of research indicating that higher frequency oscillations, often implicated in motor execution, attention, and cognitive processing, tend to exhibit significant changes primarily during active task engagement rather than during resting-state EEG recordings (85-88). This suggests that the resting-state paradigm may limit the detectability of DN-induced alterations in high-frequency connectivity, and future studies might benefit from employing task-based or open-eyes EEG protocols to capture a broader spectrum of DN's neurophysiological effects.

Crucially, the observed normalization in low-frequency bands (delta, theta, alpha) holds significant clinical relevance, as these oscillations are commonly associated with fundamental processes of neural plasticity, sensorimotor integration, and inter-regional communication, functions essential for post-stroke recovery. This is in agreement with previous studies that emphasize the role of low-frequency network dynamics in supporting neurorehabilitation (20). Moreover, although beta and gamma bands did not exhibit large-scale network remodeling, subtle but consistent improvements in betweenness centrality, even within these higher frequencies, suggest that DN might influence the efficiency of network communication hubs, laying the groundwork for future plastic changes.

The increase in small-worldness across delta, theta, and alpha bands further supports earlier reports of disrupted network segregation and integration in stroke patients (20, 89, 90). Small-worldness reflects an optimal balance between local specialization and global integration, a property that is typically compromised following stroke. DN appears to support a shift toward more efficient, small-world-like configurations in these critical low-frequency bands, which may underpin improved functional outcomes.

Despite the encouraging findings, one of the principal limitations of this study lies in its single-case design, which restricts the generalizability of the results also hinders the establishment of cause and effect. Additionally, the absence of clinical outcome measures such as spasticity grading, functional motor assessments, or quality-of-life indices limits the ability to establish direct links between EEG-based network changes and patient-centered rehabilitation outcomes. Therefore, future research should incorporate multimodal assessments and larger cohorts in randomized controlled trials to validate and extend these preliminary findings. Moreover, longitudinal follow-up could help determine DN's sustainability and long-term effects on brain network reorganization.

In conclusion, the results from Study 1 suggest that DN exerts beneficial effects on the brain's functional architecture in chronic stroke patients, particularly through enhancing low-frequency network parameters associated with recovery-related neural processes. These findings contribute to a growing body of evidence supporting DN as a neurotherapeutic tool and highlight the importance of advanced EEG-based network analysis for understanding and optimizing post-stroke interventions. Future studies with more robust methodological frameworks are essential to confirm these promising results and to translate them into clinical practice.

The review study (Study 2) underscores the profound impact of stroke on brain connectivity, with consistent evidence indicating that cerebrovascular insults lead to widespread reorganization of functional brain networks. This reorganization primarily affects brain connectivity's internal structure and efficiency, particularly in regions directly impacted by the lesion. Across multiple reviewed studies, stroke patients demonstrated weaker connections, especially within the lesioned hemisphere, reflecting disrupted local and global communication within the brain's functional architecture (20, 84, 90-93).

A central finding is that the alterations in connectivity predominantly manifest in specific EEG frequency bands, especially in the delta (1–4 Hz), theta (4–8 Hz), and alpha (8–13 Hz) ranges. These low-frequency oscillations are crucial for coordinating large-scale neural activity and are often disrupted following stroke, suggesting impaired neural synchronization and reduced integration across brain regions.

However, when examining SW, a key network parameter that captures the balance between local clustering and global integration, findings across studies remain inconsistent and inconclusive. Some investigations have reported increased SW in stroke patients (90, 93), possibly indicating a compensatory reorganization of neural networks. In contrast, others observed a decrease in SW (91, 94), reflecting network efficiency and modular integration loss. Still, some studies found no significant trend (95), highlighting the variability and complexity of brain network responses to stroke. These inconsistencies may stem from methodological differences, sample heterogeneity, and variations in stroke severity, location, and time post-onset.

While functional and topological network changes are evident, particularly in higher-frequency bands after acute stroke, no universally accepted post-stroke brain network reorganization model has emerged. Immediate changes in EEG patterns likely result from acute reductions in cerebral blood flow, leading to metabolic and synaptic dysfunction (96). These initial disturbances are often followed by long-term neuroplastic adaptations, including synaptogenesis, dendritic remodeling, and cortical reorganization,

which may serve to restore lost function (97-99). Nevertheless, the precise relationship between these neuroplastic processes and EEG-derived network metrics remains poorly understood, warranting further investigation.

Some studies also reported changes in gamma-band activity (30–100 Hz), which play a critical role in higher-order cognitive functions such as attention, working memory, and perceptual binding (100-108). These alterations may reflect disrupted cortical-hippocampal communication and impaired information integration (103, 104). However, findings were variable, with some stroke patients exhibiting increased gamma power while others showed reduced activity (91, 92), underscoring the individualized nature of cortical recovery dynamics.

Broadly, stroke is associated with a shift toward increased slow-wave activity (delta and theta) and a reduction in higher-frequency oscillations (alpha, beta, and gamma) (29, 30, 84). This frequency shift likely reflects both the acute pathophysiological effects of stroke and the subsequent compensatory mechanisms engaged during recovery.

One critical source of variability in the literature is the heterogeneity of lesion locations, which presents a major limitation in generalizing results across studies. Additionally, factors such as stroke type (ischemic vs. hemorrhagic), cortical vs. subcortical involvement, recording conditions (resting vs. task-based EEG), and patient demographics such as age and comorbidities may significantly influence EEG connectivity outcomes (109). These confounding variables likely contribute to the inconsistent findings in network parameters like small-worldness and gamma activity.

To address these limitations, future studies should prioritize larger, well-characterized patient cohorts, with careful stratification based on lesion location, size, and type and uniform EEG acquisition protocols. Moreover, incorporating resting-state and task-based paradigms may help disentangle state-dependent network changes and provide a more comprehensive picture of functional brain reorganization after stroke. Such methodological rigor will be essential for advancing our understanding of connectivity-based biomarkers and developing personalized neurorehabilitation strategies.

In addition to analyzing brain activity via EEG in stroke patients, Study 3 focused on assessing muscle tissue quality, emphasizing the limitations of conventional qualitative grading systems such as the Heckmatt scale. While these scales are widely used in clinical practice, they are inherently subjective and may suffer from inter-rater variability. Recognizing this gap, the study advocated for developing and implementing objective, quantitative markers to enhance diagnostic precision and monitoring capabilities (110).

The study identified EV, EI, and kurtosis as the most informative first-order statistical features for differentiating muscle tissue quality through advanced ultrasound image analysis. Among these, EV emerged as the most reliable biomarker, due to several advantages: it demonstrated high robustness, low dependency on ultrasound system settings, and a strong correlation with clinical severity grades, making it suitable for widespread clinical and research applications.

EV was mathematically modeled to strengthen its utility, revealing a consistent relationship between its values and tissue condition: lower EV values were associated with degraded or fibrotic muscle tissue, whereas higher EV values indicated healthier, more homogenous muscle structure. Notably, although the model was initially validated in a stroke population, its theoretical foundation suggests potential generalizability to other neuromuscular and musculoskeletal conditions.

One of the key contributions of this work is that EV provides a continuous, objective scale, enabling finer discrimination of tissue changes over time compared to the categorical nature of traditional scales like Heckmatt. This is particularly valuable for tracking rehabilitation progress, identifying subtle improvements or deteriorations, and stratifying patients by impairment level, potentially guiding therapy planning (111, 112).

Moreover, combining EV with EI may offer complementary insights, as EI captures overall brightness related to fatty infiltration and fibrotic changes. In contrast, EV reflects the heterogeneity and dispersion of pixel intensity. This dual-parameter approach could enrich clinical assessments, especially in complex cases or during longitudinal evaluations.

The findings were also consistent with prior research in other pathologies such as Amyotrophic Lateral Sclerosis (ALS) and various musculoskeletal injuries, where similar patterns in EV and EI were observed (41, 42, 72, 113-115). These parallels suggest a broader relevance of EV and EI across muscle degeneration or remodeling diseases.

Despite these promising outcomes, several technical and methodological challenges were discussed. Managing large imaging datasets, ensuring consistency in image acquisition protocols, and accounting for software variability remain critical hurdles in clinical translation. Nevertheless, first-order features like EV showed high reproducibility across different ultrasound software, reinforcing its viability for routine use (116).

Among the study's strengths were its emphasis on standardized imaging protocols, objective and automated ROI selection, and the use of quantitative, reproducible metrics. These methodological considerations help reduce bias and enhance the reliability of measurements.

However, some limitations were acknowledged, including a small sample size, lack of adjustment for demographic factors (e.g., age, sex, body composition), and the absence of inter- and intra-rater reliability analyses, which are crucial for validating the reproducibility of imaging findings in broader populations (117-121). These factors may limit the generalizability of the results and should be addressed in future investigations.

In conclusion, EV represents a promising and practical biomarker for evaluating muscle tissue integrity in stroke and potentially other neuromuscular disorders. Future research is recommended to assess the longitudinal behavior of EV and EI, evaluate their predictive value for clinical outcomes, and examine their performance across a diverse range of patient populations and pathological conditions (122). Incorporating these biomarkers into clinical workflows could significantly enhance the objectivity and sensitivity of muscle assessment in neurorehabilitation and beyond.

This secondary analysis (Study 4) builds upon the foundation laid by the earlier exploratory investigation (Study 3), with the primary aim of enhancing the clinical applicability and statistical robustness of the original findings. This study contributes critical insights into the quantitative assessment of muscle impairment following stroke by employing more sophisticated statistical techniques and refining the dataset through improved image selection and examiner standardization.

A key advancement in this analysis was the demonstration of high inter-examiner reliability, which strengthens the validity and reproducibility of the previously proposed muscle classification system that categorizes individuals into low and high impairment groups. Notably, including a third independent examiner helped to reduce potential bias further, minimize subjectivity, and enhance the consistency and credibility of the classification outcomes.

Consistent with the original findings, this study reaffirmed the clinical relevance of echotexture features, particularly EI and EV, as reliable indicators of muscle tissue degradation in post-stroke individuals. Using logistic regression models and Receiver Operating Characteristic (ROC) curve analysis, the study showed that these features possess excellent discriminative power, yielding high sensitivity and specificity in detecting clinically relevant muscle changes. These statistical measures support the strong predictive capability of EV and EI as biomarkers of muscle integrity.

In addition to confirming prior results, the study identified the diagnostic potential of additional second-order texture features, such as dissimilarity, entropy, and Gray-Level Uniformity (GLU), extracted through GLCM and GLRLM analyses. While these features received limited attention in the initial study, their significance in the present analysis suggests that higher-order textural properties of muscle images may capture subtle pathophysiological alterations not easily discernible through first-order metrics alone.

This reinforces that while expert visual evaluation remains a cornerstone of ultrasound-based assessments, it may miss nuanced structural changes that are only detectable through quantitative texture analysis. The study therefore advocates for integrating automated image feature extraction with clinician expertise to maximize diagnostic precision.

Crucially, the analysis reconfirmed the inverse relationship between EV and muscle health, with lower EV values indicating greater impairment, and the direct relationship between EI and damage severity, which aligns with earlier findings and broader literature. However, it also highlighted that while first-order features such as EV and EI are foundational, higher-order texture descriptors could further enhance diagnostic granularity, particularly for differentiating between intermediate stages of impairment or predicting recovery trajectories.

One of this study's methodological strengths lies in its correction of a notable limitation from the original investigation: previously, three images per limb were analyzed, potentially introducing redundancy and artificially inflating statistical power. In contrast, this study adhered to a more clinically realistic approach, selecting only one representative image per limb, thereby improving ecological validity and better reflecting the time-constrained realities of clinical practice.

Nonetheless, several limitations remain. Chief among them is the small sample size, which restricts the generalizability of findings and precludes more detailed subgroup analyses, such as comparisons across age, sex, stroke duration, or affected limb dominance. These variables may significantly influence muscle degradation patterns and thus warrant inclusion in future work.

In conclusion, this study strongly supports using echotexture analysis as an objective, quantitative method to evaluate muscle quality in post-stroke individuals. It adds to the growing body of evidence that advanced texture features, particularly those derived from GLCM and GLRLM, can enhance the accuracy of assessments beyond what is possible through visual inspection or simple grayscale metrics alone. Looking ahead, larger-scale studies are needed to validate these findings, assess their predictive value for

functional recovery, and work toward standardizing ultrasound acquisition and analysis protocols to facilitate wider clinical adoption.

In Study 5, we critically examined the reliability of the patch-based method in histogram-based echotexture analysis of ultrasound images. While histogram-derived features have been widely used to quantify tissue characteristics in musculoskeletal and neurological imaging (123, 124), many studies have sought to enhance accuracy by segmenting the ROI before analysis. However, to date, no research has rigorously explored whether subdividing the ROI into smaller patches alters the extracted histogram-based metrics or how the size of these patches may influence the interpretation of echotexture features.

To address this gap, we applied a systematic patch-based strategy to the gastrocnemius medialis muscle, a muscle often affected in post-stroke patients. Specifically, the full ROI was segmented into smaller square patches of various sizes, and the resulting histogram features, particularly EI and EV, were compared against values derived from the original, unsegmented ROI.

The findings revealed that mean EI values calculated from patches closely approximated the values derived from the full ROI. This suggests that EI maintains robustness across spatial subdivisions and may be a reliable parameter for patch-based analysis. In contrast, median EV values obtained from patches deviated significantly from those calculated over the entire ROI. This inconsistency is particularly important given that EV is commonly used to classify muscle quality in individuals with stroke (73), and raises critical concerns about the validity of patch-based EV analysis in clinical and research settings.

Further analysis of variability metrics provided additional insights. The standard deviation of EI remained stable regardless of patching, indicating low sensitivity to ROI partitioning. However, EV's interquartile range (IQR) systematically increased with larger patch sizes, suggesting that patch dimensions introduce artificial variability in EV, which could compromise diagnostic reliability. These findings are especially relevant in light of EV's proposed role as a quantitative and device-independent ultrasonographic biomarker in neurological disorders (41, 73).

Importantly, our results align with concerns raised in other imaging modalities, such as MRI and CT, where segmentation methods have been shown to influence texture-derived outcomes significantly and lead to variable interpretations of tissue characteristics (125, 126). These parallels emphasize the broader relevance of evaluating preprocessing strategies across imaging disciplines.

Despite its novel contributions, this study is not without limitations. The analysis was based on a single ultrasound image and one large ROI, which limits generalizability. Although findings suggest that EI may

be suitable for patch-based evaluation, EV appears more sensitive to patching artifacts and warrants cautious interpretation. Future research should include larger and more diverse datasets, multiple muscle groups, and standardized ROI and patching protocols to validate whether patch-based methods can be reliably applied, particularly for clinically significant features like EV.

Ultimately, this study underscores the need for methodological rigor in quantitative ultrasound analysis, especially when using EV as a surrogate marker for muscle integrity. Future efforts should determine whether patch-based strategies improve the diagnostic precision of ultrasonographic tools compared to conventional clinical grading systems such as the Heckmatt scale, potentially enabling more objective and reproducible assessments in clinical and research environments.

Future Research

The research presented in this dissertation lays the groundwork for a broader exploration of neuromuscular alterations in stroke patients using EEG and ultrasound imaging. Moving forward, several avenues of investigation are anticipated. First, while the initial case study demonstrated that dry needling can modulate brain network architecture in a stroke patient, future research should validate this finding in a larger cohort to enhance generalizability and statistical power. Moreover, a critical question remains unanswered: do structural and functional changes in brain networks correspond with muscle tissue alterations post-stroke? Investigating this potential interplay between neuroplasticity and echotexture will be central to our upcoming studies.

Building upon our findings that Echovariation (EV) may be a reliable biomarker of muscle involvement, future work should assess its responsiveness to physiotherapeutic interventions. Specifically, longitudinal studies could evaluate whether changes in EV can reflect treatment efficacy, thus establishing it as a dynamic indicator for clinical follow-up.

Another promising line of inquiry involves ROI segmentation in ultrasound imaging. Our results suggest that patch-based ROI analysis yields different EV and EI values compared to whole-ROI measurements, with patch size influencing EV more significantly. However, the diagnostic relevance of these two approaches, particularly concerning clinical grading systems such as the Heckmatt scale, remains unclear. Future research with larger samples is needed to determine which ROI strategy aligns more closely with clinical assessments.

Additional ongoing investigations include evaluating the effect of ROI size on extracted features and further refining our methodological framework. Integrating EEG and ultrasound data presents a unique

opportunity to uncover meaningful associations between central and peripheral systems in stroke pathology. Future studies that examine the effects of physiotherapy on both neural and muscular domains and the interrelationship between them are likely to open new frontiers in personalized rehabilitation strategies for stroke survivors.

Conclusion

1. Study 1 demonstrated the positive impact of dry needling on brain networks in a post-stroke patient, as evidenced by improvements in delta, theta, and alpha band parameters, namely density, average shortest path, global clustering coefficient, and small-worldness, toward more normalized values. These promising findings highlight the need for further investigation through well-designed clinical trials.

2. Study 2 is the first systematic review to examine EEG connectivity alterations for the diagnosis and characterization of stroke. The results revealed structural differences and similarities between the brain networks of post-stroke individuals and healthy controls. However, no distinct distribution pattern has yet been identified for differentiation, underscoring the need for more specialized and integrative research in this field.

3. In study 3, using a combined technical and clinical approach, Echovariance (EV) emerged as the most informative echotexture feature for quantifying muscle tissue impairment in the gastrocnemius medialis of individuals post-stroke. Higher EV values were associated with better muscle quality, suggesting that EV is a cost-effective, non-invasive alternative for evaluating muscle characteristics. Furthermore, EV shows promise as a monitoring tool in stroke rehabilitation and may have potential applications in other neuromuscular conditions.

4. Study 4 strengthens the validity of echotexture analysis for assessing muscle quality in post-stroke individuals by incorporating advanced statistical methods and addressing limitations from a previous exploratory study. The findings affirm EV and EI as the most reliable indicators of muscle impairment while also identifying additional features such as dissimilarity, entropy, and GLU from GLCM and GLRLM matrices. However, further studies are required to standardize imaging protocols, validate these findings in larger populations, and explore the role of echotexture features in guiding rehabilitation strategies and therapeutic decision-making.

5. Study 5 introduced a complementary patch-based histogram analysis for assessing muscle tissue characteristics in ultrasound imaging, focusing on EI and EV features. Results indicated that EI values from divided patches were consistent with the original region of interest (ROI), supporting their reliability for muscle characterization. However, EV values showed significant variation in smaller patches, raising concerns about their clinical applicability. Although the study was limited to a single ultrasound image and ROI size, the findings emphasize the necessity for standardized

analysis methods and further research to refine the diagnostic utility of EV in ultrasound-based evaluations.

Conclusión

- El Estudio 1 demostró el impacto positivo de la punción seca en las redes cerebrales de un paciente en fase post-ictus, evidenciado por mejoras en los parámetros de las bandas delta, theta y alfa, como la densidad, la longitud promedio del camino más corto, el coeficiente global de agrupamiento y la propiedad de small-world, acercándose a valores más normalizados. Estos hallazgos prometedores resaltan la necesidad de continuar la investigación mediante ensayos clínicos bien diseñados.

- El Estudio 2 es la primera revisión sistemática que examina las alteraciones en la conectividad del EEG para el diagnóstico y la caracterización del ictus. Los resultados revelaron diferencias y similitudes estructurales entre las redes cerebrales de personas post-ictus y controles sanos. Sin embargo, aún no se ha identificado un patrón de distribución claro que permita su diferenciación, lo que subraya la necesidad de investigaciones más especializadas e integradoras en este campo.

- En el Estudio 3, mediante un enfoque técnico y clínico combinado, la Ecovariación (EV) surgió como la característica de ecotextura más informativa para cuantificar el daño en el tejido muscular del gastrocnemio medial en personas post-ictus. Los valores más altos de EV se asociaron con mejor calidad muscular, lo que sugiere que EV es una alternativa rentable y no invasiva para evaluar las características del músculo. Además, EV muestra potencial como herramienta de monitoreo en la rehabilitación del ictus y podría tener aplicaciones en otras afecciones neuromusculares.

- El Estudio 4 refuerza la validez del análisis de ecotextura para evaluar la calidad muscular en personas post-ictus, mediante la incorporación de métodos estadísticos avanzados y abordando las limitaciones de un estudio exploratorio previo. Los hallazgos confirman que EV y EI son los indicadores más confiables del deterioro muscular, al tiempo que identifican características adicionales como disimilitud, entropía y GLU, provenientes de las matrices GLCM y GLRLM. Sin embargo, se requieren más estudios para estandarizar los protocolos de imagen, validar estos resultados en poblaciones más amplias y explorar el papel de las características de ecotextura en la orientación de estrategias de rehabilitación y toma de decisiones terapéuticas.

- El Estudio 5 introdujo un análisis complementario del histograma basado en parches para evaluar las características del tejido muscular en imágenes de ultrasonido, centrándose en las características EI y EV. Los resultados indicaron que los valores de EI en los parches divididos fueron consistentes con los de la región de interés (ROI) original, lo que respalda su fiabilidad para

la caracterización muscular. Sin embargo, los valores de EV mostraron una variación significativa en los parches más pequeños, lo que plantea dudas sobre su aplicabilidad clínica. Aunque el estudio se limitó a una única imagen de ultrasonido y un tamaño de ROI, los hallazgos enfatizan la necesidad de métodos de análisis estandarizados y de más investigaciones para perfeccionar la utilidad diagnóstica de EV en evaluaciones basadas en ultrasonido.

References

1.   Duncan PW, Zorowitz R, Bates B, Choi JY, Glasberg JJ, Graham GD, et al. Management of Adult Stroke Rehabilitation Care: a clinical practice guideline. Stroke. 2005;36(9):e100-43.

2.   Ma VY, Chan L, Carruthers KJ. Incidence, prevalence, costs, and impact on disability of common conditions requiring rehabilitation in the United States: stroke, spinal cord injury, traumatic brain injury, multiple sclerosis, osteoarthritis, rheumatoid arthritis, limb loss, and back pain. Arch Phys Med Rehabil. 2014;95(5):986-95 e1.

3.   Collaborators GBDF. Burden of disease scenarios for 204 countries and territories, 2022-2050: a forecasting analysis for the Global Burden of Disease Study 2021. Lancet. 2024;403(10440):2204-56.

4.   Saini V, Guada L, Yavagal DR. Global Epidemiology of Stroke and Access to Acute Ischemic Stroke Interventions. Neurology. 2021;97(20 Suppl 2):S6-S16.

5.   Bejot Y, Bailly H, Durier J, Giroud M. Epidemiology of stroke in Europe and trends for the 21st century. Presse Med. 2016;45(12 Pt 2):e391-e8.

6.   Calvo S, Brandín-de la Cruz N, Jiménez-Sánchez C, Bravo-Esteban E, Herrero P. Effects of dry needling on function, hypertonia and quality of life in chronic stroke: a randomized clinical trial. Acupuncture in Medicine. 2022;40(4):312-21.

7.   Ansari NN, Naghdi S, Fakhari Z, Radinmehr H, Hasson S. Dry needling for the treatment of poststroke muscle spasticity: a prospective case report. NeuroRehabilitation. 2015;36(1):61-5.

8.   Fakhari Z, Ansari NN, Naghdi S, Mansouri K, Radinmehr H. A single group, pretest-posttest clinical trial for the effects of dry needling on wrist flexors spasticity after stroke. NeuroRehabilitation. 2017;40(3):325-36.

9.   Mohammadpour F, Ali Oghabian M, Nakhostin Ansari N, Naghdi S, Dommerholt J. Effects of dry needling on post-stroke brain activity and muscle spasticity of the upper limb: a case report. Acupunct Med. 2021;39(1):69-71.

10.   Fernandez-Sanchis D, Brandin-de la Cruz N, Jimenez-Sanchez C, Gil-Calvo M, Herrero P, Calvo S. Cost-Effectiveness of Upper Extremity Dry Needling in Chronic Stroke. Healthcare (Basel). 2022;10(1).

11.   Cohen BA, Bravo-Fernandez EJ, Sances A, Jr. Automated electroencephalographic analysis as a prognostic indicator in stroke. Med Biol Eng Comput. 1977;15(4):431-7.

12.   Cohen BA, Bravo-Fernandez EJ, Sances A, Jr. Quantification of computer analyzed serial EEGs from stroke patients. Electroencephalogr Clin Neurophysiol. 1976;41(4):379-86.

13.   Juhasz C, Kamondi A, Szirmai I. Spectral EEG analysis following hemispheric stroke: evidences of transhemispheric diaschisis. Acta neurologica scandinavica. 1997;96(6):397-400.

14.   Luu P, Tucker DM, Englander R, Lockfeld A, Lutsep H, Oken B. Localizing acute stroke-related EEG changes: assessing the effects of spatial undersampling. J Clin Neurophysiol. 2001;18(4):302-17.

15.   Ajcevic M, Furlanis G, Miladinovic A, Buoite Stella A, Caruso P, Ukmar M, et al. Early EEG Alterations Correlate with CTP Hypoperfused Volumes and Neurological Deficit: A Wireless EEG Study in Hyper-Acute Ischemic Stroke. Ann Biomed Eng. 2021;49(9):2150-8.

16.   Bullmore E, Sporns O. Complex brain networks: graph theoretical analysis of structural and functional systems. Nat Rev Neurosci. 2009;10(3):186-98.

17.   Liao X-Y, Jiang Y-E, Xu R-J, Qian T, Che Y. A bibliometric analysis of electroencephalogram research in stroke: current trends and future directions. Frontiers in Neurology. 2025;16:1539736.

18.   Sporns O. Networks of the Brain: MIT press; 2016.

19.   Watts DJ, Strogatz SH. Collective dynamics of 'small-world' networks. Nature. 1998;393(6684):440-2.

20.   Caliandro P, Vecchio F, Miraglia F, Reale G, Della Marca G, La Torre G, et al. Small-World Characteristics of Cortical Connectivity Changes in Acute Stroke. Neurorehabil Neural Repair. 2017;31(1):81-94.

21.   Carter AR, Astafiev SV, Lang CE, Connor LT, Rengachary J, Strube MJ, et al. Resting interhemispheric functional magnetic resonance imaging connectivity predicts performance after stroke. Ann Neurol. 2010;67(3):365-75.

22.   Yin D, Song F, Xu D, Sun L, Men W, Zang L, et al. Altered topological properties of the cortical motor-related network in patients with subcortical stroke revealed by graph theoretical analysis. Hum Brain Mapp. 2014;35(7):3343-59.

23.   Miraglia F, Vecchio F, Rossini PM. Searching for signs of aging and dementia in EEG through network analysis. Behav Brain Res. 2017;317:292-300.

24.   van Wijk BC, Stam CJ, Daffertshofer A. Comparing brain networks of different size and connectivity density using graph theory. PLoS One. 2010;5(10):e13701.

25.   Siegel JS, Ramsey LE, Snyder AZ, Metcalf NV, Chacko RV, Weinberger K, et al. Disruptions of network connectivity predict impairment in multiple behavioral domains after stroke. Proc Natl Acad Sci U S A. 2016;113(30):E4367-76.

26.   Rubinov M, Sporns O. Complex network measures of brain connectivity: uses and interpretations. Neuroimage. 2010;52(3):1059-69.

27.   Onnela JP, Saramaki J, Kertesz J, Kaski K. Intensity and coherence of motifs in weighted complex networks. Phys Rev E Stat Nonlin Soft Matter Phys. 2005;71(6 Pt 2):065103.

28.   Andrew C, Pfurtscheller G. Event-related coherence as a tool for studying dynamic interaction of brain regions. Electroencephalogr Clin Neurophysiol. 1996;98(2):144-8.

29.   Weiss S, Mueller HM. The contribution of EEG coherence to the investigation of language. Brain Lang. 2003;85(2):325-43.

30.   Hallett M. The Adrian Lecture. Can EEG coherence help solve the binding problem? Suppl Clin Neurophysiol. 2000;53:19-26.

31.   Buzsáki G. Rhythms of the Brain: Oxford university press; 2006.

32.   Dougherty G. Medical image processing: techniques and applications: Springer Science & Business Media; 2011.

33.   Chowdhary CL, Acharjya DP. Segmentation and feature extraction in medical imaging: a systematic review. Procedia Computer Science. 2020;167:26-36.

34.   Chen X, Wang X, Zhang K, Fung KM, Thai TC, Moore K, et al. Recent advances and clinical applications of deep learning in medical image analysis. Med Image Anal. 2022;79:102444.

35.   Hilbert A, Ramos LA, van Os HJA, Olabarriaga SD, Tolhuisen ML, Wermer MJH, et al. Data-efficient deep learning of radiological image data for outcome prediction after endovascular treatment of patients with acute ischemic stroke. Comput Biol Med. 2019;115:103516.

36.   Whittaker JL, Stokes M. Ultrasound imaging and muscle function. J Orthop Sports Phys Ther. 2011;41(8):572-80.

37.   Chang KV, Wu WT, Ozcakar L. Ultrasound Imaging and Rehabilitation of Muscle Disorders: Part 1. Traumatic Injuries. Am J Phys Med Rehabil. 2019;98(12):1133-41.

38.   Hodges PW. Ultrasound imaging in rehabilitation: just a fad? J Orthop Sports Phys Ther. 2005;35(6):333-7.

39.   Molinari F, Caresio C, Acharya UR, Mookiah MR, Minetto MA. Advances in quantitative muscle ultrasonography using texture analysis of ultrasound images. Ultrasound Med Biol. 2015;41(9):2520-32.

40.   Paris MT, Mourtzakis M. Muscle Composition Analysis of Ultrasound Images: A Narrative Review of Texture Analysis. Ultrasound Med Biol. 2021;47(4):880-95.

41.   Martinez-Paya JJ, Rios-Diaz J, Del Bano-Aledo ME, Tembl-Ferrairo JI, Vazquez-Costa JF, Medina-Mirapeix F. Quantitative Muscle Ultrasonography Using Textural Analysis in Amyotrophic Lateral Sclerosis. Ultrason Imaging. 2017;39(6):357-68.

42.   De-la-Cruz-Torres B, Romero-Morales C. Muscular Echovariation as a New Biomarker for the Classification of Soleus Muscle Pathology: A Cross-Sectional Study. Diagnostics (Basel). 2021;11(10).

43.   Sahinis C, Kellis E. Hamstring Muscle Quality Properties Using Texture Analysis of Ultrasound Images. Ultrasound Med Biol. 2023;49(2):431-40.

44.   Zwanenburg A, Vallieres M, Abdalah MA, Aerts H, Andrearczyk V, Apte A, et al. The Image Biomarker Standardization Initiative: Standardized Quantitative Radiomics for High-Throughput Image-based Phenotyping. Radiology. 2020;295(2):328-38.

45.   Scalco E, Rizzo G. Texture analysis of medical images for radiotherapy applications. Br J Radiol. 2017;90(1070):20160642.

46.   Albuquerque A, Almeida E, Queiroz F. A Comparative Study of Texture Analysis Methods on the Classification Problem of DPLDs in HRCT scans. Annu Int Conf IEEE Eng Med Biol Soc. 2024;2024:1-4.

47.   Nailon WH. Texture analysis methods for medical image characterisation. Biomedical imaging. 2010;75:100.

48.   Mailloux GE, Bertrand M, Stampfler R, Ethier S. Local histogram information content of ultrasound B-mode echographic texture. Ultrasound Med Biol. 1985;11(5):743-50.

49.   Pillen S, Van Alfen N. Muscle ultrasound from diagnostic tool to outcome measure--Quantification is the challenge. Muscle Nerve. 2015;52(3):319-20.

50.   Pillen S, Arts IM, Zwarts MJ. Muscle ultrasound in neuromuscular disorders. Muscle & Nerve: Official Journal of the American Association of Electrodiagnostic Medicine. 2008;37(6):679-93.

51.   Sogawa K, Nodera H, Takamatsu N, Mori A, Yamazaki H, Shimatani Y, et al. Neurogenic and Myogenic Diseases: Quantitative Texture Analysis of Muscle US Data for Differentiation. Radiology. 2017;283(2):492-8.

52.   Ismail C, Zabal J, Hernandez HJ, Woletz P, Manning H, Teixeira C, et al. Diagnostic ultrasound estimates of muscle mass and muscle quality discriminate between women with and without sarcopenia. Front Physiol. 2015;6:302.

53.   Pagan-Conesa A, Garcia-Ortiz MT, Salmeron-Martinez EJ, Moya-Martinez A, Lopez-Prats F. Diagnostic Ultrasound Shows Reversal of Supraspinatus Muscle Atrophy Following Arthroscopic Rotator Cuff Repair. Arthroscopy. 2021;37(10):3039-48.

54.   Harris-Love MO, Gonzales TI, Wei Q, Ismail C, Zabal J, Woletz P, et al. Association Between Muscle Strength and Modeling Estimates of Muscle Tissue Heterogeneity in Young and Old Adults. J Ultrasound Med. 2019;38(7):1757-68.

55.   Calvo-Lobo C, Useros-Olmo AI, Almazan-Polo J, Martin-Sevilla M, Romero-Morales C, Sanz-Corbalan I, et al. Quantitative Ultrasound Imaging Pixel Analysis of the Intrinsic Plantar Muscle Tissue between Hemiparesis and Contralateral Feet in Post-Stroke Patients. Int J Environ Res Public Health. 2018;15(11).

56.   Haralick RM, Shanmugam K, Dinstein IH. Textural features for image classification. IEEE Transactions on systems, man, and cybernetics. 1973(6):610-21.

57.   Haralick RM. Statistical and structural approaches to texture. Proceedings of the IEEE. 1979;67(5):786-804.

58.   Galloway MM. Texture analysis using grey level run lengths. Nasa Sti/recon Technical Report N. 1974;75:18555.

59.   Lubner MG, Smith AD, Sandrasegaran K, Sahani DV, Pickhardt PJ. CT Texture Analysis: Definitions, Applications, Biologic Correlates, and Challenges. Radiographics. 2017;37(5):1483-503.

60.   Gillies RJ, Kinahan PE, Hricak H. Radiomics: images are more than pictures, they are data. Radiology. 2016;278(2):563-77.

61.   Berenguer R, Pastor-Juan MDR, Canales-Vazquez J, Castro-Garcia M, Villas MV, Mansilla Legorburo F, et al. Radiomics of CT Features May Be Nonreproducible and Redundant: Influence of CT Acquisition Parameters. Radiology. 2018;288(2):407-15.

62.   Pillen S, van Alfen N. Skeletal muscle ultrasound. Neurological research. 2011;33(10):1016-24.

63.	Michailovich OV, Tannenbaum A. Despeckling of medical ultrasound images. IEEE Trans Ultrason Ferroelectr Freq Control. 2006;53(1):64-78.
64.	Alter KE, Karp BI. Reply to Comment on Ultrasound Guidance for Botulinum Neurotoxin Chemodenervation Procedures. Toxins 2018, 10, 18-Quintessential Use of Ultrasound Guidance for Botulinum Toxin Injections. Toxins (Basel). 2018;10(10).
65.	Pillen S, Arts IM, Zwarts MJ. Muscle ultrasound in neuromuscular disorders. Muscle Nerve. 2008;37(6):679-93.
66.	Heckmatt JZ, Dubowitz V. Ultrasound imaging and directed needle biopsy in the diagnosis of selective involvement in muscle disease. J Child Neurol. 1987;2(3):205-13.
67.	Akazawa N, Harada K, Okawa N, Kishi M, Tamura K, Moriyama H. Changes in Quadriceps Thickness and Echo Intensity in Chronic Stroke Survivors: A 3-Year Longitudinal Study. J Stroke Cerebrovasc Dis. 2021;30(3):105543.
68.	Ryan AS, Dobrovolny CL, Smith GV, Silver KH, Macko RF. Hemiparetic muscle atrophy and increased intramuscular fat in stroke patients. Arch Phys Med Rehabil. 2002;83(12):1703-7.
69.	Heckmatt JZ, Leeman S, Dubowitz V. Ultrasound imaging in the diagnosis of muscle disease. J Pediatr. 1982;101(5):656-60.
70.	Moreta MC, Fleet A, Reebye R, McKernan G, Berger M, Farag J, et al. Reliability and Validity of the Modified Heckmatt Scale in Evaluating Muscle Changes With Ultrasound in Spasticity. Arch Rehabil Res Clin Transl. 2020;2(4):100071.
71.	Martinez-Paya JJ, Rios-Diaz J, Medina-Mirapeix F, Vazquez-Costa JF, Del Bano-Aledo ME. Monitoring Progression of Amyotrophic Lateral Sclerosis Using Ultrasound Morpho-Textural Muscle Biomarkers: A Pilot Study. Ultrasound Med Biol. 2018;44(1):102-9.
72.	Rios-Diaz J, Martinez-Paya JJ, del Bano-Aledo ME, de Groot-Ferrando A, Botia-Castillo P, Fernandez-Rodriguez D. Sonoelastography of Plantar Fascia: Reproducibility and Pattern Description in Healthy Subjects and Symptomatic Subjects. Ultrasound Med Biol. 2015;41(10):2605-13.
73.	Asadi B, Pujol-Fuentes C, Carcasona-Otal A, Calvo S, Herrero P, Lapuente-Hernandez D. Characterizing Muscle Tissue Quality Post-Stroke: Echovariation as a Clinical Indicator. J Clin Med. 2024;13(24).
74.	Serra MC. EFFECTS OF MUSCLE ALTERATIONS AND REHABILITATION ON MOBILITY IN CHRONIC CONDITIONS OF AGING. Innovation in Aging. 2019;3(Supplement_1):S573-S4.
75.	Chow RS, Medri MK, Martin DC, Leekam RN, Agur AM, McKee NH. Sonographic studies of human soleus and gastrocnemius muscle architecture: gender variability. Eur J Appl Physiol. 2000;82(3):236-44.
76.	Reeves ND, Maganaris CN, Narici MV. Ultrasonographic assessment of human skeletal muscle size. Eur J Appl Physiol. 2004;91(1):116-8.
77.	Tok F, Ozcakar L, Safaz I, Alaca R. Effects of botulinum toxin-A on the muscle architecture of stroke patients: the first ultrasonographic study. J Rehabil Med. 2011;43(11):1016-9.
78.	Yang YB, Zhang J, Leng ZP, Chen X, Song WQ. Evaluation of spasticity after stroke by using ultrasound to measure the muscle architecture parameters: a clinical study. Int J Clin Exp Med. 2014;7(9):2712-7.
79.	Hadi S, Khadijeh O, Hadian M, Niloofar AY, Olyaei G, Hossein B, et al. The effect of dry needling on spasticity, gait and muscle architecture in patients with chronic stroke: A case series study. Top Stroke Rehabil. 2018;25(5):326-32.
80.	Picelli A, Tamburin S, Cavazza S, Scampoli C, Manca M, Cosma M, et al. Relationship between ultrasonographic, electromyographic, and clinical parameters in adult stroke patients with spastic equinus: an observational study. Arch Phys Med Rehabil. 2014;95(8):1564-70.

81.   Escriche-Escuder A, Trinidad-Fernandez M, Pajares B, Iglesias-Campos M, Alba E, Garcia-Almeida JM, et al. Responsiveness of the new index muscular echotexture in women with metastatic breast cancer: an exercise intervention study. Sci Rep. 2022;12(1):15148.

82.   Del-Canto-Fernández A, Calleja-Martínez P, Descalzo-Hoyas B, Rodríguez-Posada S, Cuenca-Zaldívar N, Fernández-Carnero S, et al. The Application of Image Texture Analysis Techniques on the Effects of Dry Needling versus Placebo in Low-Back Pain Patients: A Pilot-Study. Applied Sciences. 2022;12(11):5556.

83.   Guggisberg AG, Koch PJ, Hummel FC, Buetefisch CM. Brain networks and their relevance for stroke rehabilitation. Clinical Neurophysiology. 2019;130(7):1098-124.

84.   de Vico Fallani F, Astolfi L, Cincotti F, Mattia D, la Rocca D, Maksuti E, et al. Evaluation of the brain network organization from EEG signals: a preliminary evidence in stroke patient. Anat Rec (Hoboken). 2009;292(12):2023-31.

85.   Jin SH, Lin P, Hallett M. Reorganization of brain functional small-world networks during finger movements. Hum Brain Mapp. 2012;33(4):861-72.

86.   Gerloff C, Bushara K, Sailer A, Wassermann EM, Chen R, Matsuoka T, et al. Multimodal imaging of brain reorganization in motor areas of the contralesional hemisphere of well recovered patients after capsular stroke. Brain. 2006;129(Pt 3):791-808.

87.   Westlake KP, Hinkley LB, Bucci M, Guggisberg AG, Byl N, Findlay AM, et al. Resting state alpha-band functional connectivity and recovery after stroke. Exp Neurol. 2012;237(1):160-9.

88.   Dubovik S, Pignat JM, Ptak R, Aboulafia T, Allet L, Gillabert N, et al. The behavioral significance of coherent resting-state oscillations after stroke. Neuroimage. 2012;61(1):249-57.

89.   Adhikari MH, Hacker CD, Siegel JS, Griffa A, Hagmann P, Deco G, et al. Decreased integration and information capacity in stroke measured by whole brain models of resting state activity. Brain. 2017;140(4):1068-85.

90.   Fanciullacci C, Panarese A, Spina V, Lassi M, Mazzoni A, Artoni F, et al. Connectivity Measures Differentiate Cortical and Subcortical Sub-Acute Ischemic Stroke Patients. Front Hum Neurosci. 2021;15:669915.

91.   Vecchio F, Tomino C, Miraglia F, Iodice F, Erra C, Di Iorio R, et al. Cortical connectivity from EEG data in acute stroke: A study via graph theory as a potential biomarker for functional recovery. Int J Psychophysiol. 2019;146:133-8.

92.   Rutar Gorisek V, Zupanc Isoski V, Belic A, Manouilidou C, Koritnik B, Bon J, et al. Beyond aphasia: Altered EEG connectivity in Broca's patients during working memory task. Brain Lang. 2016;163:10-21.

93.   Vecchio F, Caliandro P, Reale G, Miraglia F, Piludu F, Masi G, et al. Acute cerebellar stroke and middle cerebral artery stroke exert distinctive modifications on functional cortical connectivity: A comparative study via EEG graph theory. Clin Neurophysiol. 2019;130(6):997-1007.

94.   Vecchio F, Miraglia F, Romano A, Bramanti P, Rossini PM. Small world brain network characteristics during EEG Holter recording of a stroke event. Clin Neurophysiol. 2017;128(1):1-3.

95.   Asadi B, Fard KR, Ansari NN, Marco A, Calvo S, Herrero P. The Effect of dry Needling in Chronic Stroke with a complex Network Approach: A Case Study. Clin EEG Neurosci. 2023;54(2):179-88.

96.   Rabiller G, He JW, Nishijima Y, Wong A, Liu J. Perturbation of Brain Oscillations after Ischemic Stroke: A Potential Biomarker for Post-Stroke Function and Therapy. Int J Mol Sci. 2015;16(10):25605-40.

97.   Colcombe SJ, Kramer AF, Erickson KI, Scalf P, McAuley E, Cohen NJ, et al. Cardiovascular fitness, cortical plasticity, and aging. Proc Natl Acad Sci U S A. 2004;101(9):3316-21.

98.   Cramer SC, Sur M, Dobkin BH, O'Brien C, Sanger TD, Trojanowski JQ, et al. Harnessing neuroplasticity for clinical applications. Brain. 2011;134(Pt 6):1591-609.

99.   Felling RJ, Song H. Epigenetic mechanisms of neuroplasticity and the implications for stroke recovery. Exp Neurol. 2015;268:37-45.

100.   Busch NA, Groh-Bordin C, Zimmer HD, Herrmann CS. Modes of memory: early electrophysiological markers of repetition suppression and recognition enhancement predict behavioral performance. Psychophysiology. 2008;45(1):25-35.

101.   Osipova D, Takashima A, Oostenveld R, Fernandez G, Maris E, Jensen O. Theta and gamma oscillations predict encoding and retrieval of declarative memory. J Neurosci. 2006;26(28):7523-31.

102.   Gruber T, Tsivilis D, Montaldi D, Muller MM. Induced gamma band responses: an early marker of memory encoding and retrieval. Neuroreport. 2004;15(11):1837-41.

103.   Herrmann CS, Munk MH, Engel AK. Cognitive functions of gamma-band activity: memory match and utilization. Trends Cogn Sci. 2004;8(8):347-55.

104.   Tallon-Baudry C, Bertrand O, Peronnet F, Pernier J. Induced gamma-band activity during the delay of a visual short-term memory task in humans. J Neurosci. 1998;18(11):4244-54.

105.   Gruber T, Muller MM, Keil A, Elbert T. Selective visual-spatial attention alters induced gamma band responses in the human EEG. Clin Neurophysiol. 1999;110(12):2074-85.

106.   Herrmann CS, Mecklinger A, Pfeifer E. Gamma responses and ERPs in a visual classification task. Clin Neurophysiol. 1999;110(4):636-42.

107.   Gruber T, Muller MM. Oscillatory brain activity dissociates between associative stimulus content in a repetition priming task in the human EEG. Cereb Cortex. 2005;15(1):109-16.

108.   Keil A, Muller MM, Ray WJ, Gruber T, Elbert T. Human gamma band activity and perception of a gestalt. J Neurosci. 1999;19(16):7152-61.

109.   Achard S, Bullmore E. Efficiency and cost of economical brain functional networks. PLoS Comput Biol. 2007;3(2):e17.

110.   Nijholt W, Scafoglieri A, Jager-Wittenaar H, Hobbelen JSM, van der Schans CP. The reliability and validity of ultrasound to quantify muscles in older adults: a systematic review. J Cachexia Sarcopenia Muscle. 2017;8(5):702-12.

111.   Picelli A, Bonetti P, Fontana C, Barausse M, Dambruoso F, Gajofatto F, et al. Is spastic muscle echo intensity related to the response to botulinum toxin type A in patients with stroke? A cohort study. Arch Phys Med Rehabil. 2012;93(7):1253-8.

112.   Wijntjes J, Saris C, Doorduin J, van Alfen N, van Engelen B, Mul K. Improving Heckmatt muscle ultrasound grading scale through Rasch analysis. Neuromuscul Disord. 2024;42:14-21.

113.   Molina-Paya FJ, Rios-Diaz J, Carrasco-Martinez F, Martinez-Paya JJ. Infrared Thermography, Intratendon Vascular Resistance, and Echotexture in Athletes with Patellar Tendinopathy: A Cross-Sectional Study. Ultrason Imaging. 2023;45(2):47-61.

114.   Canosa-Carro L, Lopez-Lopez D, Garcia-Sanz F, Diaz-Meco-Conde R, Garcia-Bermejo P, de-la-Cruz-Torres B, et al. Features of Extrinsic Plantar Muscles in Patients with Plantar Fasciitis by Ultrasound Imaging: A Retrospective Case Control Research. Diagnostics (Basel). 2022;12(4).

115.   Martinez-Paya JJ, Del Bano-Aledo ME, Rios-Diaz J, Tembl-Ferrairo JI, Vazquez-Costa JF, Medina-Mirapeix F. Muscular Echovariation: A New Biomarker in Amyotrophic Lateral Sclerosis. Ultrasound Med Biol. 2017;43(6):1153-62.

116.   Foy JJ, Robinson KR, Li H, Giger ML, Al-Hallaq H, Armato SG, 3rd. Variation in algorithm implementation across radiomics software. J Med Imaging (Bellingham). 2018;5(4):044505.

117.   Pingel J, Bartels EM, Nielsen JB. New perspectives on the development of muscle contractures following central motor lesions. J Physiol. 2017;595(4):1027-38.

118.   Young HJ, Jenkins NT, Zhao Q, McCully KK. Measurement of intramuscular fat by muscle echo intensity. Muscle Nerve. 2015;52(6):963-71.

119.   Pillen S, Tak RO, Zwarts MJ, Lammens MM, Verrijp KN, Arts IM, et al. Skeletal muscle ultrasound: correlation between fibrous tissue and echo intensity. Ultrasound Med Biol. 2009;35(3):443-6.

120.   Strasser EM, Draskovits T, Praschak M, Quittan M, Graf A. Association between ultrasound measurements of muscle thickness, pennation angle, echogenicity and skeletal muscle strength in the elderly. Age (Dordr). 2013;35(6):2377-88.

121.   Watanabe Y, Ikenaga M, Yoshimura E, Yamada Y, Kimura M. Association between echo intensity and attenuation of skeletal muscle in young and older adults: a comparison between ultrasonography and computed tomography. Clin Interv Aging. 2018;13:1871-8.

122.   Lopez-Lopez S, Pareja-Galeano H, Almazan-Polo J, Cotteret C, Tellez-Gonzalez P, Calvo-Lobo C, et al. Quantitative Ultrasound Changes in Echotexture and Functional Parameters after a Multicomponent Training Program in Pre-Frailty Individuals: A Pilot Randomized Clinical Trial. Healthcare (Basel). 2021;9(10).

123.   Zhu Q, editor Ultrasonic Image Analysis of Cardiac Space-occupying Diseases Based on Grey Clustering Algorithm. 2023 International Conference on Telecommunications, Electronics and Informatics (ICTEI); 2023: IEEE.

124.   Kermani A, Ayatollahi A, Talebi M, editors. Segmentation of medical ultrasound image based on local histogram range image. 2010 3rd International Conference on Biomedical Engineering and Informatics; 2010: IEEE.

125.   Dos Santos E, Yoshizawa M, Tanaka A, Saijo Y, Iwamoto T. Detection of luminal contour using fuzzy clustering and mathematical morphology in intravascular ultrasound images. Conf Proc IEEE Eng Med Biol Soc. 2005;2005:3471-4.

126.   Zhang D, Liu Y, Yang Y, Xu M, Yan Y, Qin Q. A region-based segmentation method for ultrasound images in HIFU therapy. Med Phys. 2016;43(6):2975-89.

Acknowledgements

I would like to express my deepest gratitude to my wife, whose unwavering support and presence have been my strength throughout this challenging journey. Her sacrifices, patience, and encouragement during my years of study have meant more to me than words can express. This achievement would not have been possible without her constant love and dedication.

Annexes

Studies 1 to 5 are presented as image files in this document; these files are also provided separately as PDF documents in the supplementary materials.

Study 1

Since Study 1, titled The effect of dry needling in chronic stroke with a complex network approach: a case study, is fully copyrighted by its publisher, we were unable to include the entire article here. Therefore, only the abstract and the DOI link to the article have been provided at: https://journals.sagepub.com/doi/abs/10.1177/15500594221120136.

Abstract

Background: Dry Needling (DN) has been demonstrated to be effective in improving sensorimotor function and spasticity in patients with chronic stroke. Electroencephalogram (EEG) has been used to analyze if DN has effects on the central nervous system of patients with stroke. There are no studies on how DN works in patients with chronic stroke based on EEG analysis using complex networks. Objective: The aim of this study was to assess how DN works when it is applied in a patient with stroke, using the graph theory. Methods: One session of DN was applied to the spastic brachialis muscle of a 62-year-old man with right hemiplegia after stroke. EEG was used to analyze the effects of DN following metrics that measure the topological configuration: 1) network density, 2) clustering coefficient, 3) average shortest path length, 4) betweenness centrality, and 5) small-worldness. Measurements were taken before and during DN. Results: An improvement of the brain activity was observed in this patient with stroke after the application of DN, which led to variations of local parameters of the brain network in the delta, theta and alpha bands, and inclined towards those of the healthy control bands. Conclusions: This case study showed the positive effects of DN on brain network of a patient with chronic stroke.

Study 2

Review

Brain Analysis with a Complex Network Approach in Stroke Patients Based on Electroencephalography: A Systematic Review and Meta-Analysis

Borhan Asadi [1], Juan Nicolás Cuenca-Zaldivar [2,3,4], Noureddin Nakhostin Ansari [5,6], Jaime Ibáñez [7,8], Pablo Herrero [1,*] and Sandra Calvo [1]

1 Department of Physiatry and Nursing, Faculty of Health Sciences, IIS Aragon, University of Zaragoza, C/Domingo Miral s/n, 50009 Zaragoza, Spain
2 Grupo de Investigación en Fisioterapia y Dolor, Departamento de Enfermería y Fisioterapia, Facultad de Medicina y Ciencias de la Salud, Universidad de Alcalá, 28801 Alcalá de Henares, Spain
3 Physical Therapy Unit, Primary Health Care Center "El Abajón", 28231 Las Rozas de Madrid, Spain
4 Research Group in Nursing and Health Care, Puerta de Hierro Health Research Institute—Segovia de Arana (IDIPHISA), 28222 Majadahonda, Spain
5 Research Center for War-Affected People, Tehran University of Medical Sciences, Tehran P.O. Box 14155-6559, Iran
6 Department of Physiotherapy, School of Rehabilitation, Tehran University of Medical Sciences, Tehran P.O. Box 14155-6559, Iran
7 BSICoS Group, IIS Aragón, Universidad de Zaragoza, 50018 Zaragoza, Spain
8 Department of Bioengineering, Imperial College, London SW7 2AZ, UK
* Correspondence: pherrero@unizar.es

Abstract: Background and purpose: Brain function can be networked, and these networks typically present drastic changes after having suffered a stroke. The objective of this systematic review was to compare EEG-related outcomes in adults with stroke and healthy individuals with a complex network approach. Methods: The literature search was performed in the electronic databases PubMed, Cochrane and ScienceDirect from their inception until October 2021. Results: Ten studies were selected, nine of which were cohort studies. Five of them were of good quality, whereas four were of fair quality. Six studies showed a low risk of bias, whereas the other three studies presented a moderate risk of bias. In the network analysis, different parameters such as the path length, cluster coefficient, small-world index, cohesion and functional connection were used. The effect size was small and not significant in favor of the group of healthy subjects (Hedges'g = 0.189 [−0.714, 1.093], Z = 0.582, p = 0.592). Conclusions: The systematic review found that there are structural differences between the brain network of post-stroke patients and healthy individuals as well as similarities. However, there was no specific distribution network to allows us to differentiate them and, therefore, more specialized and integrated studies are needed.

Keywords: brain function network; electroencephalography; stroke

1. Introduction

Stroke represents one of the most common causes of disability with regards to its impact on functional limitations [1]. In addition, because of the aging population, the absolute number of strokes is expected to increase in the coming years [2]. Apart from the positive and negative clinical features that may appear after a stroke, this type of neural lesion is typically associated with alterations in the oscillatory brain activity that can be measured from the lesioned areas in the brain. Typically, lesioned brain regions present a slowing of rhythmic activity as compared to the contralesional side. This can be observed by computing the ratio between the power at low frequency (e.g., delta) and high frequency (alpha/beta/gamma) of spectral components in the EEG [3] Brain connectivity

also undergoes changes, and this has been researched during the last years [4–13]. At present, we mainly rely on structural images of the brain affected areas to take clinical decisions and make predictions about evolution. Brain networks are a relevant feature of brain function, and these networks typically present drastic changes after a certain region gets damaged.

Taking all this into account, network analysis can help to improve the clinical characterization of patients with a stroke, since brain networks determine which areas of the brain are physically or functionally connected to support cognitive and behavioral functions during the brain's rest/default state [14]. A "small-world index" (SW) network reproduces the competence of the brain networks to locally and globally process the flow of information [15]. In this regard, through the analysis of EEG graphs, it has been shown that ischemic stroke leads to a rearrangement of the information flow between the two hemispheres in the brain, which is frequency-dependent [13]. Regarding the interest in this field, the number of articles with the 'Brain Network' keyword has grown very fast since 1985, and this interest has increased exponentially in the last years, from 8387 research manuscripts published in 2016 to 14,256 in 2021 in Pubmed.

Studies on network topology highlight functional reorganization after stroke [16,17], suggesting that changes in the spontaneous functional architecture of the brain connectivity affecting function could be produced by ischemic lesions [18]. The complexity of functional brain connectivity can be studied using graph theory, a mathematical approach used to analyze networks that may be used to analyze the brain's complex networks through simplified schemes of nodes and edges [19]. In this field, a network is a mathematical representation of a complex system in the real world and is defined by a set of nodes (vertices) and links (edges) between pairs of nodes. Different parameters define the properties of a network, each of which defines the network in some way. These parameters are used for network analysis and comparison between networks created from healthy humans and stroke patients. Brain network theory considers brain segregation as the network tendency to be organized in clusters and analyzes them using the local and global clustering coefficient (CC). The local CC calculates the local cohesion of a node with its neighbors [20]. Additionally, it provides an overall measure of the cohesion of the nodes in the whole network.

The average shortest path length (PL) parameter is also used to analyze brain integration. This parameter represents the network ability to exchange information between distant regions [15–19]. The measure of network small-world index (SW) is defined as the ratio between CC and PL [21,22]. The SW coefficient is used to describe the balance between the local connectedness and the global integration of a network. When SW is larger than 1, a network is said to have small-world index properties. SW organization mixes short PL and high CC.

The rapid development of imaging technology, such as computed tomography (CT), positron emission tomography, magnetic resonance imaging (MRI) and EEG, allows researchers to access latent knowledge about brain changes during stroke onset and the recovery process [23]. EEG provides a continuous, real-time and non-invasive measurement of brain function and provides new insights into brain pathophysiology after stroke [24–26]. This technology has the advantage of being widely available, having a low cost and providing a good compromise in terms of spatio-temporal resolution for superficial structures in the brain. EEG-based measures can provide neurophysiological biomarkers in the early pre-treatment phase that may be used to make short- and long-term predictions regarding the evolution of a patient, and that may even provide relevant information to determine optimal treatment strategies [3]. Moreover, EEG technologies have advanced significantly in recent years, making it possible to record signals unobtrusively without needing to move patients from their beds; it is also possible to test neurofeedback interventions based on the EEG signal and to modulate certain brain rhythms to study its potential therapeutic effect [3,27].

In EEG studies, functional connectivity between two signals can be evaluated by using a measure of general synchronization [28], such as EEG coherence [29]. The increase of EEG coherence can be interpreted as a functional coupling between two anatomically separated regions [30]. In addition, EEG coherence can also be used as a measure of binding by synchrony and is a proposed solution to the connecting problem [31], the way that the brain integrates signals separated in space and time [32].

Stroke leads to a large variability in clinical presentation and outcomes [33]. There is substantial heterogeneity in the procedures and tools used for outcome assessment after stroke, most of which are poorly validated [34]. Consequently, the heterogeneity in the use of outcome tools comprises the data quality [33]. No previous works looked into the brain network changes as an outcome post-stroke. To the authors' knowledge, there are not any previous reviews of studies that have carried out brain network analysis of EEG in stroke patients. Because of this, in this systematic review, our objective is to review the research carried out on different stroke areas (Broca, cerebellum, middle cerebral artery, thalamus) and clinical phases (i.e., acute, sub-acute), by networking analysis of EEG and to perform a meta-analysis of the EEG-related outcomes in stroke patients.

2. Materials and Methods

2.1. Study Design

This systematic review was performed following the Preferred Reporting Items for Systematic Reviews and Meta-Analyses (PRISMA) statement [35] and was registered with the International Prospective Register of Systematic Reviews (PROSPERO), registration number (reference number: 285761).

2.2. Data Sources

The electronic databases PubMed, Cochrane and ScienceDirect were searched from their inception until October 2021. Search strategies were performed following the instructions described by Greenhalgh [36] (see Appendix A). The research question followed the PICO format: in adults who suffered a stroke episode (P = population), taking EEG from participants (I = intervention), comparing patients with stroke with healthy individuals (C = comparison) and analyzing outcomes related to brain network (O = outcome). Due to the limited number of cohort studies, cross-sectional studies and case reports were also considered.

2.3. Study Eligibility Criteria

Experimental studies were eligible for inclusion if they met the following criteria: (1) included patients with stroke, (2) used EEG tools for assessment, (3) used network analysis and (4) were published in English language. Rehabilitation studies, effect of physical therapy and/or effect of any other procedure on stroke were excluded. Two independent reviewers (BA and NC) performed the systematic search and screened the title and abstract of the articles, with duplicates being removed. The full text of eligible papers was carefully read to decide whether the eligibility criteria were met. The two reviewers compared their findings, and a third reviewer (SC) helped to solve any possible discrepancies if needed. After the selected articles were considered suitable for inclusion, one reviewer (BA) extracted the following information: (1) study author(s), (2) year of publication, (3) characteristics of participants (e.g., sample size, study groups, mean age, sex distribution, and types of strokes), (4) type of study, (5) type of method used to measure connectivity between nodes, (6) outcome measures, (7) assessment and intervention protocol and (8) main results. Then, a second reviewer (NC) verified the findings, and possible disagreements were discussed.

The Newcastle–Ottawa Scale was used to assess the risk of bias and the quality of nonrandomized studies in meta-analyses [37]. Three factors were considered to score the quality of included studies: (1) selection, including representativeness of the exposed cohort, selection of the non-exposed cohort, ascertainment of exposure and demonstration that at the start of the study the outcome of interest was not present; (2) comparability,

assessed on the basis of study design and analysis, and whether any confounding variables were adjusted for; and (3) outcome, based on the follow-up period and cohort retention and ascertained by independent blind assessment, record linkage or self-report. The quality of the studies (good, fair and poor) was rated by awarding stars in each domain following the guidelines of the Newcastle–Ottawa Scale. A "good" quality score required 3 or 4 stars in selection, 1 or 2 stars in comparability and 2 or 3 stars in outcomes. A "fair" quality score required 2 stars in selection, 1 or 2 stars in comparability and 2 or 3 stars in outcomes. A "poor" quality score reflected 0 or 1 star(s) in selection, 0 stars in comparability or 0 or 1 star(s) in outcomes.

2.4. Data Analysis

For the statistical analysis, the program R Ver. 4.1.2 was used (R Foundation for Statistical Computing, Institute for Statistics and Mathematics, Welthandelsplatz 1, 1020 Vienna, Austria). In the articles showing the results with median and interquartile range, these were transformed into mean and standard deviation using the appropriate formulas [38,39]. The combination of groups and the average of the means and standard deviations were performed using the appropriate formulas [40]. Data were obtained by request from the authors and, when it was not possible, by extracting data from the graphs available in the articles (since these did not present them in table format) using the webplotdigitizer software [41].

A meta-analysis was carried out taking the small-world index (SW) as measure of brain networks. A random effects model was applied given the heterogeneity between the studies and analyzing the level of significance between the groups of patients and healthy participants through the standardized difference of means (SMD), based on the mean, standard deviation and sample size in each group. Heterogeneity was analyzed by estimating the between-studies variance τ^2 (calculated with the DerSimonian–Laird estimator with Hartung–Knapp correction), with the Cochran Q test as well as with the I^2 estimator being defined with the latter as: 0–30%, unimportant heterogeneity; 30–50%, moderate heterogeneity; 50–75%, large heterogeneity; and 75–100%, significant heterogeneity. The effect size was calculated with Hedges'g, defined as small effect below 0.2, moderate effect between 0.2 and 0.8 and big effect above 0.8.

Heterogeneity was assessed by detecting the following: (1) outlier studies, defined as studies with extreme effect sizes whose confidence interval does not overlap with the confidence interval of the pooled effect and differs significantly from the overall effect [42]; and (2) influencing studies, defined as those which have a large impact on the pooled effect or heterogeneity, regardless how high or low the effect is [42]. To analyze heterogeneity, the following were used: (1) influence graphs, which indicate the fit of the studies to the model; (2) Baujat plots, which detect studies that overly contribute to the heterogeneity in a meta-analysis ([43]); and (3) leave-one-out meta-analysis, which are forest plots with recalculated pooled effects, with one study omitted each time. In addition, a Graphic Display of Heterogeneity (GOSH) was used, which plots the pooled effect size on the *x*-axis and the between-study heterogeneity on the *y*-axis, which allows for looking for specific patterns or clusters with different effect sizes and amounts of heterogeneity [44].

Subgroup meta-analysis were performed to explore the detected heterogeneity depending on the mode to calculate SW brain networks: direct SW (SW calculated directly), ratio of the raw weighted clustering coefficient (Cw), weighted characteristic path length (Lw) or the ratio of raw global efficiency (Eg) to local efficiency (El). Publication bias was analyzed using the Begg and Eggers tests and standard and trim and fill funnel plots [45]. Finally, the overall and subgroup meta-analysis powers were calculated.

3. Results

The PRISMA flow diagram (Figure 1) illustrates the screening process. The electronic search identified 64 records, and 2 other results were added through alternative sources. After removing 2 duplicated articles, 47 manuscripts were excluded for not meeting the

inclusion criteria. From the 17 results selected, 7 of them were removed for not meeting the eligibility criteria. Finally, a total of 10 studies were kept, 9 of which were cohort studies.
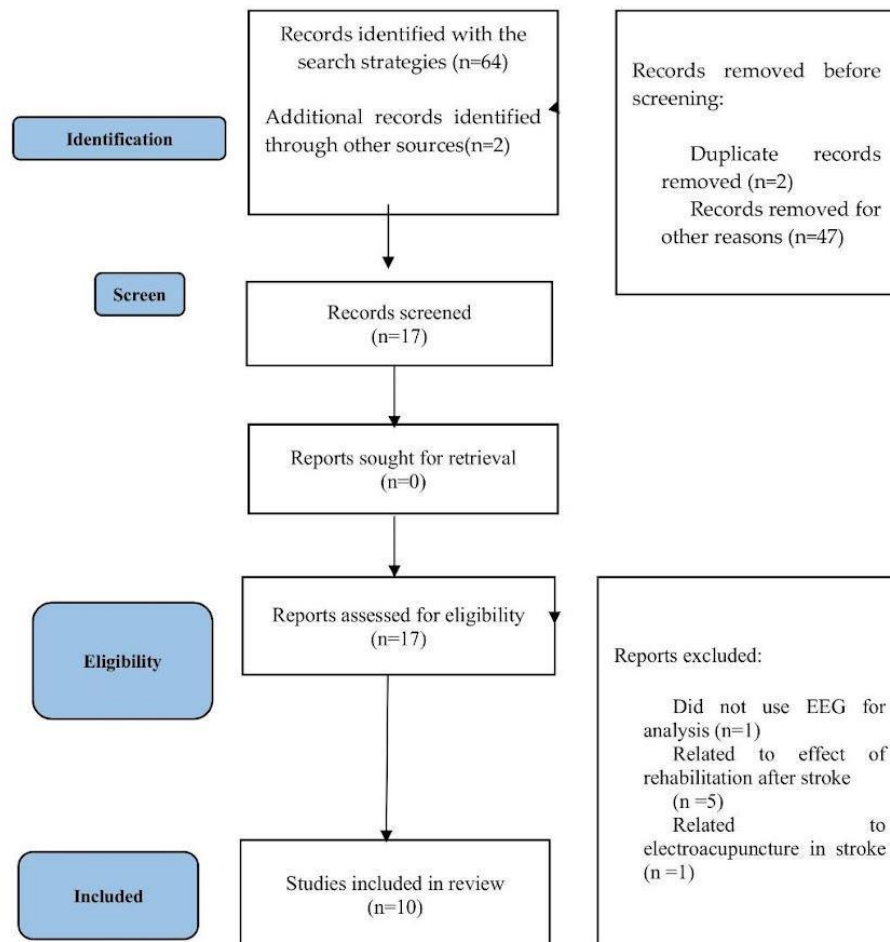
Figure 1. Preferred Reporting Items for Systematic reviews and Meta-Analyses (PRISMA) flowchart.

Table 1 summarizes the studies included in this systematic review investigating the analysis of brain networks in stroke patients [4–13]. These studies include research on stroke that has had effects such as hemianopsia [8] and Broca [5] in patients. In all the included studies, the presence of a lesion in the brain was observed, and in fact, the lesion caused a change in the network, which is discussed below. All included studies are case–cohort studies [4–10,12,13] except one, which was a cross-sectional study [11] that helps to understand the network change at the time of stroke and after. The networking methods in the studies were different, as well as the analysis performed, although they all had some similarities. In the network analysis, different parameters were used, which include the PL, CC, SW, cohesion and functional connection (FC). Each of the articles examined some parameters and were not consistent in this regard.

Table 1. Data of the studies investigating the analysis of brain networks in stroke patients.

Study	Population	Control	Intervention	Outcome	Results
Liu, Shuang et al., 2016 [6]	30 acute thalamic ischemic stroke patients	30 healthy subjects	EEG in resting condition with eyes closed was recorded.	The functional connectivity was estimated with partial directed coherence (PDC) [46].	Compared to the control group, the stroke group showed a trend of weaker cortical connectivity and a symmetrical pattern of functional connectivity; that is, there was less information transfer between electrodes on the brain.
Vecchio, Fabrizio et al., 2019 [4]	30 patients with middle cerebral artery stroke and 11 with cerebellar stroke.	30 healthy subjects	EEG was measured in resting state (at least 5 min) with eyes closed with 19 electrodes in the International 10–20 system position and sampling rate fixed at 256 Hz.	Functional connectivity of EEG data was carried out with eLORETA. The eLORETA algorithm is a linear inverse solution for detection of the EEG signals' source [47].	Beta2 and gamma small-world index were increased in the right hemisphere of patients with cerebellar stroke, respectively, compared to healthy subjects, while the alpha 2 small-world index was increased only in patients with middle cerebral stroke. Cerebellar stroke differed from MCA in that it did not cause reorganization of the alpha 2 network, whereas it caused reorganization of the high-frequency network in the beta 2 and gamma bands with small-world index enhancement.
Rutar Gorišek, Veronika et al., 2016 [5]	10 Broca's patients	10 healthy subjects	The testing and EEG recordings were performed from 10 to 90 days (mean 54.4 ± SD 30.7) after the ischemic stroke.	Coherences were calculated by using the mscohere function in Matlab.	It was shown that the precise balance between task-related theta synchronization and desynchronization found in healthy subjects was severely disrupted in Broca's patients, and functional networks in the theta frequency band were significantly altered in the patient group. Gamma desynchronization was widespread in healthy controls, but in Broca patients, task-related desynchronization was less in the right hemisphere, and functional networks in the gamma frequency band were significantly altered in the patient group.
Vecchio, Fabrizio et al., 2019 [7]	139 consecutive patients were enrolled in the acute phase of stroke	110 healthy subjects	The EEG recording was performed at rest, with closed eyes.	EEG functional connectivity analysis has been performed using the eLORETA.	When comparing the patients with the control group, there were significant differences, with higher levels of SW in the healthy subjects. A strong negative correlation was found between the NIHSS at follow-up and the small-world index gamma index in the acute phase, giving the SW gamma index a predictive weight for recovery.
Wang, Lei et al., 2012 [8]	7 stroke patients with hemianopia	7 healthy control subjects	EEG data were recorded with 30 scalp electrodes with the patient kept awake with eyes closed throughout the EEG recording for 2 min.	Phase synchronization index (PSI) [48] has been used.	For each case of the brain network with a different number of edges, the weighted clustering coefficient of the network of hemianopia stroke patients seems to be generally higher than that of the normal control group. Hemianopia stroke patients generally had a lower weighted characteristic path length than the control group.

Table 1. *Cont.*

Study	Population	Control	Intervention	Outcome	Results
Dubovik, Sviatlana et al., 2013 [9]	20 stroke patients	19 healthy participants	EEG was recorded with a 128-channel EEG system in an awake, resting condition with eyes closed.	The electromagnetic neural activity at each gray matter voxel was reconstructed with an adaptive spatial filter (beamformer)	Increased functional connectivity (FC) was observed in non-lesioned areas. These changes were mostly related to the alpha frequency band, and FC in the dysfunctional brain regions was consistently reduced in the alpha frequency band.
De Vico Fallani, Fabrizio et al., 2009 [10]	1 stroke patient	8 healthy subjects	EEG signals were recorded with a sampling frequency of 2048 Hz from 128 scalp electrodes.	Brain functional connectivity is achieved through the computation of task-related coherence.	The differences mainly involved the highest spectral contents (beta and gamma bands). In these bands, the global and local performances of the patient were statistically lower than the control subjects in the PRE (during the planning period) and EXE (movement execution) intervals.Network topology changes were particularly prominent in the beta band, which is already involved in motor tasks [45], as well as in the gamma band.
Vecchio, Fabrizio et al., 2017 [11]	A 72-year-old patient with stroke	Before and during a stroke attack	EEG Holter was recorded for evaluating signs of stroke-related epilepsy.	Magnitude squared coherence used (mscohere)	SW decreases in stroke and increases after stroke.SW decrease in the delta band and SW increase in the alpha bands.Coherence decreases during stroke and increases after stroke.
Fanciullacci, Chiara et al., 2021 [12]	33 unilateral post stroke patients in the sub-acute phase: cortico-subcortical ($n = 18$) and subcortical ($n = 15$)	10 healthy subjects	EEG was recorded for 10 min with a 10/20 EEG system in an awake, resting condition with eyes closed.	to explore interconnectivity between the ROIs, and intracortical lagged linear coherence was computed	In both groups of patients, compared to healthy subjects, there was an increase in the small-world index of the resting-state network in the θ band.β-band network measures differed significantly between stroke patients, with greater resolution and small-world index in patients with cortical involvement.
Caliandro, Pietro et al., 2017 [13]	30 patients with ischemic lesion	30 healthy subjects	The EEG recording was performed at rest, with eyes closed and no task condition for at least 5 min from 19 electrodes.	Connectivity analysis using eLORETA in both hemispheres.	Resting-state network changes were mainly detected in low- and medium-frequency EEG bands, i.e., delta, theta and alpha 2 rhythms, while no network reorganization was found in alpha 1, beta and gamma bands.

The evaluation of the quality and risk of bias of cohort studies is shown in Table 2; five studies were of good quality [4,5,7,8,13] and four were of fair quality [6,9–11].

The risk of bias analysis is shown in Figure 2. Six studies showed a low overall risk of bias [5–7,9,12,13]. However, three studies presented an overall moderate risk of bias due to some concerns about outcome measures and reported outcomes [4,8,10]. The overall risk of bias is low to moderate due to missing data and the selection of reported studies.

Only one of the studies [11] assessed was a cross-sectional study (see Table 3). The study [11] included in this review does not have a sufficiently defined protocol, and the analysis was not repeated by more than one researcher to ensure reliability. However, it has many positive strengths that are indicated in Table 3 with the answer "yes".

Table 2. Risk of bias assessment (Newcastle–Ottawa Quality Assessment Scale criteria).

	Selection				Comparability	Outcome			
Study	Representativeness of Exposed Cohort	Selection of the Non-Exposed Cohort from Same Source as Exposed Cohort	Ascertainment of Exposure	Outcome of Interest Was Not Present at Start of Study	Comparability of Cohorts	Assessment of Outcome	Follow-up Long Enough for Outcome to Occur	Adequacy of Follow-Up	Quality Score
Liu, Shuang et al., 2016 [6]	Participants were in two groups: ischemic thalamic stroke (*n* = 30) and the healthy group (*n* = 30). ★	Yes ★	Inclusion criteria of the patients consisted of focal ischemic lesion of the thalamus and hand numbness as symptoms.	Yes ★	Nothing matched	Comparison of parameters of brain network between ischemic thalamic stroke patients and healthy group.	Yes ★	All stroke patients from whom EEG was taken participated in the study. ★	Fair
Vecchio, Fabrizio et al., 2019 [4]	Patients were in two groups: cerebellar and middle cerebral artery strokes (*n* = 30) and healthy group (*n* = 30). ★	Yes ★	The patients were clinically assessed by the National Institutes of Health Stroke Scale (NIHSS) during the acute phase.	Yes ★	Age and gender matched ★	Comparison of parameters of brain network between stroke patients and healthy group.	Yes ★	All stroke patients from whom EEG was taken participated in the study. ★	Good
Rutar Gorišek, Veronika et al., 2016 [5]	Participants were in two groups: Broca's patients (*n* = 10) and healthy group (*n* = 10). ★	Yes ★	Boston Diagnostic Aphasia Evaluation (BDAE)	Yes ★	Sex and education matched ★	Comparison of parameters of brain network between stroke patients and healthy group.	Yes ★	All patients from whom EEG was taken participated in the study. ★	Good
Vecchio, Fabrizio et al., 2019 [7]	Participants were in two groups: patients with stroke in the acute phase (*n* = 139) and healthy group (*n* = 110). ★	Yes ★	All patients were clinically evaluated with three scales for stroke: NIHSS, Barthel and ARAT.	Yes ★	Sex and age matched ★	Comparison of parameters of brain network between stroke patients and healthy group.	Yes ★	All patients from whom EEG was taken participated in the study. ★	Good
Wang, Lei et al., 2012 [8]	Participants were in two groups: stroke patients (*n* = 7) and healthy controls (*n* = 7). ★	Yes ★	All patients were diagnosed with hemianopia stroke according to visual threshold test and MRI/CT scanning.	Yes ★	Sex and age matched ★	Comparison of parameters of brain network between stroke patients and healthy group.	Yes ★	All patients from whom EEG was taken participated in the study. ★	Good

Table 2. *Cont.*

Study	Selection				Comparability		Outcome		Quality Score
	Representativeness of Exposed Cohort	Selection of the Non-Exposed Cohort from Same Source as Exposed Cohort	Ascertainment of Exposure	Outcome of Interest Was Not Present at Start of Study	Comparability of Cohorts	Assessment of Outcome	Follow-up Long Enough for Outcome to Occur	Adequacy of Follow-Up	
Dubovik, Sviatlana et al., 2013 [9]	Participants were in two groups: patients with ischemic stroke (n = 20) and healthy participants (n = 19). ★	Yes ★	Motor function was evaluated by means of the Jamar dynamometer, the Nine Hole Peg test, the Stroke Rehabilitation Assessment of Movement (STREAM) and the Fugl–Meyer score.	Yes ★	Age matched	Assessment resting-state functional connectivity with (EEG).	Yes ★	All patients from whom EEG was taken participated in the study. ★	Fair
de Vico Fallani, Fabrizio et al., 2009 [10]	Participants were in two groups: healthy subjects (n = 8) and one patient with stroke. ★	Yes ★	No information	Yes ★	Nothing matched	Analysis of cerebral electro-physiological activity during planning or execution of movement in in stroke patients.	Yes ★	All patients and healthy people from whom EEG was taken participated in the study. ★	Fair
Fanciullacci, Chiara et al., 2021 [12]	Participants were in two groups: stroke patients in the sub-acute phase (n = 33) and healthy subjects (n = 10). ★	Yes ★	Brain injury was assessed by means of a standard CT scan.	Yes ★	Age matched	Characterizing resting-state EEG activity and functional connectivity changes in a cohort of unilateral ischemic patients compared with the healthy group.	Yes ★	All patients from whom EEG was taken participated in the study. ★	Fair
Caliandro, Pietro et al., 2017 [13]	Participants were in 2 groups: patients with ischemic lesion (n = 30) and healthy subjects (n = 30). ★	Yes ★	Patients were clinically evaluated by the National Institutes of Health Stroke Scale.	Yes ★	Age and sex matched ★	Whether and how ischemic stroke in the acute stage may determine changes in the small-world index of cortical networks.	Yes ★	All patients from whom EEG was taken participated in the study. ★	Good

★ The quality of the studies (good, fair and poor) was rated by awarding stars in each domain following the guidelines of the Newcastle–Ottawa Scale. A "good" quality score required 3 or 4 stars in selection, 1 or 2 stars in comparability and 2 or 3 stars in outcomes. A "fair" quality score required 2 stars in selection, 1 or 2 stars in comparability and 2 or 3 stars in outcomes. A "poor" quality score reflected 0 or 1 star(s) in selection, 0 stars in comparability or 0 or 1 star(s) in outcomes.
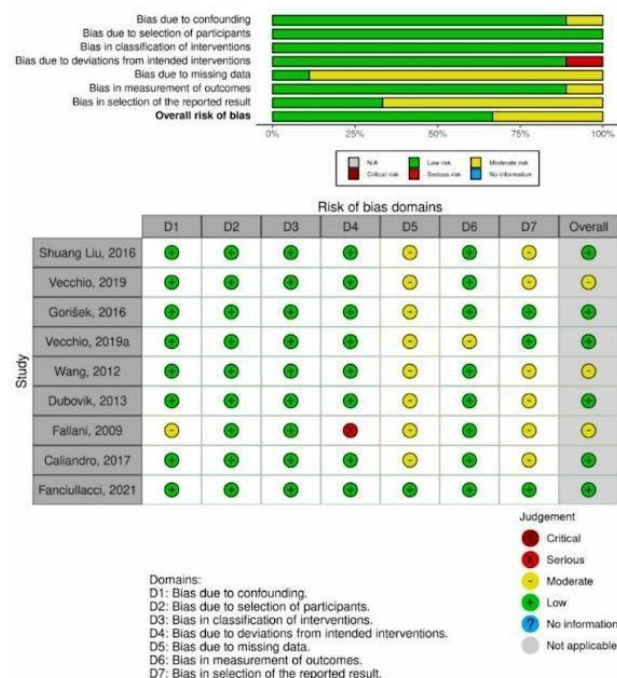
Figure 2. Risk of bias (RoB) traffic light plot. Assessment of the risk of bias via the traffic light plot of the RoB of each included clinical trial and the weighted plot for the assessment of the overall risk of bias via the Cochrane Robins-I tool (*n* = 9 studies). Yellow circle indicates some concerns on the risk of bias, and green circle represents low risk of bias [4–10,12,13].

Table 3. Quality assessment for cross-sectional study.

Vecchio, Fabrizio et al., 2017 [11]	
Did the study address a clearly focused question/issue?	Yes
Is the study design appropriate for answering the research question?	Yes
Does the study have a well-defined protocol?	No
Are both the setting and the subjects representative with regard to the population to which the findings will correlate?	Yes
Is the researcher's perspective clearly described and taken into account?	Yes
Are the methods for collecting data clearly described?	Yes
Are the methods for analyzing the data likely to be valid and reliable? Are quality control measures used?	Yes
Was the analysis repeated by more than one researcher to ensure reliability?	No
Are the results credible, and if so, are they relevant for practice? Are results easy to understand?	Yes
Were there clinically relevant outcomes?	Yes
Are the conclusions drawn justified by the results?	Yes
Are the findings of the study transferable to other settings?	No

Meta-Analysis

The presence of relatively high values for τ^2 (0.25), the significant Cochrane Q test ($p = 0.04$) and the value of I^2 of the 60% indicate large heterogeneity. The effect size is small and not significant in favor of the group of healthy subjects (Hedges'g = 0.189 [-0.714, 1.093], Z = 0.582, $p = 0.592$) (Figure 3).

	Patients			**Healthy**				**Std. Mean Difference**	**Std. Mean Difference**
Study	**Mean**	**SD**	**Total**	**Mean**	**SD**	**Total**	**Weight**	**IV, Random, 95% CI**	**IV, Random, 95% CI**
Wang, 2012	0.18	0.04	7	0.16	0.05	7	16.8%	0.38 [-0.68; 1.44]	
Vecchio, 2019	1.00	0.02	41	1.00	0.03	10	24.3%	-0.03 [-0.72; 0.66]	
Fallani, 2009	0.13	0.00	1	0.24	0.08	80	7.1%	-1.43 [-3.42; 0.55]	
Fanciullacci, 2021	1.02	0.18	33	0.79	0.26	10	23.0%	1.12 [0.37; 1.87]	
Caliandro, 2017	0.98	0.28	30	1.01	0.45	30	28.8%	-0.08 [-0.58; 0.43]	
Total (95% CI)			**112**			**137**	**100.0%**	**0.19 [-0.71; 1.09]**	
Prediction Interval								**[-1.71; 2.09]**	

Heterogeneity: Tau^2 = 0.2502; Chi^2 = 10.02, df = 4 (P = 0.04); I^2 = 60%

Figure 3. Meta-analysis forest plot for small-world index brain network measure on healthy subjects vs. stroke patients. SD: standard deviation; SMD: standardized mean difference; 95%CI: 95% confidence interval; Tau2: τ^2 between studies variance estimation; Chi^2: Cochran Q test; df: degrees of freedom; I^2: proportion of the variance in observed effect is due to variance in true effects rather than sampling error [7,8,10,12,13].

No study analyzed is an outlier that exceeds the 95% CI (Appendix A, Figure A1). The influence analysis shows how the study published by Fanciullacci (red dot) exerts a great influence on the result of the meta-analysis (Appendix A, Figure A2). The Baujat graph shows again that the Fanciullacci study (upper right square dot) also exerts an excessive influence on the heterogeneity detected (Appendix A, Figure A3). The sensitivity analysis to the withdrawal of a study indicates, both by effect size and by I2 values, that the study published by Fanciullacci is the one that most influences the result of the meta-analysis (Appendix A, Figure A4). The GOSH graph shows the presence of two clusters of studies with a heterogeneity around 60–80% and 0–20% respectively, with an effect that oscillates around 0 and 0.5 in both (Appendix A, Figure A5).

When the meta-analysis of subgroups was carried out, we found that there is a decrease in heterogeneity in the studies carried out with Raw Cw, Lw (I^2 changes from 60% to 0%), whereas there is an increase in the studies carried out with Direct SW (I^2 changes from 60% to 79%). Therefore, it is possible that studies with Direct SW are responsible for part of the heterogeneity detected. We verified how the effect size in the studies carried out with Raw Cw-Lw is small and not significant in favor of the group of healthy subjects (Hedges's g = 0.008, [-2.229, 2.245], Z = 0.047, $p = 0.97$). In the group of studies carried out with Direct SW, the effect size is moderate and not significant and displaced in favor of the group of healthy subjects (Hedges's g = 0.535, [-6.76, 7.831], Z = 0.932, $p = 0.522$). Finally, in the study carried out with Raw Eg-El, the effect size is large and not significant and displaced in favor of the patient group (Hedges's g = -1.431, [$-3.416,0.555$], Z = -1.412, $p = 0.158$). Therefore, it can be concluded that none of the study groups produced significant effects. Despite the disparity of the effect in each group (0.008 vs. 0.535 vs. -1.431), there are no significant differences in the effect between groups depending on the calculation mode of the SW (X2(2) = 2.86, $p = 0.239$) (Figure 4).

The tests of Begg (Kendall's $\tau = 0$, $p = 1$) and Eggers (t(3) = -1.187, $p = 0.321$) were not significant and indicate the absence of publication bias. The funnel plots (both the standard and the one obtained with trim and fill method) show a symmetrical distribution except for the study carried out by Fallani, which corroborates the absence of publication bias (Appendix A, Figure A6).
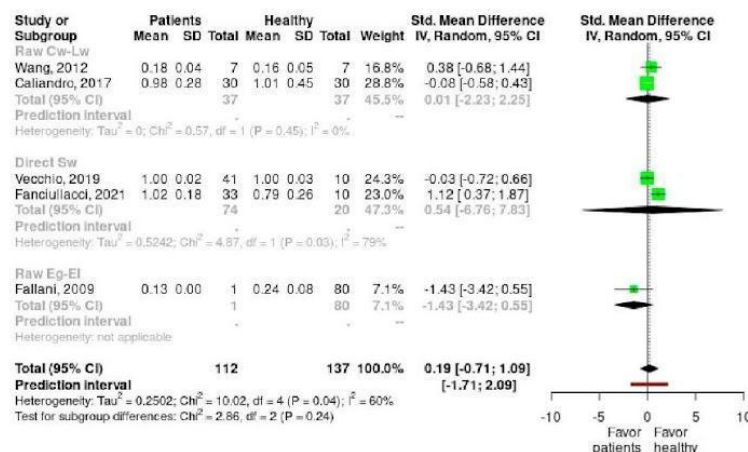
Figure 4. Subgroup forest plots for the different calculation methods of small-world index on healthy subjects vs. stroke patients. Cw: weighted clustering coefficient; Lw: weighted characteristic path length; Eg: global efficiency; El: local efficiency. SD: standard deviation; SMD: standardized mean difference; 95%CI: 95% confidence interval; Tau^2: τ^2 between studies variance estimation; Chi^2: Cochran Q test; df: degrees of freedom; I^2: proportion of the variance in observed effect is due to variance in true effects rather than sampling error [7,8,10,12,13].

4. Discussion

Studying cortical connectivity changes in stroke can provide novel ways to characterize clinical rehabilitation and suitable therapies for patients with brain lesions leading to cognitive or motor disability. Here, we revise the existing literature supporting the use of EEG-based metrics to analyze brain networks and how they are altered in stroke patients. Despite the identified differences between the studies considered here in terms of recording conditions (e.g., devices or number of channels used) and metrics used to assess cortico-cortical connectivity, it was possible to find a common conclusion in them: the brain network of stroke patients was shown to be different from that of healthy people. These differences were only found in specific frequency bands. For example, there were neither significant differences between post-stroke patients with hemianopia and the healthy controls in the global weighted CC and PL [8] parameters nor in the network rearrangement in alpha 1, beta and gamma bands [13].

In all the studies analyzed, the internal structure of the brain network changed compared to healthy humans. The greatest impact was observed in the affected areas, which showed weaker connections. If we consider delta, theta and alpha bands as low-frequency bands, and assume beta and gamma as high-frequency bands, the functional and topological network in high-frequency bands in patients after an acute stroke show changes [4,5,7,10,12,13]. However, no conclusion can be drawn with certainty about the SW index: in some studies, the patients had a higher SW in different bands [4,12], whereas in others [11], the SW index increased after stroke. However, another study showed that the SW parameter was higher in the control group [7]. It could be expected that healthy patients have a higher SW so that transfer data in the brain is done faster from one point to another, following the shortest path length, but this is still unclear, and data obtained in different populations are still controversial.

As in the case of the small-world index, no statistically significant differences were found in indices, such as the shortest path length and clustering coefficient, although recently a case study showed significant changes in these parameters when the analysis was performed by dynamic complex network, which shows higher variations in the global

clustering coefficient and small-world index and lower variations in the average shortest path length in the low-frequency bands, such as delta, theta and alpha bands, in the chronic stroke patients [49].

Although evidence suggests that connections are less in the brain of post-stroke patients, a model of brain network cannot be clearly considered, or there is not a standard by which patients with stroke can be recognized. However, the immediate EEG changes observed after stroke are a direct consequence of cerebral blood flow reduction that later results in neuronal impairment or neuronal death. This neuronal impairment in turn leads to a disorganization of the electrical activity that is reflected by the global EEG changes [50]. Subsequent neuroplastic changes after stroke have been largely reported [51]. Post-stroke neuroplasticity can lead to reorganization in neural circuits that allow for regaining the lost functionality [52,53]. However, according to our knowledge, there have not been any publications discussing how neuroplasticity after a stroke leads to changes in brain network parameters measured with EEG.

Oscillating neural activity in the gamma frequency band is involved in several cognitive functions, including visual object processing [54,55], attention [56,57] and memory [58,59]. Additionally, several studies have demonstrated that gamma band activity is strongly associated with behavioral performance in several memory tasks [60,61] and that there is a higher gamma band activity in participants exhibiting superior recognition memory performance [62]. Other findings [63,64] suggest that gamma oscillations not only reflect brain activity related to memory processes, but also vary with the memory ability of individuals. Two of the studies included in the review [5,7] described variation in the gamma band, which could be supported by evidence that suggests that gamma oscillations mediate information transfer between cortical and hippocampal structure for memory abilities [58,59].

With some exceptions, a consensus is reached on how an increase in the slow band frequencies, referred to as slow oscillation and delta oscillation, and is associated with not only the slow-wave sleep state, but also brain ischemia. Conversely, high band frequencies, such as the alpha, beta and gamma oscillations, are associated with wake states or cognitive task engagement, and their presence frequently reduces after stroke. As it was found in one study [10], changes were seen in gamma and beta bands. A possible explanation could be that coherence in higher bands may be more involved in active (either motor or cognitive) tasks [30–32].

In our review, differences in EEG signals were observed not only in parameters, but also in different bands. For example, in one study [13], changes were seen in low-frequency bands (delta, theta and alpha2), and no difference was seen in higher-frequency bands (alpha1, beta and gamma), which is consistent with the results of a recent case study [49]. In other studies, changes were seen in alpha [7,9] and theta and beta bands [12]. The changes in the different bands that are seen can be related to the type of stroke, the type of networking of the brain regions, the resting or active state, the examined area of the brain and the age of the patient [65].

Regarding the usefulness of EEG-based connectivity measures to assess brain function in stroke, we found some limitations related to the heterogeneity of the injured areas in the patients participating in the studies included in our meta-analysis. Future studies should include larger samples and grouping patients in terms of the exact locations of their lesions, which would allow us to further understand how the spatial location of a brain lesion affects the rearrangement of brain connections at the local and global scales.

5. Conclusions

This is the first systematic review carried out about EEG connectivity changes to diagnose or characterize stroke. The systematic review found that there are structural differences between the brain network of post-stroke patients and healthy individuals as well as similarities. However, there is no specific distribution network that allows us to differentiate them and, therefore, more specialized and integrated studies are needed.

Appendix A

Figure A1. Outliers forest plot. SD: standard deviation; SMD: standardized mean difference; 95%CI: 95% confidence interval; Tau^2: τ^2 between studies variance estimation; p: Cochran Q test p v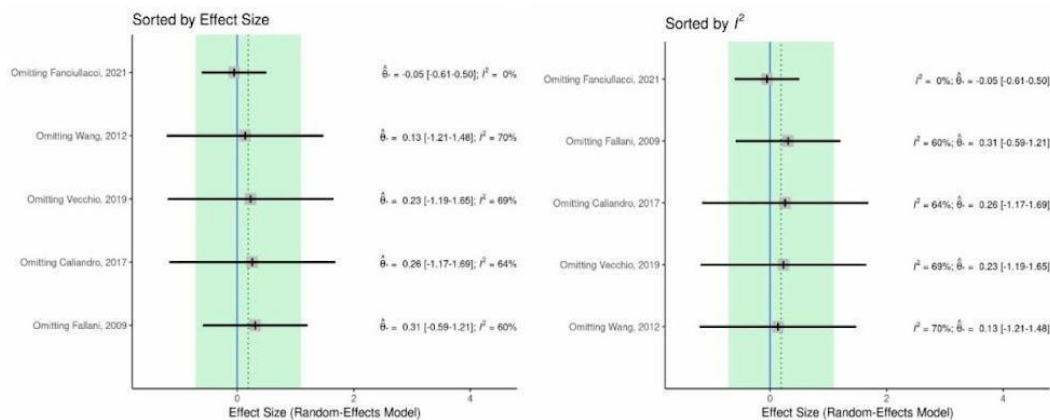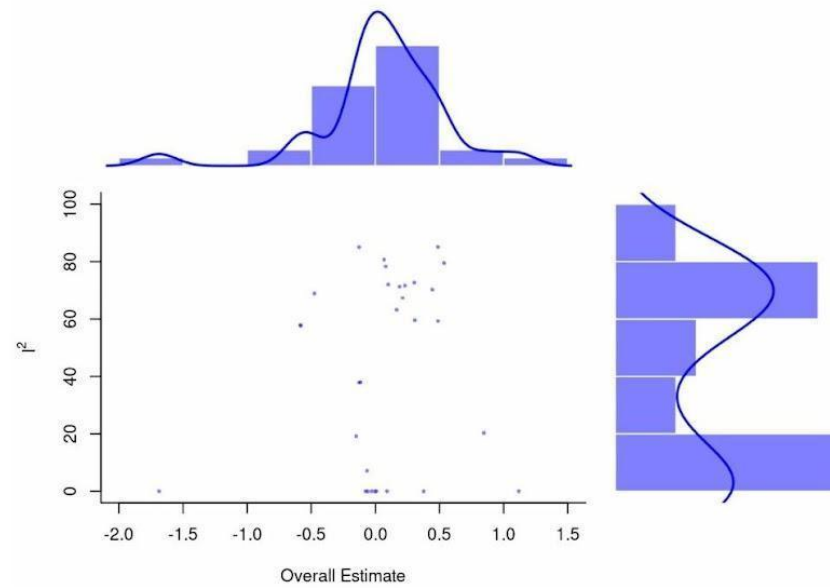alue; I^2: proportion of the variance in observed effect is due to variance in true effects rather than sampling error [7,8,10,12,13].
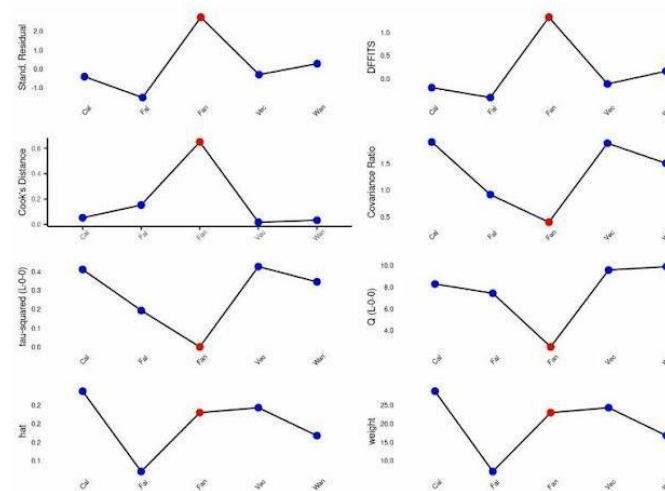
Figure A2. Influence graph. Stand. Residual: standardized residuals for each study; DFFITS: difference in fit(s) of studentized residuals for each study; Cook's distance: residuals removing each

time from one study; Covariance ratio: ratio between variance pooled effect and initial average effect; tau-squared (L-O-O): tau squared leave-one-out plot is the heterogeneity measure by tau squared removing a single study each time; Q (L-O-O): Cochrane test leave-one-out plot is the heterogeneity measure Cochran Q test removing a single study each time; hat: model predictions for each study; weight: studies' weight. Red points are influencing studies, blue points are not influencing studies.
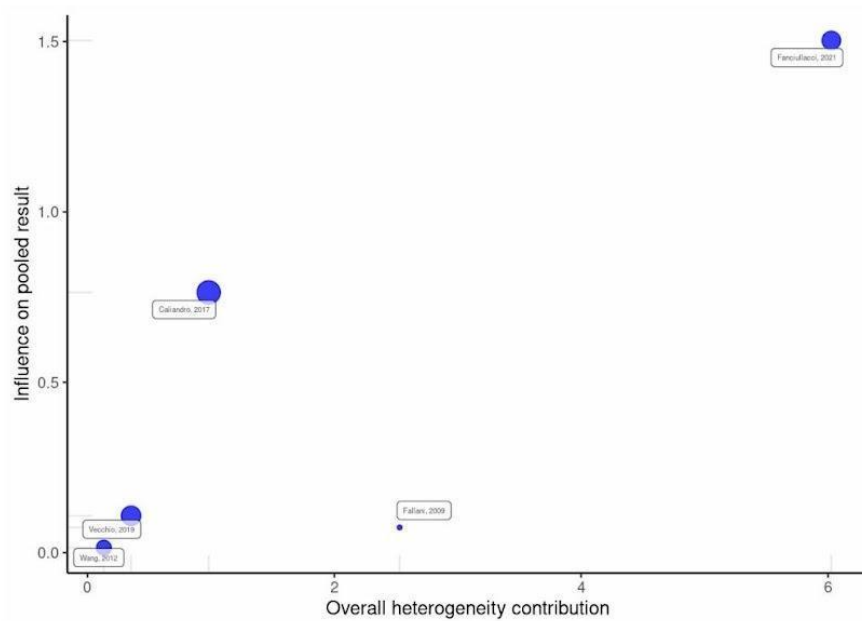
Figure A3. Baujat plot [7,8,10,12,13].

Figure A4. Leave-one-out plots. I^2: proportion of the variance in observed effect is due to variance in true effects rather than sampling error [7,8,10,12,13].

Figure A5. GOSH plot. I^2: proportion of the variance in observed effect is due to variance in true effects rather than sampling error.
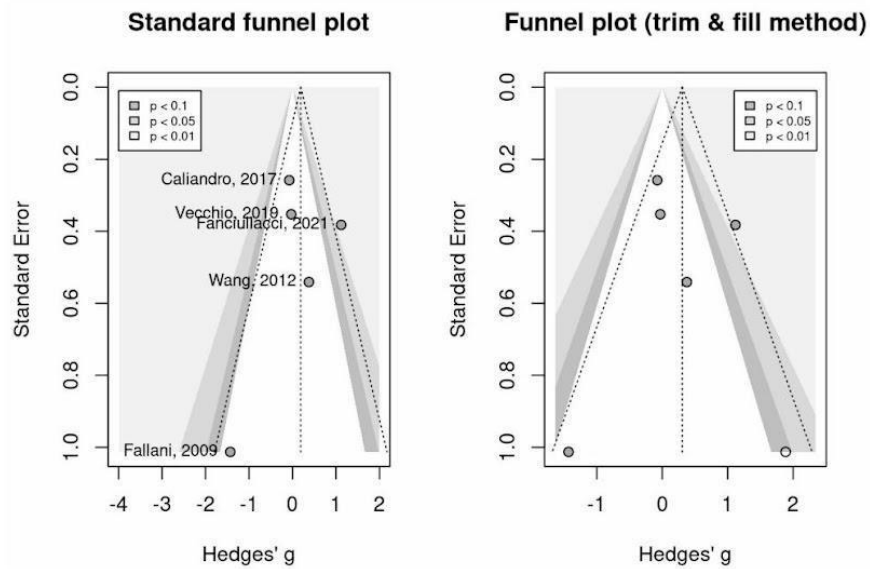
Figure A6. Publication bias funnel plots. Grey scale bands: significance levels from $p < 0.1$ (darker gray) to $p < 0.01$ (lighter gray) [7,8,10,12,13].

References

1. Ma, V.Y.; Chan, L.; Carruthers, K.J. Incidence, prevalence, costs, and impact on disability of common conditions requiring rehabilitation in the United States: Stroke, spinal cord injury, traumatic brain injury, multiple sclerosis, osteoarthritis, rheumatoid arthritis, limb loss, and back pain. *Arch. Phys. Med. Rehabil.* **2014**, *95*, 986–995.e981.
2. Béjot, Y.; Bailly, H.; Durier, J.; Giroud, M. Epidemiology of stroke in Europe and trends for the 21st century. *La Presse Méd.* **2016**, *45*, e391–e398. [CrossRef]
3. Ajčević, M.; Furlanis, G.; Miladinović, A.; Buoite Stella, A.; Caruso, P.; Ukmar, M.; Cova, M.A.; Naccarato, M.; Accardo, A.; Manganotti, P. Early EEG alterations correlate with CTP hypoperfused volumes and neurological deficit: A wireless EEG study in hyper-acute ischemic stroke. *Ann. Biomed. Eng.* **2021**, *49*, 2150–2158. [CrossRef]
4. Vecchio, F.; Caliandro, P.; Reale, G.; Miraglia, F.; Piludu, F.; Masi, G.; Iacovelli, C.; Simbolotti, C.; Padua, L.; Leone, E. Acute cerebellar stroke and middle cerebral artery stroke exert distinctive modifications on functional cortical connectivity: A comparative study via EEG graph theory. *Clin. Neurophysiol.* **2019**, *130*, 997–1007. [CrossRef]
5. Gorišek, V.R.; Isoski, V.Z.; Belič, A.; Manouilidou, C.; Koritnik, B.; Bon, J.; Meglič, N.P.; Vrabec, M.; Žibert, J.; Repovš, G. Beyond aphasia: Altered EEG connectivity in Broca's patients during working memory task. *Brain Lang.* **2016**, *163*, 10–21. [CrossRef]
6. Liu, S.; Guo, J.; Meng, J.; Wang, Z.; Yao, Y.; Yang, J.; Qi, H.; Ming, D. Abnormal EEG complexity and functional connectivity of brain in patients with acute thalamic ischemic stroke. *Comput. Math. Methods Med.* **2016**, *2016*, 2582478. [CrossRef]
7. Vecchio, F.; Tomino, C.; Miraglia, F.; Iodice, F.; Erra, C.; Di Iorio, R.; Judica, E.; Alù, F.; Fini, M.; Rossini, P.M. Cortical connectivity from EEG data in acute stroke: A study via graph theory as a potential biomarker for functional recovery. *Int. J. Psychophysiol.* **2019**, *146*, 133–138. [CrossRef]
8. Wang, L.; Guo, X.; Sun, J.; Jin, Z.; Tong, S. Cortical networks of hemianopia stroke patients: A graph theoretical analysis of EEG signals at resting state. In Proceedings of the 2012 Annual International Conference of the IEEE Engineering in Medicine and Biology Society, San Diego, CA, USA, 28 August–1 September 2012; pp. 49–52.
9. Dubovik, S.; Ptak, R.; Aboulafia, T.; Magnin, C.; Gillabert, N.; Allet, L.; Pignat, J.-M.; Schnider, A.; Guggisberg, A.G. EEG alpha band synchrony predicts cognitive and motor performance in patients with ischemic stroke. *Behav. Neurol.* **2013**, *26*, 187–189. [CrossRef]
10. De Vico Fallani, F.; Astolfi, L.; Cincotti, F.; Mattia, D.; La Rocca, D.; Maksuti, E.; Salinari, S.; Babiloni, F.; Vegso, B.; Kozmann, G. Evaluation of the brain network organization from EEG signals: A preliminary evidence in stroke patient. *Anat. Rec. Adv. Integr. Anat. Evol. Biol. Adv. Integr. Anat. Evol. Biol.* **2009**, *292*, 2023–2031. [CrossRef]
11. Vecchio, F.; Miraglia, F.; Romano, A.; Bramanti, P.; Rossini, P.M. Small world brain network characteristics during EEG Holter recording of a stroke event. *Clin. Neurophysiol.* **2017**, *128*, 1–3. [CrossRef]
12. Fanciullacci, C.; Panarese, A.; Spina, V.; Lassi, M.; Mazzoni, A.; Artoni, F.; Micera, S.; Chisari, C. Connectivity measures differentiate cortical and subcortical sub-acute ischemic stroke patients. *Front. Hum. Neurosci.* **2021**, *15*, 669915. [CrossRef]
13. Caliandro, P.; Vecchio, F.; Miraglia, F.; Reale, G.; Della Marca, G.; La Torre, G.; Lacidogna, G.; Iacovelli, C.; Padua, L.; Bramanti, P. Small-world characteristics of cortical connectivity changes in acute stroke. *Neurorehabilit. Neural Repair* **2017**, *31*, 81–94. [CrossRef]
14. Sporns, O. *Networks of the Brain*; MIT press: Cambridge, MA, USA, 2016.
15. Watts, D.J.; Strogatz, S.H. Collective dynamics of 'small-world' networks. *Nature* **1998**, *393*, 440–442. [CrossRef]
16. Carter, A.R.; Astafiev, S.V.; Lang, C.E.; Connor, L.T.; Rengachary, J.; Strube, M.J.; Pope, D.L.; Shulman, G.L.; Corbetta, M. Resting interhemispheric functional magnetic resonance imaging connectivity predicts performance after stroke. *Ann. Neurol.* **2010**, *67*, 365–375.
17. Yin, D.; Song, F.; Xu, D.; Sun, L.; Men, W.; Zang, L.; Yan, X.; Fan, M. Altered topological properties of the cortical motor-related network in patients with subcortical stroke revealed by graph theoretical analysis. *Hum. Brain Mapp.* **2014**, *35*, 3343–3359. [CrossRef]
18. Siegel, J.S.; Ramsey, L.E.; Snyder, A.Z.; Metcalf, N.V.; Chacko, R.V.; Weinberger, K.; Baldassarre, A.; Hacker, C.D.; Shulman, G.L.; Corbetta, M. Disruptions of network connectivity predict impairment in multiple behavioral domains after stroke. *Proc. Natl. Acad. Sci. USA* **2016**, *113*, E4367–E4376. [CrossRef]
19. Miraglia, F.; Vecchio, F.; Rossini, P.M. Searching for signs of aging and dementia in EEG through network analysis. *Behav. Brain Res.* **2017**, *317*, 292–300. [CrossRef]
20. Van Wijk, B.C.; Stam, C.J.; Daffertshofer, A. Comparing brain networks of different size and connectivity density using graph theory. *PLoS ONE* **2010**, *5*, e13701. [CrossRef]
21. Rubinov, M.; Sporns, O. Complex network measures of brain connectivity: Uses and interpretations. *Neuroimage* **2010**, *52*, 1059–1069. [CrossRef]
22. Onnela, J.-P.; Saramäki, J.; Kertész, J.; Kaski, K. Intensity and coherence of motifs in weighted complex networks. *Phys. Rev. E* **2005**, *71*, 065103. [CrossRef]
23. Eliassen, J.C.; Boespflug, E.L.; Lamy, M.; Allendorfer, J.; Chu, W.-J.; Szaflarski, J.P. Brain-mapping techniques for evaluating poststroke recovery and rehabilitation: A review. *Top. Stroke Rehabil.* **2008**, *15*, 427–450. [CrossRef]
24. Cohen, B.A.; Bravo-Fernández, E.J.; Sances Jr, A. Quantification of computer analyzed serial EEGs from stroke patients. *Electroencephalogr. Clin. Neurophysiol.* **1976**, *41*, 379–386. [CrossRef]

25. Cohen, B.; Bravo-Fernandez, E.; Sances, A. Automated electroencephalographic analysis as a prognostic indicator in stroke. *Med. Biol. Eng. Comput.* **1977**, *15*, 431–437. [CrossRef]

26. Luu, P.; Tucker, D.M.; Englander, R.; Lockfeld, A.; Lutsep, H.; Oken, B. Localizing acute stroke-related eeg changes:: Assessing the effects of spatial undersampling. *J. Clin. Neurophysiol.* **2001**, *18*, 302–317. [CrossRef]

27. Finnigan, S.P.; Rose, S.E.; Walsh, M.; Griffin, M.; Janke, A.L.; McMahon, K.L.; Gillies, R.; Strudwick, M.W.; Pettigrew, C.M.; Semple, J. Correlation of quantitative EEG in acute ischemic stroke with 30-day NIHSS score: Comparison with diffusion and perfusion MRI. *Stroke* **2004**, *35*, 899–903. [CrossRef]

28. Bullmore, E.; Sporns, O. Complex brain networks: Graph theoretical analysis of structural and functional systems. *Nat. Rev. Neurosci.* **2009**, *10*, 186–198. [CrossRef]

29. Andrew, C.; Pfurtscheller, G. Event-related coherence as a tool for studying dynamic interaction of brain regions. *Electroencephalogr. Clin. Neurophysiol.* **1996**, *98*, 144–148. [CrossRef]

30. Weiss, S.; Mueller, H.M. The contribution of EEG coherence to the investigation of language. *Brain Lang.* **2003**, *85*, 325–343. [CrossRef]

31. Hallett, M. Can EEG coherence help solve the binding problem?: The Adrian Lecture. In *Supplements to Clinical Neurophysiology*; Elsevier: Amsterdam, The Netherlands, 2000; Volume 53, pp. 19–26.

32. Buzsaki, G. *Rhythms of the Brain*; Oxford University Press: Oxford, UK, 2006.

33. Quinn, T.; Dawson, J.; Walters, M.; Lees, K. Functional outcome measures in contemporary stroke trials. *Int. J. Stroke* **2009**, *4*, 200–205. [CrossRef]

34. Lees, R.; Fearon, P.; Harrison, J.K.; Broomfield, N.M.; Quinn, T.J. Cognitive and mood assessment in stroke research: Focused review of contemporary studies. *Stroke* **2012**, *43*, 1678–1680. [CrossRef]

35. Moher, D.; Liberati, A.; Tetzlaff, J.; Altman, D.G.; Group, P. Preferred reporting items for systematic reviews and meta-analyses: The PRISMA statement. *Int. J. Surg.* **2010**, *8*, 336–341. [CrossRef]

36. Greenhalgh, T. How to read a paper: The Medline database. *BMJ* **1997**, *315*, 180–183. [CrossRef]

37. Wells, G.A.; Shea, B.; O'Connell, D.; Peterson, J.; Welch, V.; Losos, M.; Tugwell, P. *The Newcastle-Ottawa Scale (NOS) for Assessing the Quality of Nonrandomised Studies in Meta-Analyses*; ScienceOpen, Inc.: Burlington, MA, USA, 2000.

38. Wan, X.; Wang, W.; Liu, J.; Tong, T. Estimating the sample mean and standard deviation from the sample size, median, range and/or interquartile range. *BMC Med. Res. Methodol.* **2014**, *14*, 135. [CrossRef]

39. Luo, D.; Wan, X.; Liu, J.; Tong, T. Optimally estimating the sample mean from the sample size, median, mid-range, and/or mid-quartile range. *Stat. Methods Med. Res.* **2018**, *27*, 1785–1805. [CrossRef]

40. Higgins, J.P.; Thomas, J.; Chandler, J.; Cumpston, M.; Li, T.; Page, M.J.; Welch, V.A. *Cochrane Handbook for Systematic Reviews of Interventions*; John Wiley & Sons: Hoboken, NJ, USA, 2019.

41. Drevon, D.; Fursa, S.R.; Malcolm, A.L. Intercoder reliability and validity of WebPlotDigitizer in extracting graphed data. *Behav. Modif.* **2017**, *41*, 323–339. [CrossRef]

42. Viechtbauer, W.; Cheung, M.W.L. Outlier and influence diagnostics for meta-analysis. *Res. Synth. Methods* **2010**, *1*, 112–125. [CrossRef]

43. Baujat, B.; Mahé, C.; Pignon, J.P.; Hill, C. A graphical method for exploring heterogeneity in meta-analyses: Application to a meta-analysis of 65 trials. *Stat. Med.* **2002**, *21*, 2641–2652. [CrossRef]

44. Olkin, I.; Dahabreh, I.J.; Trikalinos, T.A. GOSH–a graphical display of study heterogeneity. *Res. Synth. Methods* **2012**, *3*, 214–223. [CrossRef]

45. Duval, S.; Tweedie, R. Trim and fill: A simple funnel-plot–based method of testing and adjusting for publication bias in meta-analysis. *Biometrics* **2000**, *56*, 455–463. [CrossRef]

46. Sakkalis, V. Review of advanced techniques for the estimation of brain connectivity measured with EEG/MEG. *Comput. Biol. Med.* **2011**, *41*, 1110–1117. [CrossRef]

47. Pascual-Marqui, R.D.; Lehmann, D.; Koukkou, M.; Kochi, K.; Anderer, P.; Saletu, B.; Tanaka, H.; Hirata, K.; John, E.R.; Prichep, L. Assessing interactions in the brain with exact low-resolution electromagnetic tomography. *Philos. Trans. R. Soc. A Math. Phys. Eng. Sci.* **2011**, *369*, 3768–3784. [CrossRef] [PubMed]

48. Sun, J.; Small, M. Unified framework for detecting phase synchronization in coupled time series. *Phys. Rev. E* **2009**, *80*, 046219. [CrossRef] [PubMed]

49. Asadi, B.; Fard, K.R.; Ansari, N.N.; Marco, Á.; Calvo, S.; Herrero, P. The Effect of dry Needling in Chronic Stroke with a complex Network Approach: A Case Study. *Clin. EEG Neurosci.* **2023**, *54*, 179–188. [CrossRef] [PubMed]

50. Rabiller, G.; He, J.-W.; Nishijima, Y.; Wong, A.; Liu, J. Perturbation of brain oscillations after ischemic stroke: A potential biomarker for post-stroke function and therapy. *Int. J. Mol. Sci.* **2015**, *16*, 25605–25640. [CrossRef]

51. Felling, R.J.; Song, H. Epigenetic mechanisms of neuroplasticity and the implications for stroke recovery. *Exp. Neurol.* **2015**, *268*, 37–45. [CrossRef]

52. Cramer, S.C.; Sur, M.; Dobkin, B.H.; O'Brien, C.; Sanger, T.D.; Trojanowski, J.Q.; Rumsey, J.M.; Hicks, R.; Cameron, J.; Chen, D. Harnessing neuroplasticity for clinical applications. *Brain* **2011**, *134*, 1591–1609. [CrossRef]

53. Colcombe, S.J.; Kramer, A.F.; Erickson, K.I.; Scalf, P.; McAuley, E.; Cohen, N.J.; Webb, A.; Jerome, G.J.; Marquez, D.X.; Elavsky, S. Cardiovascular fitness, cortical plasticity, and aging. *Proc. Natl. Acad. Sci. USA* **2004**, *101*, 3316–3321. [CrossRef]

54. Keil, A.; Müller, M.M.; Ray, W.J.; Gruber, T.; Elbert, T. Human gamma band activity and perception of a gestalt. *J. Neurosci.* **1999**, *19*, 7152–7161. [CrossRef]
55. Gruber, T.; Müller, M.M. Oscillatory brain activity dissociates between associative stimulus content in a repetition priming task in the human EEG. *Cereb. Cortex* **2005**, *15*, 109–116. [CrossRef]
56. Herrmann, C.S.; Mecklinger, A.; Pfeifer, E. Gamma responses and ERPs in a visual classification task. *Clin. Neurophysiol.* **1999**, *110*, 636–642. [CrossRef]
57. Gruber, T.; Müller, M.M.; Keil, A.; Elbert, T. Selective visual-spatial attention alters induced gamma band responses in the human EEG. *Clin. Neurophysiol.* **1999**, *110*, 2074–2085. [CrossRef] [PubMed]
58. Tallon-Baudry, C.; Bertrand, O.; Peronnet, F.; Pernier, J. Induced γ-band activity during the delay of a visual short-term memory task in humans. *J. Neurosci.* **1998**, *18*, 4244–4254. [CrossRef] [PubMed]
59. Herrmann, C.S.; Munk, M.H.; Engel, A.K. Cognitive functions of gamma-band activity: Memory match and utilization. *Trends Cogn. Sci.* **2004**, *8*, 347–355. [CrossRef] [PubMed]
60. Gruber, T.; Tsivilis, D.; Montaldi, D.; Müller, M.M. Induced gamma band responses: An early marker of memory encoding and retrieval. *Neuroreport* **2004**, *15*, 1837–1841. [CrossRef] [PubMed]
61. Osipova, D.; Takashima, A.; Oostenveld, R.; Fernández, G.; Maris, E.; Jensen, O. Theta and gamma oscillations predict encoding and retrieval of declarative memory. *J. Neurosci.* **2006**, *26*, 7523–7531. [CrossRef]
62. Busch, N.A.; Groh-Bordin, C.; Zimmer, H.D.; Herrmann, C.S. Modes of memory: Early electrophysiological markers of repetition suppression and recognition enhancement predict behavioral performance. *Psychophysiology* **2008**, *45*, 25–35. [CrossRef]
63. Park, J.Y.; Lee, K.S.; An, S.K.; Lee, J.; Kim, J.-J.; Kim, K.H.; Namkoong, K. Gamma oscillatory activity in relation to memory ability in older adults. *Int. J. Psychophysiol.* **2012**, *86*, 58–65. [CrossRef]
64. Lenz, D.; Jeschke, M.; Schadow, J.; Naue, N.; Ohl, F.W.; Herrmann, C.S. Human EEG very high frequency oscillations reflect the number of matches with a template in auditory short-term memory. *Brain Res.* **2008**, *1220*, 81–92. [CrossRef]
65. Achard, S.; Bullmore, E. Efficiency and cost of economical brain functional networks. *PLoS Comput. Biol.* **2007**, *3*, e17. [CrossRef]

Study 3

Article

Characterizing Muscle Tissue Quality Post-Stroke: Echovariation as a Clinical Indicator

Borhan Asadi [1,2], Clara Pujol-Fuentes [1,2], Alberto Carcasona-Otal [1,2], Sandra Calvo [1,2], Pablo Herrero [1,2,*] and Diego Lapuente-Hernández [1,2]

[1] Department of Physiatry and Nursing, Faculty of Health Sciences, University of Zaragoza, 50009 Zaragoza, Spain; basadi@iisaragon.es (B.A.); cpujol@iisaragon.es (C.P.-F.); acarcasona@unizar.es (A.C.-O.); sandracalvo@unizar.es (S.C.); d.lapuente@unizar.es (D.L.-H.)
[2] iHealthy Research Group, Instituto de Investigación Sanitaria (IIS) Aragón, University of Zaragoza, 50009 Zaragoza, Spain
*   Correspondence: pherrero@unizar.es; Tel.: +34-646-16-82-48

Abstract: Background/Objectives: Strokes remain a major global health concern, contributing significantly to disability and healthcare costs. Currently, there are no established indicators to accurately assess the degree of muscle tissue impairment in stroke-affected individuals. However, ultrasound imaging with an echotexture analysis shows potential as a quantitative tool to assess muscle tissue quality. This study aimed to identify specific echotexture features in the gastrocnemius medialis that effectively characterize muscle impairment in post-stroke individuals. **Methods**: An observational study was conducted with 22 post-stroke individuals. A total of 21 echotexture features were extracted and analyzed, including first-order metrics, a grey-level co-occurrence matrix, and a grey-level run length matrix. The modified Heckmatt scale was also applied to correlate with the most informative echotexture features. **Results**: Among the features analyzed, echovariation (EV), echointensity, and kurtosis emerged as the most informative indicators of muscle tissue quality. The EV was highlighted as the primary feature due to its strong and significant correlation with the modified Heckmatt scale ($r = -0.81$, $p < 0.001$) and its clinical and technical robustness. Lower EV values were associated with poorer muscle tissue quality, while higher values indicated better quality. **Conclusions**: The EV may be used as a quantitative indicator for characterizing the gastrocnemius medialis muscle tissue quality in post-stroke individuals, offering a more nuanced assessment than traditional qualitative scales. Future studies should investigate the correlation between the EV and other clinical outcomes and explore its potential to monitor the treatment efficacy, enhancing its applicability in clinical practice.

Keywords: stroke; ultrasonography; echotexture analysis; muscle tissue; Heckmatt scale; gastrocnemius medialis

1. Introduction

Strokes are a significant health issue with a profound socioeconomic impact, being one of the leading causes of disability worldwide [1]. Recent data indicate that approximately 13.7 million people experience a stroke annually, with substantial costs associated with long-term care and rehabilitation [2]. The effective management of strokes implies objective, accurate, and reproducible measurement tools that can be integrated into clinical practice to assess patient progress and optimize therapeutic outcomes to ensure that interventions are appropriately tailored to individual patient needs, enhancing their recovery and quality of life.

Over the years, a texture analysis has emerged as a key technique to characterize muscle composition in various diagnostic imaging technologies. A texture image is defined by the mathematical evaluation of pixel intensities and their spatial distribution within a region of interest (ROI) [3,4]. Statistical methods, classified into first-order (individual pixel

intensities), second-order (ratios between pixel pairs), and higher-order features, provide information on tissue patterns [5,6]. However, reproducibility and validation problems have limited the clinical application of these methods [7–10].

In the concrete case of ultrasound (US), it has emerged as a readily accessible, non-invasive, and cost-effective method for assessing skeletal muscle composition [11]. Furthermore, the acoustic power levels employed in US devices are designed to minimize the risk of adverse biological effects [6]. To date, US image analyses of muscle tissue have mainly focused on muscle architecture characteristics, including the cross-sectional area, thickness, fascicle length, and fascicle pennation angle [12,13]. Nonetheless, muscle echotexture features have also been explored in the context of certain medical conditions, such as amyotrophic lateral sclerosis [14], myofascial pain syndrome [15], or low back pain [16], as well as in healthy tissue [6]. However, considerable research is still required before these features can be reliably implemented in clinical practice.

Regarding muscle echotexture features in individuals who have suffered a stroke, the most extensively studied feature is the echogenicity/echointensity (EI), defined as the mean pixel brightness within the muscle fascia boundaries [17]. This feature appears to be altered in this population due to changes in histopathological features like atrophy and the fibro-adipose replacement of hypoechoic contractile elements [18], resulting in a higher EI due to the increased reflection of sound waves [19–21]. The EI can be assessed both qualitatively and quantitatively. The original or modified Heckmatt scale can be used for a qualitative analysis, which simply classifies the image into four possible degrees of impairment without an extensive analysis [22]. This scale has demonstrated a good reliability and validity in evaluating muscle changes in patients with spasticity [23]. Several free software programs for quantitative analyses exist to calculate the EI, but their clinical application is still limited due to the complexity and variability of the measurements. This variability is influenced by factors such as the type of US device, the settings, the operator technique, and image artifacts [24–26].

Another promising parameter for characterizing muscle composition in neuromuscular or neurological disorders is echovariation (EV), as a measure of the EI variation [27,28]. However, its application in the context of strokes has not yet been investigated. Additionally, a critical issue in existing studies on other conditions is the substantial variability of the echotexture features employed and the resulting data, often leading to the occurrence of spurious findings [29]. Consequently, this study aimed to identify the most informative echotexture features for characterizing gastrocnemius medialis muscle tissue in stroke-affected individuals. This effort could assist future research in selecting these features and evaluating their potential as reliable indicators for assessing the extent of muscle impairment and determining any relationships with other clinical outcomes in stroke-affected individuals.

2. Materials and Methods

2.1. Study Design

This observational study included stroke-affected individuals and analyzed the echotexture features of the gastrocnemius medialis muscle. The study followed the STROBE recommendations for observational studies [30] and the Declaration of Helsinki [31].

The Aragon Ethics Committee (PI24/030) approved the study and registered on ClinicalTrials.gov (NTC06411587, https://clinicaltrials.gov/study/NCT06411587, accessed on 7 February 2024). This study was based on a subset of data from the trial registered under the specified ClinicalTrials number, in which an analysis of the echotexture from various US images was conducted.

2.2. Participants

Stroke-affected individuals were recruited at the Hospital Clínico Universitario Lozano Blesa from February to April 2024 by a physician specializing in physical medicine and rehabilitation. During consultations, the specialists assessed the patients based on the

predefined inclusion and exclusion criteria. The inclusion criteria were as follows: (1) to be aged over 18 years; (2) to have a stroke diagnosis confirmed by computed tomography (CT) or magnetic resonance imaging (MRI); (3) to have more than 6 months of evolution since the onset of the stroke; and (4) to be able to walk independently, with or without assistance. The exclusion criteria were the following: (1) to have other neurological disorders (e.g., ataxia or dystonia); (2) to have undergone surgical intervention in the lower limb; and (3) to have other medical conditions that may interfere with data collection.

Patients meeting the criteria were given detailed explanations about the study, including its purpose, potential benefits, and associated risks. Those interested in participating were given an informed consent form, and any questions or concerns were addressed. Upon obtaining written informed consent, the patients were scheduled for an appointment to be evaluated at the Hospital Clínico Universitario Lozano Blesa.

2.3. Data Collection

US images of the gastrocnemius medialis muscle were obtained using the Butterfly iQ+ portable US system, specifically designed for external US imaging, manufactured by Butterfly Network, Inc. The imaging protocol utilized a standardized preset of a 50% gain and a 5 to 7 cm depth. The scans were conducted by a physiotherapist experienced in using the US in stroke-affected individuals. The images were taken with the participant seated, with 90° of knee flexion. The probe was placed at a point located proximally at 30% of the distance between the medial condyle of the tibia and the medial malleolus [32], while adjusting the angle from horizontal to obtain the best possible image (usually around 35–45° from horizontal). Six images were taken in total, three for each lower limb of the participant.

2.4. Variables and Data Analysis

The whole process, from data collection to analysis, is summarized in Figure 1. After the physiotherapist (C.P.-F) collected the US images, they were uploaded into a cloud server and analyzed by an independent researcher (B.A.). Subsequently, two expert physiotherapists (D.L.-H and P.H.) manually selected the ROI for each image by consensus, including the maximum gastrocnemius medialis muscle tissue, while excluding superficial and deep fascia [33] (Figure 2). Images with an unclear delineation of the fascia or significant artifacts that could affect the image analysis were excluded. This ROI selection process followed a standardized image-acquisition protocol to minimize the variability. A specific ROI size was not predefined to avoid bias. Instead, the ROI was selected manually for each image, aiming to include the maximum amount of muscle tissue. This approach ensured a more representative analysis, as chronic conditions are expected to affect the muscle uniformly, unlike acute injuries, where selecting a specific ROI is necessary to target localized damage.
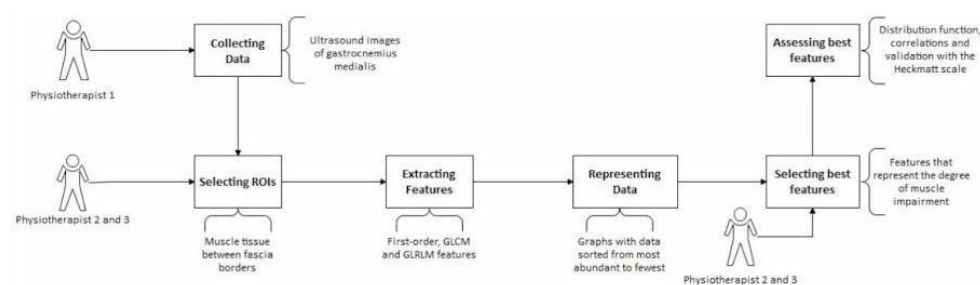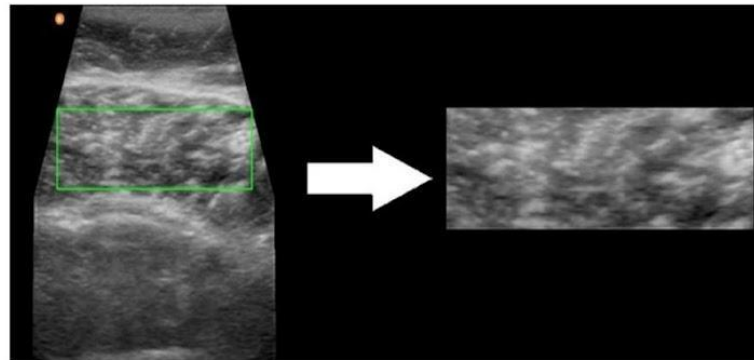

Figure 1. Research pipeline.

Figure 2. Manual ROI selection process with as much muscle tissue as possible. The green rectangle indicates the final selection of the ROI after consensus between two physiotherapists.

Three main types of features were extracted from each of the US images (Table 1) without any image pre-processing:

- Histogram-based (first-order features): the EI [25], EV [28], variance, standard deviation, skewness, and kurtosis [34]. These features were computed directly from the pixel matrix of the images.
- Grey-level co-occurrence matrix (GLCM): the correlation, dissimilarity, contrast, homogeneity, angular second moment (ASM), energy, maximum probability, entropy [35], cluster shade, and cluster prominence [36]. The GLCM was calculated using the skimage.feature library (https://scikit-image.org/docs/stable/api/skimage.feature.html, accessed on 20 October 2024), with distances = 5, angles = 0, and levels = 256.
- Grey-level run length matrix (GLRLM): the short run emphasis (SRE), long run emphasis (LRE) [37], grey-level Uuniformity (GLU), run length uniformity (RLU) [38], and run percentage (RPC) [39]. The GLRLM was calculated using a custom library (https://pypi.org/project/glrlm/, accessed on 20 October 2024). The final output of the GLRLM was obtained for all angles: 0°, 45°, 90°, 135°, and 180°, using a level parameter of 16. The features were then extracted from each matrix, and the final output was derived by averaging the features across all angles.

The methodology to select the most informative features for assessing muscle impairment or muscle tissue quality assumed that each feature's top and bottom 10 values should correspond to the images with the most and the least affected tissue. Each feature's images were ordered from the highest to the lowest values for this exploratory analysis and graphically represented. The 20 images with the top and bottom 10 values were then selected for each feature, and two physiotherapists (D.L.-H and P.H.) assessed the degree of muscle impairment, considering that more significant impairment was indicated by an increased loss of muscle echotexture (e.g., diffuse areas). These two physiotherapists underwent joint training sessions before the analysis to standardize the evaluation process. Following training, each evaluator independently assessed the images while blinded to the participants' clinical outcomes to ensure objective evaluations solely based on image-derived features. Features were selected only when the top and bottom 10 values corresponded 100% with high or low muscle impairment and when the images with high or low quality were in the opposite extreme for both evaluators. For example, features characterizing 100% of the images as highly affected for both the top and bottom 10 values were not considered informative features. Following this process, the two evaluators summarized the number of images grouped at each extreme according to the degree of impairment, allowing them to determine the most informative features.

Table 1. Description of the echotexture features extracted from each of the US images.

Statistical Approach	Feature	Brief Description
Histogram-based (first-order) features	Echogenicity, also called echointensity (EI)	The ability of tissues to reflect ultrasound waves. Specifies the average brightness of the ultrasound image.
	Variance	Measures the dispersion of pixel intensity values.
	Standard deviation	The square root of variance.
	Echovariation (EV), also called coefficient of variation	Variation in echointensities in an ultrasound image.
	Skew	Measures the asymmetry of the distribution of pixel intensity values.
	Kurtosis	Measures the "tailedness" of the distribution of pixel intensity values.
Grey-level co-occurrence matrix (GLCM)	Correlation	Measures the statistical correlation between neighboring pixels.
	Dissimilarity	Measures the mean absolute difference between neighboring pixel values.
	Contrast	Measures the intensity contrast between a pixel and its neighbor across the ROI.
	Homogeneity, also called inverse different moment	Measures the closeness of the distribution of elements in the GLCM to the GLCM diagonal.
	Angular second moment (ASM)	Similar to energy, it measures the uniformity of the GLCM.
	Energy	Sum of squared elements in the GLCM, representing texture uniformity.
	Max probability	The highest value in the GLCM.
	Entropy	Measures the randomness or complexity of the texture.
	Cluster shade	Measures the skewness of the distribution of the GLCM.
	Cluster prominence	Measures the peakedness of the distribution of the GLCM.
Grey-level run length matrix (GLRLM)	Short run emphasis (SRE)	Measures the distribution of short runs.
	Long run emphasis (LRE)	Measures the distribution of long runs.
	Grey-level uniformity (GLU)	Measures the uniformity of grey levels.
	Run length uniformity (RLU)	Measures the uniformity of run lengths.
	Run percentage (RPC)	The ratio of the number of runs to the number of pixels.

After this, a third independent physiotherapist (C.P.-F) classified the 130 US images based on the four grades of the modified Heckmatt scale, which has been proven to be both reliable and valid for assessing spastic muscle and is easier to use in clinical practice compared to the original Heckmatt scale [23]. The relationship between the most informative selected features and the modified Heckmatt scale was examined with Pearson's correlation coefficient. The correlations were assessed based on established criteria [40]: (1) correlations greater than 0.80 were considered very strong; (2) correlations between 0.60 and 0.80 were considered moderately strong; (3) correlations between 0.30 and 0.50 were considered moderate; and (4) correlations below 0.30 were considered weak. Before the correlation analysis, all the data were normalized using Min-Max normalization to ensure that the variables were on a comparable scale. The p-values for each correlation coefficient were calculated to assess the statistical significance, with a threshold of $p < 0.05$ indicating significance.

An additional secondary analysis was carried out after identifying the most informative features for muscle tissue characterization through the preliminary exploratory process and correlation analysis. This analysis was based on the available scientific evidence and/or the inherent characteristics of each feature to select only one as the reference feature. The distribution of this feature was mathematically represented using a function. This approach facilitated the characterization of the extent of muscle tissue impairment in individuals who have experienced a stroke. Additionally, Pearson's correlation coefficient between the reference feature and each of the other 20 extracted features was calculated, following the same established criteria as before [40]. Features exhibiting a correlation coefficient greater than 0.8 with the reference feature and a p-value < 0.05 were selected as possible features of interest. These features were chosen due to their potential to complement the reference feature, indicating the strongest and statistically significant associations.

Finally, the mean and standard deviation of each of the four grades of the modified Heckmatt scale were calculated using the reference feature values, allowing its dispersion to be visualized along the distribution graph. In addition, to determine whether statistically significant differences existed between the groups, an ANOVA test or a Kruskal–Wallis test was performed, depending on the normality of the data distribution. Normality was assessed by examining histograms and Q-Q plots. If statistically significant differences ($p < 0.05$) between groups were detected, a post hoc analysis was performed using Tukey's honest significant difference or the Bonferroni correction to identify which specific pairs of groups showed significant differences.

Data pre-processing and visualization, the image analysis, and the machine learning analysis were performed in Python, version 3.11.5, using libraries such as numpy, os, matplotlib, random, string, PIL, skimage.feature, mahotas.features.texture, cv2, pandas, scipy.stats, scipy.optimize, sklearn.metrics, and sklearn. The programming environment used was JupyterLab, version 4.0.11. The statistical analyses were performed in RStudio, version 2024.09.0.

3. Results

A total of 130 ROIs extracted from US images of the gastrocnemius medialis muscles of both the lower limbs of 22 stroke-affected individuals were analyzed. The sample consisted of 16 (72.73%) men and 6 (27.27%) women, with a mean age of 64.32 ± 13.25 years. The distribution of time since the stroke onset among the participants was as follows: five participants (6 to <12 months), eleven participants (12 to <24 months), five participants (24 to <36 months), and one participant (36 to <40 months). Of the participants, 5 had experienced a hemorrhagic stroke and 17 had an ischemic stroke. Notably, only one participant was on spasticity medication during the study.

Following the selection of the ROIs and a subsequent analysis of the extracted features, three features (EV, EI, and kurtosis) were identified based on the methodology described. These features were the most informative for assessing gastrocnemius medialis muscle tissue impairment in individuals who had experienced a stroke. Specifically, reduced values of EV and kurtosis indicated greater muscle tissue impairment, while the EI had the highest values (Table 2). After the image classification by the third physiotherapist using the modified Heckmatt scale, the analysis revealed a very strong and significant correlation for the EV ($r = -0.81$, $p < 0.001$) and the EI ($r = 0.87$, $p < 0.001$), but not for kurtosis ($r = -0.37$, $p < 0.001$).

The mathematical function for the distribution of the EV was calculated and fitted using the model $y = ae^{bx} + ce^{dx} + E$ with parameter estimates of $a = 37.13$, $b = -0.14$, $c = 132{,}052.16$, $d = -2 \times 10^{-6}$, and $E = -131{,}990.30$. This model demonstrated a high degree of accuracy, as evidenced by an R^2 error rate of 0.993, indicating that the function effectively represents the distribution of the EV. The graphical representation of this distribution is shown in Figure 3, where lower EV values along the Y-axis correspond to images in which experts identified the muscle tissue as having a poorer quality and more significant impairment (as illustrated in Supplementary Figure S1). Conversely, higher EV values were

associated with images of less impaired muscle tissue, suggesting an improved quality (Supplementary Figure S2). The location of each of the US images shown as an example of low and high EV along the distribution in Figure 3 is presented as Supplementary Figure S3.

Table 2. The evaluation process was conducted by two physiotherapists using ultrasound images with the top and bottom 10 values of each echotexture feature. The number of images was categorized based on consistency with more affected muscle tissue patterns.

Features	Top 10 Values		Bottom 10 Values	
	Physiotherapist 1	Physiotherapist 2	Physiotherapist 1	Physiotherapist 2
Echointensity *	10/10	10/10	0/10	0/10
Variance	8/10	10/10	7/10	8/10
Standard deviation	9/10	10/10	7/10	7/10
Echovariation *	0/10	0/10	10/10	10/10
Skew	2/10	3/10	10/10	10/10
Kurtosis *	0/10	0/10	10/10	10/10
Correlation	8/10	8/10	4/10	3/10
Dissimilarity	1/10	1/10	5/10	5/10
Contrast	3/10	4/10	5/10	5/10
Homogeneity	2/10	2/10	5/10	5/10
ASM	3/10	4/10	7/10	9/10
Energy	0/10	0/10	5/10	7/10
Max probability	0/10	0/10	7/10	8/10
Entropy	7/10	7/10	8/10	8/10
Cluster shade	8/10	10/10	2/10	2/10
Cluster prominence	7/10	10/10	1/10	1/10
SRE	8/10	9/10	7/10	8/10
LRE	3/10	3/10	7/10	9/10
GLU	8/10	8/10	10/10	10/10
RLU	10/10	10/10	10/10	10/10
RPC	10/10	10/10	9/10	9/10

Features marked with an asterisk (*) indicate those that met the criteria to be selected as the most informative features. For example, an indicator showing a score of 0/10 for the top 10 values and 10/10 for the bottom 10 values (or vice versa) would be optimal.
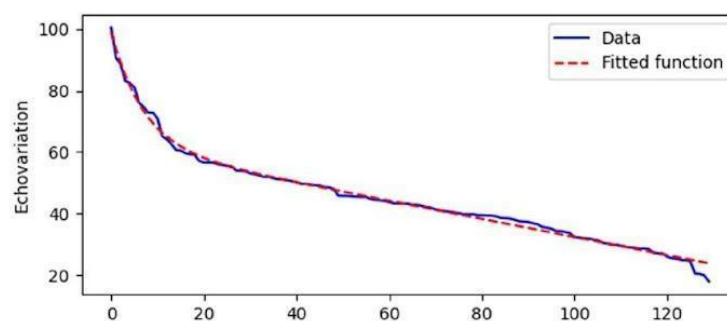
Figure 3. Graph showing the fitted distribution of EV values across ROIs. The scale on the X-axis shows the number of the US image, while the Y-axis shows the echovariation (EV) values.

The correlations between the EV and the other features are detailed in Table 3. Among these features, only the EI showed a Pearson's correlation coefficient greater than 0.8, demonstrating a statistically significant relationship ($p < 0.05$) with a value of -0.90. This indicates a strong inverse correlation, suggesting that, as the EI increases, the EV decreases, and vice versa. The correlation plot illustrating the relationship between the EI and the EV is presented in Figure 4. In this plot, the data were sorted by the EV in descending order,

and the values were subsequently normalized on a scale from 0 to 1 (Figure 4). Additional correlations are provided in the Supplementary Material (Supplementary Figure S4).

Table 3. Correlations between each echotexture feature with echovariation (EV) as a reference.

Feature	Correlation	*p*-Value
Echointensity	−0.90 *	<0.001 [a]
Variance	0.34	<0.001 [a]
Standard deviation	0.35	<0.001 [a]
Skew	0.68	<0.001 [a]
Kurtosis	0.46	<0.001 [a]
Correlation	0.21	0.019 [a]
Dissimilarity	0.03	0.753
Contrast	0.18	0.040 [a]
Homogeneity	0.53	<0.001 [a]
ASM	0.62	<0.001 [a]
Energy	0.65	<0.001 [a]
Max probability	0.72	<0.001 [a]
Entropy	−0.20	0.024 [a]
Cluster shade	−0.23	0.009 [a]
Cluster prominence	−0.37	<0.001 [a]
SRE	−0.12	0.190
LRE	0.38	<0.001 [a]
GLU	−0.14	0.116
RLU	−0.08	0.349
RPC	0.03	0.740

[a] Statistically significant differences (*p*-value < 0.05); * correlations with a Pearson's coefficient > 0.80.
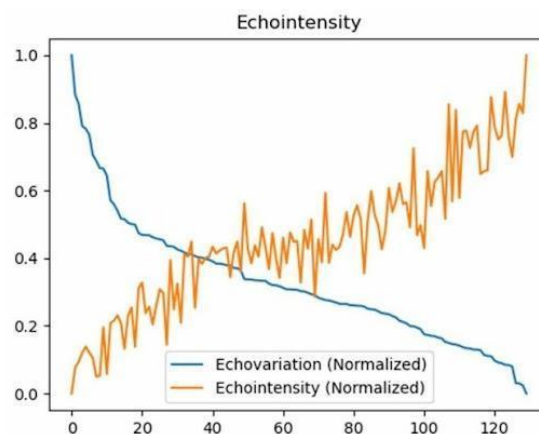
Figure 4. Graphical representation of the correlation between echovariation (EV) and echointensity (EI), the only one that showed a Pearson's correlation coefficient > 0.80. The scale on the X-axis shows the number of the US image, while the Y-axis shows the echovariation (EV) and echointensity (EI) values normalized on a scale from 0 to 1.

After assessing the normality of the data, the Kruskal–Wallis test was performed to assess any differences that existed between the EV values according to the four grades of the modified Heckmatt scale, which revealed statistically significant differences between the four grades ($p < 0.001$) (Table 4). A subsequent post hoc analysis, using the Bonferroni correction, confirmed that significant differences existed between all possible pairs of groups, with each comparison reaching statistical significance ($p < 0.001$) (Table 4). Figure 5 illustrates the distribution of EV values across the four grades of the modified Heckmatt

scale. For each grade, the mean and standard deviation are shown, providing a clear visualization of the distribution and variability of the data (Figure 5).

Table 4. Descriptive data and comparison analyses of echovariation (EV) values across the four grades of the modified Heckmatt scale.

Feature	Grade 1 (n = 24)	Grade 2 (n = 58)	Grade 3 (n = 24)	Grade 4 (n = 24)	Between-Group Comparison (Kruskal–Wallis Test)	Post Hoc Analysis (Wilcoxon Tests with Bonferroni Correction)
Echovariation	67.28 ± 15.05	46.62 ± 7.17	37.16 ± 4.94	26.85 ± 4.06	<0.001 [a]	Grade 1 vs. Grade 2: <0.001 [a] Grade 1 vs. Grade 3: <0.001 [a] Grade 1 vs. Grade 4: <0.001 [a] Grade 2 vs. Grade 3: <0.001 [a] Grade 2 vs. Grade 4: <0.001 [a] Grade 3 vs. Grade 4: <0.001 [a]

Data are presented as mean ± standard deviation; [a] statistically significant difference (p-value < 0.05).
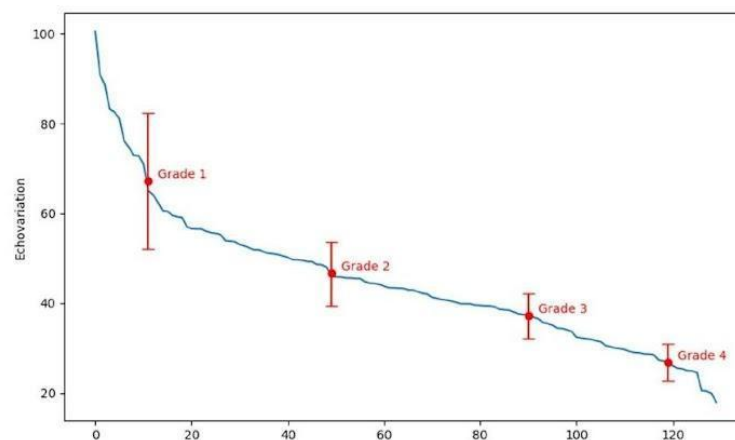
Figure 5. Distribution of the four grades of the modified Heckmatt scale along echovariation (EV) values, with mean and standard error bars for each grade. The scale on the X-axis shows the number of the US image, while the Y-axis shows the echovariation (EV) values.

4. Discussion

One of the existing needs in the analysis of muscle tissue quality is to have an indicator that can be used to quantify the degree of muscle impairment more objectively than qualitative scales such as the original or modified Heckmatt scale, which has been the most widely used to date, despite its limitations. An US is cost-effective in assessing muscle tissue and could serve as an objective tool [41]. In line with our aim to identify the most informative echotexture features for characterizing the degree of muscle tissue impairment in the gastrocnemius medialis of stroke-affected individuals, the findings of our study suggest that the EV, EI, and kurtosis may be the most informative features initially.

Considering the correlation between the modified Heckmatt scale and the three most informative features, the EV and EI seemed the most informative. Different factors were considered to propose only one feature that would be more easily transferable to clinical practice, resulting in the EV being considered the most suitable feature for several reasons: (1) previous studies have consistently identified the EV as a significant metric for assessing muscle tissue across various neuromusculoskeletal conditions; (2) the EV includes the EI in its calculation, as it is defined as the standard deviation of pixel intensity divided by the mean pixel intensity (which constitutes the EI); (3) the EV can be considered a relative measure that is inherently less susceptible to variations in the US image and device settings,

unlike the EI, which is significantly influenced by settings such as the gain; (4) the EV is a better measure of the overall relative variability when compared with kurtosis, that takes into account only the extreme values, losing the information between the extremes; and (5) when the EV values were analyzed, there were significant differences between the different grades in the modified Heckmatt scale, which supports the use of this indicator as a complement to quantify the degree of muscle impairment objectively. The decision to retain only one feature was made to enhance its clinical applicability and facilitate its transferability to practical settings.

Based on a mathematical model and considering that the pixel intensity values from greyscale images may range from 0 (black) to 255 (white), when the image is uniform (i.e., standard deviation—σ—is small) and the mean (μ) approaches its maximum value of 255 (all pixels white), the EV is at its lowest. Conversely, when the image is more heterogeneous (i.e., σ is big) and μ approaches its minimum value (all pixels blacker), the EV is at its highest. These observations led us to hypothesize that lower EV values correspond to poorer muscle tissue quality, while higher EV values indicate better muscle tissue quality. Additional details regarding this hypothesis are provided in Supplementary Figure S5.

This hypothesis recognizes the relationship between EV and muscle tissue quality without attempting to restrict the EV range artificially. Although this study was performed specifically on stroke-affected individuals, we believe its underlying principles can potentially be extended to assessing healthy muscles and muscles in other populations with different pathologies/conditions. However, further research into its use is needed to validate the applicability and determine with confidence the generalizability of this model to other populations, including the healthy population, in an attempt to define a normalized score for muscle tissue.

The proposed model offers a robust framework for quantitatively assessing muscle tissue quality in stroke-affected individuals, addressing limitations inherent to the modified Heckmatt scale, which categorizes impairment into four discrete grades. By providing a more detailed measurement of muscle tissue quality, our model enables physiotherapists to detect subtle variations in muscle tissue that categorical scales may overlook. This capability is crucial for tracking changes over time, responding to therapeutic interventions, and objectively evaluating injury progression and prognoses. For instance, the modified Heckmatt scale might categorize two images as reflecting the same degree of muscle impairment, despite variations in their EV values. Though clinically relevant, such differences remain undetected by the modified Heckmatt scale or even through visual inspection by clinicians. Therefore, using an indicator like the EV may provide additional value in clinical practice compared to a clinical scale like the Heckmatt scale, since it allows for the more granular or objective quantification of muscle impairment. There is still controversy about the modified Heckmatt scale, with recent studies suggesting that it would be better to reduce it from four to three grades [42].

Although the modified Heckmatt scale is based on the EI, we propose the EV as a more reliable indicator than the EI based on our results. Our results indicate that higher EV values are associated with healthier or higher-quality muscle tissue, while lower EV values correspond to more severely impaired muscle tissue in stroke-affected individuals. Conversely, the relationship is inverted for the EI; higher EI values mean a poorer muscle tissue quality, whereas lower EI values indicate a greater similarity to healthy muscle tissue. The strong correlation between the EV and EI allows us to assert that, as muscle tissue becomes increasingly impaired, the EI values will rise while the EV values will decline.

From a clinical perspective, it may be beneficial to consider the complementary use of both the EV and EI in assessing muscle tissue characteristics. While we have presented evidence supporting the relevance of the EV, the EI remains a familiar metric among physiotherapists. Utilizing both may mitigate the limitations inherent to each when assessed in isolation, thereby reducing potential biases and enhancing the overall characterization of muscle tissue. In light of this, the EV shows great potential for practical applications

in clinical settings, particularly as an indicator for monitoring rehabilitation progress and guiding therapeutic decisions. By providing quantitative assessments of muscle tissue quality, the EV complements existing qualitative scales, enabling the detection of subtle changes in muscle composition. For instance, during the rehabilitation process, changes in the EV values may help a clinician quantify the treatment's effects over time or the adverse effects of some treatments, such as botulinum toxin injection. Furthermore, the EV could serve as a diagnostic tool for stratifying patients according to the severity of muscle impairment, helping to develop personalized rehabilitation plans and more targeted therapeutic strategies [43]. Our findings establish EV as a promising indicator, but its clinical implementation requires further validation and research.

Our results are similar to those observed in individuals with amyotrophic lateral sclerosis, where the muscles affected also show an increased EI and a reduced EV [44]. However, in contrast to our findings, GLCM features have been identified as relevant in amyotrophic lateral sclerosis [14]. Similarly, the EV has been shown to discriminate between different types of soleus injuries based on the EI patterns [45]. It has also been used to differentiate between the plantar extrinsic musculature and the plantar fascia in individuals with plantar fasciitis compared to healthy controls [28,46], as well as in individuals with patellar tendinopathy who have a higher EV compared to healthy controls [47].

One of the challenges of a texture analysis is knowing how to handle the large amount of data that can be extracted from a single image, as there can be hundreds of parameters, which means that, even for that reason alone, high correlations can be found between them [4]. In our study, we reduced twenty-one initial features to just one, combining an exploratory analysis and different factors that may affect the possibility of comparing the results and translating them into clinical practice. Another critical challenge is the significant variability between the programs/software that calculate these echotexture features, which makes it difficult to compare and interpret the results. However, concerning the first-order features, an excellent concordance has been demonstrated between software packages [48]. This reinforces our results regarding considering the EV (first-order feature) as the main feature for characterizing muscle tissue quality in individuals who have suffered a stroke.

The results presented in this study mix a clinical point of view, based on expert physiotherapists, with a technical point of view, based on a data analysis and programming without any data pre-processing. The main strengths of our study are the absence of possible biases in the selection of the ROI, with the collection of the maximum amount of muscle tissue to prevent the loss of relevant information, together with the standardization of the US image collection protocol and the clarity with which all the settings, features, and programs used have been shown. However, the results of this study are subject to certain limitations inherent in its observational design. Firstly, various factors that could affect US imaging, such as the age [49], sex [6], muscle strength [50], amount of skin, fascia, subcutaneous adipose tissue [51,52], genetic and epigenetic components [53], time from stroke onset, and prior therapeutic interventions received, among others, were not considered. We considered the standardized image collection procedure to be a strength, although it could also be understood as a limitation, since we do not know if it can be extrapolated to the rest of the gastrocnemius muscle areas or if there are differences between both sides or between different muscles. However, considering that this is a chronic condition, we assumed that the degree of impairment would be similarly distributed throughout the muscle, which does not occur in other conditions like muscle tears. Furthermore, despite the large number of US images used, they were only extracted from 22 stroke-affected individuals, which is a notable limitation of the study, as it restricts the generalizability of the findings to the general population. However, the results are a starting point for other studies on the same population and on populations with different pathologies. Lastly, another limitation is the absence of formal inter- and intra-rater reliability testing for the muscle tissue quality assessments. Although minimal inter-rater discrepancies were observed, conducting such

assessments in future research would strengthen the robustness and reproducibility of the findings.

Although this was an observational study in which the capacity of different echotexture features to characterize the gastrocnemius medialis muscle tissue quality in stroke-affected individuals was studied, it could be interesting to explore their use in the follow-up and evolution of patients and the analysis of the effectiveness of treatments, as has been proposed for other echotexture features in different populations [54].

5. Conclusions

Based on a mixed technical and clinical approach, the EV proved to be the most informative echotexture feature for quantifying the degree of muscle tissue impairment in the gastrocnemius medialis of post-stroke individuals, with a higher EV indicating a better muscle tissue quality. The EV represents a cost-effective and non-invasive method for assessing muscle tissue characteristics, providing a valuable alternative to other imaging modalities. Furthermore, the EV offers a promising tool for monitoring stroke rehabilitation and could be explored in other neuromuscular conditions.

Supplementary Materials: The following supporting information can be downloaded at: https://www.mdpi.com/article/10.3390/jcm13247800/s1. Figure S1: Example of an ultrasound image exhibiting a high value of echovariation; Figure S2: Example of an ultrasound image exhibiting a low value of echovariation; Figure S3: Location of the US images presented as Figures S1 and S2 along the EV distribution graph; Figure S4: Correlation plots of each feature with the reference feature (echovariation); Figure S5: Proposed hypothesis for echovariation as an informative feature of muscle tissue quality.

Author Contributions: Conceptualization, B.A. and P.H.; methodology, B.A., C.P.-F., P.H. and D.L.-H.; software, B.A.; validation, C.P.-F., P.H. and D.L.-H.; formal analysis, B.A. and D.L.-H.; investigation, B.A., C.P.-F. and D.L.-H.; data curation, B.A.; writing—original draft, B.A., A.C.-O., S.C., P.H. and D.L.-H.; writing—review & editing, B.A., C.P.-F., A.C.-O., S.C., P.H. and D.L.-H.; supervision, P.H.; project administration, P.H. and D.L.-H. All authors have read and agreed to the published version of the manuscript.

Funding: This research received no external funding.

Institutional Review Board Statement: This study was conducted in accordance with the Declaration of Helsinki and approved by the Aragon Ethics Committee (protocol code PI24/030 and date of 7 February 2024).

Informed Consent Statement: Informed consent was obtained from all the subjects involved in this study. Written informed consent was obtained from the patients to publish this paper.

Data Availability Statement: The data presented in this study are available from the corresponding author upon request, due to the fact that these data are part of a larger, ongoing project and may not yet be fully available for public sharing until the project is completed.

Acknowledgments: The authors want to thank Alberto Cebollada from the Biocomputing Unit, Institute for Health Sciences in Aragon (IACS), Zaragoza, Spain, for his support and advice on the statistical analysis.

Conflicts of Interest: The authors declare no conflicts of interest.

References

1. Vollset, S.E.; Ababneh, H.S.; Abate, Y.H.; Abbafati, C.; Abbasgholizadeh, R.; Abbasian, M.; Abbastabar, H.; Abd Al Magied, A.H.A.; ElHafeez, S.A.; Abdelkader, A.; et al. Burden of Disease Scenarios for 204 Countries and Territories, 2022–2050: A Forecasting Analysis for the Global Burden of Disease Study 2021. *Lancet* **2024**, *403*, 2204–2256. [CrossRef] [PubMed]
2. Saini, V.; Guada, L.; Yavagal, D.R. Global Epidemiology of Stroke and Access to Acute Ischemic Stroke Interventions. *Neurology* **2021**, *97*, S6–S16. [CrossRef] [PubMed]
3. Zwanenburg, A.; Vallières, M.; Abdalah, M.A.; Aerts, H.J.W.L.; Andrearczyk, V.; Apte, A.; Ashrafinia, S.; Bakas, S.; Beukinga, R.J.; Boellaard, R.; et al. The Image Biomarker Standardization Initiative: Standardized Quantitative Radiomics for High-Throughput Image-Based Phenotyping. *Radiology* **2020**, *295*, 328–338. [CrossRef] [PubMed]

4. Scalco, E.; Rizzo, G. Texture Analysis of Medical Images for Radiotherapy Applications. *Br. J. Radiol.* **2017**, *90*, 20160642. [CrossRef]
5. Bharati, M.H.; Liu, J.J.; MacGregor, J.F. Image Texture Analysis: Methods and Comparisons. *Chemom. Intell. Lab. Syst.* **2004**, *72*, 57–71. [CrossRef]
6. Molinari, F.; Caresio, C.; Acharya, U.R.; Mookiah, M.R.K.; Minetto, M.A. Advances in Quantitative Muscle Ultrasonography Using Texture Analysis of Ultrasound Images. *Ultrasound Med. Biol.* **2015**, *41*, 2520–2532. [CrossRef]
7. Gillies, R.J.; Kinahan, P.E.; Hricak, H. Radiomics: Images Are More than Pictures, They Are Data. *Radiology* **2016**, *278*, 563–577. [CrossRef]
8. Berenguer, R.; Del Rosario Pastor-Juan, M.; Canales-Vázquez, J.; Castro-García, M.; Villas, M.V.; Legorburo, F.M.; Sabater, S. Radiomics of CT Features May Be Nonreproducible and Redundant: Influence of CT Acquisition Parameters. *Radiology* **2018**, *288*, 407–415. [CrossRef]
9. Sollini, M.; Antunovic, L.; Chiti, A.; Kirienko, M. Towards Clinical Application of Image Mining: A Systematic Review on Artificial Intelligence and Radiomics. *Eur. J. Nucl. Med. Mol. Imaging* **2019**, *46*, 2656. [CrossRef]
10. Hatt, M.; Tixier, F.; Pierce, L.; Kinahan, P.E.; Le Rest, C.C.; Visvikis, D. Characterization of PET/CT Images Using Texture Analysis: The Past, the Present... Any Future? *Eur. J. Nucl. Med. Mol. Imaging* **2017**, *44*, 151–165. [CrossRef]
11. Correa-de-Araujo, R.; Harris-Love, M.O.; Miljkovic, I.; Fragala, M.S.; Anthony, B.W.; Manini, T.M. The Need for Standardized Assessment of Muscle Quality in Skeletal Muscle Function Deficit and Other Aging-Related Muscle Dysfunctions: A Symposium Report. *Front. Physiol.* **2017**, *8*, 87. [CrossRef] [PubMed]
12. Chow, R.S.; Medri, M.K.; Martin, D.C.; Leekam, R.N.; Agur, A.M.; McKee, N.H. Sonographic Studies of Human Soleus and Gastrocnemius Muscle Architecture: Gender Variability. *Eur. J. Appl. Physiol.* **2000**, *82*, 236–244. [CrossRef]
13. Reeves, N.D.; Maganaris, C.N.; Narici, M. Ultrasonographic Assessment of Human Skeletal Muscle Size. *Eur. J. Appl. Physiol.* **2004**, *91*, 116–118. [CrossRef] [PubMed]
14. Martínez-Payá, J.J.; Ríos-Díaz, J.; Del Baño-Aledo, M.E.; Tembl-Ferrairó, J.I.; Vazquez-Costa, J.F.; Medina-Mirapeix, F. Quantitative Muscle Ultrasonography Using Textural Analysis in Amyotrophic Lateral Sclerosis. *Ultrason. Imaging* **2017**, *39*, 357–368. [CrossRef] [PubMed]
15. Behr, M.; Noseworthy, M.; Kumbhare, D. Feasibility of a Support Vector Machine Classifier for Myofascial Pain Syndrome: Diagnostic Case-Control Study. *J. Ultrasound Med.* **2019**, *38*, 2119–2132. [CrossRef]
16. Del-Canto-fernández, A.; Calleja-Martínez, P.; Descalzo-Hoyas, B.; Rodríguez-Posada, S.; Cuenca-Zaldívar, N.; Fernández-Carnero, S.; Naranjo-Cinto, F.; Gallego-Izquierdo, T. The Application of Image Texture Analysis Techniques on the Effects of Dry Needling versus Placebo in Low-Back Pain Patients: A Pilot-Study. *Appl. Sci.* **2022**, *12*, 5556. [CrossRef]
17. Paris, M.T.; Mourtzakis, M. Muscle Composition Analysis of Ultrasound Images: A Narrative Review of Texture Analysis. *Ultrasound Med. Biol.* **2021**, *47*, 880–895. [CrossRef]
18. Alter, K.E.; Karp, B.I. Ultrasound Guidance for Botulinum Neurotoxin Chemodenervation Procedures. *Toxins* **2017**, *10*, 18. [CrossRef]
19. Pillen, S.; Arts, I.M.P.; Zwarts, M.J. Muscle Ultrasound in Neuromuscular Disorders. *Muscle Nerve* **2008**, *37*, 679–693. [CrossRef]
20. Heckmatt, J.Z.; Dubowitz, V. Ultrasound Imaging and Directed Needle Biopsy in the Diagnosis of Selective Involvement in Muscle Disease. *J. Child. Neurol.* **1987**, *2*, 205–213. [CrossRef]
21. Akazawa, N.; Harada, K.; Okawa, N.; Kishi, M.; Tamura, K.; Moriyama, H. Changes in Quadriceps Thickness and Echo Intensity in Chronic Stroke Survivors: A 3-Year Longitudinal Study. *J. Stroke Cerebrovasc. Dis.* **2021**, *30*, 105543. [CrossRef] [PubMed]
22. Heckmatt, J.Z.; Leeman, S.; Dubowitz, V. Ultrasound Imaging in the Diagnosis of Muscle Disease. *J. Pediatr.* **1982**, *101*, 656–660. [CrossRef] [PubMed]
23. Moreta, M.C.; Fleet, A.; Reebye, R.; McKernan, G.; Berger, M.; Farag, J.; Munin, M.C. Reliability and Validity of the Modified Heckmatt Scale in Evaluating Muscle Changes With Ultrasound in Spasticity. *Arch. Rehabil. Res. Clin. Transl.* **2020**, *2*, 100071. [CrossRef] [PubMed]
24. Pillen, S.; Van Alfen, N. Muscle Ultrasound from Diagnostic Tool to Outcome Measure--Quantification Is the Challenge. *Muscle Nerve* **2015**, *52*, 319–320. [CrossRef]
25. Pillen, S.; van Alfen, N. Skeletal Muscle Ultrasound. *Neurol. Res.* **2011**, *33*, 1016–1024. [CrossRef]
26. Michailovich, O.V.; Tannenbaum, A. Despeckling of Medical Ultrasound Images. *IEEE Trans. Ultrason. Ferroelectr. Freq. Control* **2006**, *53*, 64. [CrossRef]
27. Martínez-Payá, J.J.; Ríos-Díaz, J.; Medina-Mirapeix, F.; Vázquez-Costa, J.F.; del Baño-Aledo, M.E. Monitoring Progression of Amyotrophic Lateral Sclerosis Using Ultrasound Morpho-Textural Muscle Biomarkers: A Pilot Study. *Ultrasound Med. Biol.* **2018**, *44*, 102–109. [CrossRef]
28. Ríos-Díaz, J.; Martínez-Payá, J.J.; del Baño-Aledo, M.E.; de Groot-Ferrando, A.; Botía-Castillo, P.; Fernández-Rodríguez, D. Sonoelastography of Plantar Fascia: Reproducibility and Pattern Description in Healthy Subjects and Symptomatic Subjects. *Ultrasound Med. Biol.* **2015**, *41*, 2605–2613. [CrossRef]
29. Lubner, M.G.; Smith, A.D.; Sandrasegaran, K.; Sahani, D.V.; Pickhardt, P.J. CT Texture Analysis: Definitions, Applications, Biologic Correlates, and Challenges. *Radiographics* **2017**, *37*, 1483–1503. [CrossRef]
30. Vandenbroucke, J.P.; von Elm, E.; Altman, D.G.; Gøtzsche, P.C.; Mulrow, C.D.; Pocock, S.J.; Poole, C.; Schlesselman, J.J.; Egger, M.; Blettner, M.; et al. Strengthening the Reporting of Observational Studies in Epidemiology (STROBE): Explanation and Elaboration. *Int. J. Surg.* **2014**, *12*, 1500–1524. [CrossRef]

31. Shrestha, B.; Dunn, L. The Declaration of Helsinki on Medical Research Involving Human Subjects: A Review of Seventh Revision. *J. Nepal. Health Res. Counc.* **2020**, *17*, 548–552. [CrossRef] [PubMed]

32. Perkisas, S.; Baudry, S.; Bauer, J.; Beckwée, D.; De Cock, A.M.; Hobbelen, H.; Jager-Wittenaar, H.; Kasiukiewicz, A.; Landi, F.; Marco, E.; et al. Application of Ultrasound for Muscle Assessment in Sarcopenia: Towards Standardized Measurements. *Eur. Geriatr. Med.* **2018**, *9*, 739–757. [CrossRef] [PubMed]

33. Caresio, C.; Molinari, F.; Emanuel, G.; Minetto, M.A. Muscle Echo Intensity: Reliability and Conditioning Factors. *Clin. Physiol. Funct. Imaging* **2015**, *35*, 393–403. [CrossRef] [PubMed]

34. Gonzalez, R.C.; Woods, R.E. *Digital Image Processing*, 2nd ed.; Prentice Hall: Englewood Cliffs, NJ, USA, 2002; ISBN 0201180758.

35. Haralick, R.M.; Dinstein, I.; Shanmugam, K. Textural Features for Image Classification. *IEEE Trans. Syst. Man. Cybern.* **1973**, *SMC-3*, 610–621. [CrossRef]

36. Tsai, D.-M.; Hsiao, B. Automatic Surface Inspection Using Wavelet Reconstruction. *Pattern Recognit.* **2001**, *34*, 1285–1305. [CrossRef]

37. Galloway, M.M. Texture Analysis Using Gray Level Run Lengths. *Comput. Graph. Image Process.* **1975**, *4*, 172–179. [CrossRef]

38. Chu, A.; Sehgal, C.M.; Greenleaf, J.F. Use of Gray Value Distribution of Run Lengths for Texture Analysis. *Pattern Recognit. Lett.* **1990**, *11*, 415–419. [CrossRef]

39. Amadasun, M.; King, R. Texural Features Corresponding to Texural Properties. *IEEE Trans. Syst. Man. Cybern.* **1989**, *19*, 1264–1274. [CrossRef]

40. Chan, Y.H. Biostatistics 104: Correlational Analysis. *Singap. Med. J.* **2003**, *44*, 614–619.

41. Nijholt, W.; Scafoglieri, A.; Jager-Wittenaar, H.; Hobbelen, J.S.M.; van der Schans, C.P. The Reliability and Validity of Ultrasound to Quantify Muscles in Older Adults: A Systematic Review. *J. Cachexia Sarcopenia Muscle* **2017**, *8*, 702–712. [CrossRef]

42. Wijntjes, J.; Saris, C.; Doorduin, J.; van Alfen, N.; van Engelen, B.; Mul, K. Improving Heckmatt Muscle Ultrasound Grading Scale through Rasch Analysis. *Neuromuscul. Disord.* **2024**, *42*, 14–21. [CrossRef] [PubMed]

43. Picelli, A.; Bonetti, P.; Fontana, C.; Barausse, M.; Dambruoso, F.; Gajofatto, F.; Girardi, P.; Manca, M.; Gimigliano, R.; Smania, N. Is spastic muscle echo intensity related to the response to botulinum toxin type A in patients with stroke? A cohort study. *Arch. Phys. Med. Rehabil.* **2012**, *93*, 1253–1258. [CrossRef] [PubMed]

44. Martínez-Payá, J.J.; del Baño-Aledo, M.E.; Ríos-Díaz, J.; Tembl-Ferrairó, J.I.; Vázquez-Costa, J.F.; Medina-Mirapeix, F. Muscular Echovariation: A New Biomarker in Amyotrophic Lateral Sclerosis. *Ultrasound Med. Biol.* **2017**, *43*, 1153–1162. [CrossRef] [PubMed]

45. De-La-cruz-torres, B.; Romero-Morales, C. Muscular Echovariation as a New Biomarker for the Classification of Soleus Muscle Pathology: A Cross-Sectional Study. *Diagnostics* **2021**, *11*, 1884. [CrossRef] [PubMed]

46. Canosa-Carro, L.; López-López, D.; García-Sanz, F.; Díaz-Meco-conde, R.; García-Bermejo, P.; De-La-cruz-torres, B.; Marszalek, J.; Romero-Morales, C. Features of Extrinsic Plantar Muscles in Patients with Plantar Fasciitis by Ultrasound Imaging: A Retrospective Case Control Research. *Diagnostics* **2022**, *12*, 897. [CrossRef]

47. Molina-Payá, F.J.; Ríos-Díaz, J.; Carrasco-Martínez, F.; Martínez-Payá, J.J. Infrared Thermography, Intratendon Vascular Resistance, and Echotexture in Athletes with Patellar Tendinopathy: A Cross-Sectional Study. *Ultrason. Imaging* **2023**, *45*, 47–61. [CrossRef]

48. Foy, J.J.; Robinson, K.R.; Li, H.; Giger, M.L.; Al-Hallaq, H.; Armato, S.G. Variation in Algorithm Implementation across Radiomics Software. *J. Med. Imaging* **2018**, *5*, 044505. [CrossRef]

49. Watanabe, Y.; Ikenaga, M.; Yoshimura, E.; Yamada, Y.; Kimura, M. Association between Echo Intensity and Attenuation of Skeletal Muscle in Young and Older Adults: A Comparison between Ultrasonography and Computed Tomography. *Clin. Interv. Aging* **2018**, *13*, 1871–1878. [CrossRef]

50. Strasser, E.M.; Draskovits, T.; Praschak, M.; Quittan, M.; Graf, A. Association between Ultrasound Measurements of Muscle Thickness, Pennation Angle, Echogenicity and Skeletal Muscle Strength in the Elderly. *Age* **2013**, *35*, 2377–2388. [CrossRef]

51. Pillen, S.; Tak, R.O.; Zwarts, M.J.; Lammens, M.M.Y.; Verrijp, K.N.; Arts, I.M.P.; van der Laak, J.A.; Hoogerbrugge, P.M.; van Engelen, B.G.M.; Verrips, A. Skeletal Muscle Ultrasound: Correlation between Fibrous Tissue and Echo Intensity. *Ultrasound Med. Biol.* **2009**, *35*, 443–446. [CrossRef]

52. Young, H.J.; Jenkins, N.T.; Zhao, Q.; Mccully, K.K. Measurement of Intramuscular Fat by Muscle Echo Intensity. *Muscle Nerve* **2015**, *52*, 963–971. [CrossRef] [PubMed]

53. Pingel, J.; Bartels, E.M.; Nielsen, J.B. New Perspectives on the Development of Muscle Contractures Following Central Motor Lesions. *J. Physiol.* **2017**, *595*, 1027–1038. [CrossRef] [PubMed]

54. López-López, S.; Pareja-Galeano, H.; Almazán-Polo, J.; Cotteret, C.; Téllez-González, P.; Calvo-Lobo, C.; Perea-Unceta, L.; Romero-Morales, C. Quantitative Ultrasound Changes in Echotexture and Functional Parameters after a Multicomponent Training Program in Pre-Frailty Individuals: A Pilot Randomized Clinical Trial. *Healthcare* **2021**, *9*, 1279. [CrossRef] [PubMed]

Study 4

Article

Improving the Reliability of Muscle Tissue Characterization Post-Stroke: A Secondary Statistical Analysis of Echotexture Features

Borhan Asadi [1,2], Juan Nicolás Cuenca-Zaldívar [3,4,5,6], Alberto Carcasona-Otal [1,2], Pablo Herrero [1,2,*] and Diego Lapuente-Hernández [1,2]

[1] iHealthy Research Group, Instituto de Investigación Sanitaria (IIS) Aragon, University of Zaragoza, 50009 Zaragoza, Spain; basadi@iisaragon.es (B.A.); acarcasona@unizar.es (A.C.-O.); d.lapuente@unizar.es (D.L.-H.)
[2] Department of Physiatry and Nursing, Faculty of Health Sciences, University of Zaragoza, 50009 Zaragoza, Spain
[3] Grupo de Investigación en Fisioterapia y Dolor, Departamento de Enfermería y Fisioterapia, Facultad de Medicina y Ciencias de la Salud, Universidad de Alcalá, 28801 Alcalá de Henares, Spain; nicolas.cuenca@salud.madrid.org
[4] Research Group in Nursing and Health Care, Puerta de Hierro Health Research Institute—Segovia de Arana (IDIPHISA), 28222 Majadahonda, Spain
[5] Interdisciplinary Group on Musculoskeletal Disorders, Faculty of Sport Sciences, Universidad Europea de Madrid, 28670 Villaviciosa de Odón, Spain
[6] Primary Health Center "El Abajón", 28231 Las Rozas de Madrid, Spain
* Correspondence: pherrero@unizar.es; Tel.: +34-976761651 (ext. 4444)

Abstract: Background/Objectives: Ultrasound (US) imaging and echotexture analysis are emerging techniques for assessing muscle tissue quality in the post-stroke population. Clinical studies suggest that echovariation (EV) and echointensity (EI) serve as objective indicators of muscle impairment, although methodological limitations hinder their clinical translation. This secondary analysis aimed to refine the assessment of echotexture by using robust statistical techniques. **Methods:** A total of 130 regions of interest (ROIs) extracted from the gastrocnemius medialis of 22 post-stroke individuals were analyzed. First, inter-examiner reliability between two physiotherapists was assessed by using Cohen's kappa for muscle impairment classification (low/high) for each echotexture feature. For each examiner, the correlation between the classification of the degree of impairment and the modified Heckmatt scale for each feature was analyzed. The dataset was then reduced to 44 ROIs (one image per leg per patient) and assessed by three physiotherapists to analyze inter-examiner reliability by using Light´s kappa and correlation between both assessment methods globally. Statistical differences in 21 echotexture features were evaluated according to the degree of muscle impairment. A binary logistic regression model was developed by using features with a Cohen's kappa value greater than 0.9 as predictors. **Results:** A strong and significant degree of agreement was observed among the three examiners regarding the degree of muscle impairment (Kappa$_{light}$ = 0.85, $p < 0.001$), with nine of the 21 features showing excellent inter-examiner reliability. The correlation between muscle impairment classification with the modified Heckmatt scale was very high and significant both globally and for each echotexture feature. Significant differences (<0.05) were found for EV, EI, dissimilarity, energy, contrast, maximum likelihood, skewness, and the modified Heckmatt scale. Logistic regression highlighted dissimilarity, entropy, EV, Gray-Level Uniformity (GLU), and EI as the main predictors of muscle tissue impairment. The EV and EI models showed high explanatory power (Nagelkerke's pseudo-R^2 = 0.74 and 0.76) and robust classification performance (AUC = 94.20% and 95.45%). **Conclusions:** This secondary analysis confirms echotexture analysis as a reliable tool for post-stroke muscle assessment,

validating EV and EI as key indicators while identifying dissimilarity, entropy, and GLU as additional relevant features.

1. Introduction

In recent years, medical image analysis has become an essential tool in the health sciences to improve diagnostic accuracy, disease monitoring, and treatment assessment [1]. The integration of advanced algorithms, including digital image processing, deep learning, and mathematical modeling [2,3] has dramatically improved the ability to extract clinically relevant information from images. These methods facilitate the simulation and quantification of key image features such as texture, structure, and dynamic behavior of organs and tissues, providing clinicians with highly accurate, data-driven information to enhance pathology prognoses and optimize treatment selection [4]. Medical fields that have benefited the most from advanced imaging techniques include oncology [5] and cardiology [6], which remain the leading causes of morbidity and mortality worldwide.

In line with this trend, musculoskeletal research has also benefited from advanced image-based analysis, mainly through tools such as magnetic resonance imaging (MRI) or computed tomography (CT) [7,8], but more recently also through ultrasound (US) imaging and echotexture analysis [9]. Echotexture analysis involves extracting and processing structural and intensity distribution features from US images by using digital image analysis techniques. The most relevant parameters in this area include (1) first-order statistics, which describe the intensity distribution without considering spatial relationships; (2) Haralick features, derived from the gray-level co-occurrence matrix (GLCM), which quantify texture based on the spatial relationships between pixels [10,11]; and (3) gray-level run-length matrix (GLRLM) features, which assess intensity variability and uniformity within the image [12].

US imaging and echotexture analysis are particularly advantageous due to their non-invasive nature, accessibility, and cost-effectiveness, making them promising tools for assessing muscle tissue quality [9,13]. Their application has been extensively studied in various pathological conditions, such as stroke [14], amyotrophic lateral sclerosis [15,16], myofascial pain syndrome [17], chronic low back pain [18], metastatic breast cancer [19], and musculotendinous injuries [20,21], as well as in healthy individuals for various research purposes [22,23].

In the case of stroke, it is characterized by significant neuromuscular alterations produced by central motor pathway disruption, reduced voluntary activation, and peripheral disuse, which leads to pathophysiological changes such as muscle atrophy, fiber-type changes, and progressive replacement of hypoechoic contractile elements with fibrous and adipose tissue [24,25]. Early studies focused mainly on a combination of structural parameters, such as muscle thickness, pennation angle, and fascicle length [26,27], with other echotexture features, mainly echointensity (EI), which have been shown to correlate with clinical features such as spasticity and gait performance [28,29]. More recently, research interest has expanded to additional echotexture features, such as echovariation (EV), which quantifies tissue heterogeneity and may provide complementary information on muscle architecture and degeneration [14]. This research motivation directly led to the further exploration of echotexture features in the present study.

Despite its promising potential, the clinical application of echotexture analysis requires rigorous methodological validation to ensure its reliability, standardization, and repro-

ducibility before it can be incorporated into routine practice. The aforementioned study in post-stroke subjects [14] identified EV and EI as key objective indicators of muscle tissue deterioration, with EV showing a strong correlation with the modified Heckmatt scale, the current gold standard for the qualitative assessment of muscle tissue in individuals with stroke [30]. However, this initial study had several methodological limitations, including a potential selection bias in the US imaging dataset. Rather than using robust statistical validation, the analysis was based on the subjective opinion of expert physiotherapists on the 10 images with the highest values and 10 images with the lowest values for each echotexture feature from a dataset of 130 images. Given these limitations, thorough methodological validation is required before conclusions can be drawn and echotexture analysis can be implemented in daily clinical practice in the post-stroke population.

Recognizing these limitations, the present study aims to perform a secondary analysis to reduce the subjectivity and bias of the previous study by using more robust statistical methods to refine and validate its methodology [14]. In addition, this study aims to improve our understanding of the relationship between echotexture characteristics and clinical muscle classification in individuals who have suffered a stroke. Ultimately, this work aims to provide quantitative evidence to support the integration of echotexture analysis into clinical decision making for the assessment of muscle tissue.

2. Materials and Methods

To facilitate a clear understanding of the work developed in this secondary analysis, only the most relevant methodological information is presented in this section. Full details regarding the materials and methods are available in the original article [14], which this analysis is based upon.

2.1. Study Design

This secondary analysis was performed by using data from a previously published observational study of the post-stroke population by Asadi et al. [14]. The original study included 130 US images from 22 participants and is the basis for this secondary analysis. The study followed the STROBE guidelines [31] and the ethical principles described in the Declaration of Helsinki [32]. Ethical approval was granted by the Aragon Ethics Committee (PI24/030). The study was registered on ClinicalTrials.gov (NTC06411587).

2.2. Participants and Data Collection

In the original study, a physical medicine and rehabilitation specialist recruited post-stroke individuals at Hospital Clínico Universitario Lozano Blesa between February and April 2024. As this is a secondary analysis of existing data [14], the inclusion and exclusion criteria were predefined in the original study. Participants were eligible for inclusion if they were at least 18 years old, had a confirmed diagnosis of stroke based on CT or MRI, had suffered a stroke at least six months before enrollment, and could walk independently with or without assistive devices, with no additional requirements for specific motor impairment. People were excluded if they had other concurrent neurological disorders, such as ataxia or dystonia, had undergone lower-limb surgery, or had medical problems that could have interfered with data collection.

US images of the gastrocnemius medialis muscle were obtained by using the Butterfly iQ+ portable US system (Butterfly Network, Inc., Burlington, MA, USA) in B-mode, employing a linear transducer with a frequency range of 1 to 10 MHz. A standardized imaging protocol was followed with a gain setting of 50% and a depth range of 5–7 cm. Participants were seated with their knees flexed at a 90-degree angle. The US probe was placed at a point corresponding to 30% of the distance between the medial condyle of the

tibia and the medial malleolus, and the angle of the probe was adjusted to obtain an optimal image. Six images were collected from each participant, comprising three different images from each lower extremity, with only one region of interest (ROI) per image, specifically a whole-muscle ROI. The decision to assess the gastrocnemius medialis was determined in the original study design. This muscle has been analyzed in previous studies [28] since it plays a key role in gait mechanics, making it a clinically relevant muscle for assessing post-stroke impairment.

2.3. Echotexture Feature Extraction

In this secondary analysis, the researchers analyzed the original database, which contained the selected ROIs from the 130 US images used in the study by Asadi et al. [14]. In the original study, the ROIs were selected by two expert physiotherapists, who included as much muscle tissue surface area as possible in the ROI (whole-muscle ROI). In this secondary analysis, the same textural features as in the original study were extracted directly from the database: (1) first-order histogram-based features (see Table S1); (2) features derived from the gray-level co-occurrence matrix (GLCM) [10,33], computed by using an orientation of 0 degrees, a gray level of 256, and a pixel distance of 5 (see Table S2); and (3) features based on the gray-level run-length matrix (GLRLM) [12,34,35], calculated across five standard orientations (0, 45, 90, 90, 135, and 180 degrees) with a gray level of 16. The final texture features were obtained by averaging the run-length matrix data and the extracted parameters across all orientations (see Table S3).

2.4. Ultrasound Imaging Assessment

The original study published by Asadi et al. [14] performed an initial feature selection process to identify the most informative texture parameters for assessing muscle tissue impairment. Two independent expert physiotherapists (D.L.H. and P.H.) evaluated 420 ROIs (20 ROIs for each of the 21 echotexture features, selected from the 10 highest and 10 lowest values). Before the study, both physiotherapists jointly reviewed a set of sample US images to reach a consensus on the assessment criteria and standardize image interpretation procedures. Each image contained only one ROI, as it included the maximum amount of muscle, excluding fascia. Each ROI was classified according to two criteria: the degree of muscle tissue impairment, categorized as low or high loss of muscle tissue echotexture, and the modified Heckmatt scale, a four-point grading system, with higher values indicating greater impairment [36]. However, the original study did not analyze the inter-examiner reliability for the level of impairment (low–high), which was the first analysis performed in this study. After performing this reliability analysis, the correlation between the level of impairment, as assessed by the experts (low–high), and the modified Heckmatt scale was also calculated.

After this initial analysis of the original dataset, which was based on echotexture features, a secondary analysis was performed with only 44 ROIs, using a single US image per limb (whole-muscle ROI) per patient to eliminate redundancy and potential bias from multiple images of the same patient. The images were independently assessed by the first two physiotherapists (D.L.H. and P.H.) and a third expert physiotherapist (C.P.F.), who classified them according to the degree of muscle tissue impairment (low–high) and assigned a score based on the modified Heckmatt scale. To preserve methodological rigor and standardization, this third physiotherapist was trained by the first two examiners. The inter-examiner reliability for the level of impairment and the correlation between muscle tissue impairment and the modified Heckmatt scale was reassessed for this final dataset. With these 44 ROIs, a binary logistic regression model was developed by using the degree

of muscle tissue impairment as the dependent variable and the echotexture features with a Cohen's kappa coefficient greater than 0.9 as explanatory variables.

2.5. Statistical Analysis

All statistical analyses were performed by using R software (version 4.1.3; R Foundation for Statistical Computing, Vienna, Austria). A significance level of $p < 0.05$ was used. The Shapiro–Wilk test assessed the normality of quantitative variables, presented as means $\pm$ standard deviation (SD), while categorical variables were reported as absolute and relative frequencies.

The inter-examiner reliability for the level of muscle tissue impairment for each feature was assessed with Cohen's kappa statistic and that among the three examiners with Light's kappa statistic, with both cases being defined as poor (<0.6), moderate (0.6–0.8), strong (0.8–0.9), or excellent (>0.9) [37]. On the other hand, for each examiner, the correlation between the classification of the degree of impairment and the modified Heckmatt scale both globally and for each feature was analyzed based on the polychoric correlation matrix, defining it as negligible (<0.29), low (0.3–0.49), moderate (0.5–0.69), high (0.70–0.89), or very high (>0.90) [38].

In this secondary analysis, the presence of significant differences in echotexture features according to the degree of muscle tissue impairment was analyzed by using the Mann–Whitney U test, while differences in the modified Heckmatt scale were assessed by using Fisher's exact test. Regarding the binary regression model, a backward stepwise selection approach was applied to optimize the model, minimizing the Akaike Information Criterion (AIC) while excluding variables with a Variance Inflation Factor (VIF) greater than 5. Due to the correlation between EV and EI, separate models were generated by using each as the primary explanatory variable. From the final model, regression coefficients and odds ratios were estimated with their corresponding 95% confidence intervals (CIs) and significance levels. Model fit was assessed by comparing the deviation of the final model to that of the null model, assessing overall model effectiveness, and applying the Hosmer–Lemeshow goodness-of-fit test. The proportion of variance explained was quantified by using Nagelkerke's pseudo-R^2. Additionally, the relative contribution of each explanatory variable to the model was evaluated. To assess the model's predictive performance, receiver operating characteristic (ROC) curve analysis was performed, calculating sensitivity, specificity, area under the curve (AUC), and overall classification accuracy for each significant variable.

3. Results

The sample consisted of 16 (72.73%) males and 6 (27.27%) females, with a mean age of 64.32 ± 13.25 years. The inter-examiner reliability for the original 420 ROIs was excellent and significant for the variables EI, EV, dissimilarity, entropy, GLU, homogeneity, kurtosis, RLU, and RPC (Table S4). A strong and significant degree of agreement was also observed among the three examiners regarding the level of impairment (Kappa$_{light}$ = 0.85, $p < 0.001$). In addition, the correlation between each examiner's classification of muscle tissue impairment (low–high) and the modified Heckmatt scale grading was very high and significant in total (Examiner$_1$ = 0.98 (0.91, 0.99), Examiner$_2$ = 0.98 (0.90, 0.99), and Examiner$_3$ = 1 (1, 1)) and for all features (Table S5).

Of the 44 ROIs selected for this secondary analysis, 21 were classified as having low impairment, while the remaining 23 were classified as having high impairment. Statistically significant differences were observed in the level of muscle impairment for the variables EV, EI, dissimilarity, energy, contrast, maximum probability, skewness, and the modified Heckmatt scale ($p < 0.05$). Specifically, ROIs classified as low impairment had a higher

proportion of Heckmatt grades 1 and 2, while those classified as high impairment predominantly exhibited grades 3 and 4. In addition, all features evaluated, except EI, showed higher values in the low-impairment group and lower values in the high-impairment group. In contrast, EI showed opposite results, being significantly higher in the high-impairment group and significantly lower in the low-impairment group (Table 1).

Table 1. Descriptive statistics and comparison of echotexture features between ROIs classified as low and high impairment after the secondary analysis.

		Overall	Low Impairment	High Impairment	[a] *p*-Value
N		44	21	23	
Main outcomes					
Echovariation		46.26 ± 16.69	56.84 ± 16.52	36.60 ± 9.58	<0.001 *
Echointensity		82.89 ± 23.60	66.56 ± 17.92	97.80 ± 17.58	<0.001 *
Secondary outcomes					
Heckmatt scale, *n* (%)	Grade 1	3 (6.8)	3 (14.3)	0 (0.0)	<0.001 *
	Grade 2	21 (47.7)	18 (85.7)	3 (13.0)	
	Grade 3	12 (27.3)	0 (0.0)	12 (52.2)	
	Grade 4	8 (18.2)	0 (0.0)	8 (34.8)	
Variance		1237.73 ± 324.37	1267.46 ± 301.08	1210.59 ± 348.76	0.568
Standard deviation		34.87 ± 4.71	35.34 ± 4.42	34.45 ± 5.02	0.536
Skewness		0.50 ± 0.34	0.65 ± 0.32	0.37 ± 0.31	0.005 *
Kurtosis		0.03 ± 0.65	0.22 ± 0.81	−0.15 ± 0.40	0.056
Correlation		0.97 ± 0.01	0.97 ± 0.01	0.98 ± 0.01	0.103
Dissimilarity		5.97 ± 0.74	6.21 ± 0.81	5.75 ± 0.60	0.037 *
Energy		0.02 ± 0.01	0.03 ± 0.02	0.02 ± 0.00	0.042 *
Contrast		62.00 ± 14.82	68.20 ± 15.69	56.35 ± 11.65	0.007 *
Homogeneity		0.17 ± 0.03	0.18 ± 0.04	0.17 ± 0.02	0.444
Angular Second Moment		0.00 ± 0.00	0.00 ± 0.00	0.00 ± 0.00	0.058
Maximum probability		0.01 ± 0.02	0.01 ± 0.02	0.00 ± 0.00	0.013 *
Entropy		7.04 ± 0.22	7.00 ± 0.24	7.07 ± 0.20	0.275
Cluster Shade		8.03 ± 0.23	7.99 ± 0.25	8.07 ± 0.20	0.234
Cluster Prominence		10.87 ± 0.36	10.81 ± 0.42	10.92 ± 0.28	0.294
Short-Run Emphasis		0.73 ± 0.08	0.73 ± 0.07	0.72 ± 0.08	0.49
Long-Run Emphasis		440.64 ± 134.70	447.98 ± 173.53	433.94 ± 89.38	0.734
Gray-Level Uniformity		10,957.52 ± 2970.64	10,237.13 ± 2319.04	11,615.27 ± 3378.09	0.126
Run-Length Uniformity		17,268.72 ± 4566.54	17,109.75 ± 2938.33	17,413.87 ± 5732.68	0.828
Run Percentage		15.27 ± 3.28	15.37 ± 2.45	15.17 ± 3.95	0.837

Data are expressed as means ± standard deviation or as absolute and relative values (%). [a] significant if $p < 0.05$ (marked with asterisk).

After eliminating variables with a VIF greater than five and selecting the model with the lowest AIC, the final logistic regression model retained dissimilarity, entropy, EV, GLU, and EI as the main predictors of muscle tissue impairment. Additionally, the model including EV and the model including EI had a variance of 39, which is lower than the null model variance of 43, indicating a better model fit. In both models, the overall efficacy was statistically significant ($\chi^2(4) = 35.36$, $p < 0.001$ for EV; $\chi^2(4) = 37.38$, $p < 0.001$ for EI). The non-significant Hosmer–Lemeshow test ($\chi^2(8) = 4.94$, $p = 0.76$ for EV; $\chi^2(8) = 4.57$, $p = 0.80$

for EI) confirmed an overall satisfactory model fit. Nagelkerke's pseudo-R^2 indicated high explanatory power, with values of 0.74 and 0.76 for the EV and EI models, respectively. The model fit plots are shown in Figures S1 and S2.

For both models, the plot of the predicted values shows that the residuals do not exceed the band (-2, 2), indicating a good fit of the final model selected and its adequacy (Figures S1a and S2a). All the predicted values had a Cook's distance of less than 1, both with respect to the observed values and in terms of leverage, indicating the absence of influential values outside the normal limits. However, some atypical ones were observed (Figures S1b,c and S2b,c). The residuals and their standardized versions did not exceed the band (-2, 2) compared with the fitted values, indicating a good fit of the model and its adequacy (Figures S1d,e and S2d,e). The distribution of the residuals in the Q-Q plot was not normal (Figures S1f and S2f). Finally, the plot of residuals against leverage indicates the presence of some influential data (Figures S1b,S1 and S2b,h).

In the model including EV, the odds ratio indicated that for each unit increase in EV and dissimilarity, the probability of low impairment increased by 1.28 and 17.86 times, respectively. Conversely, for each unit increase in entropy, the odds of low impairment decreased significantly, by <0.001 times. In the model including EI, each unit increase in EI was associated with a 0.86-fold decrease in the probability of high impairment, while dissimilarity was associated with a 15.65-fold increase in the probability of high impairment. Of all the predictors, EV and EI contributed the most to their respective models (Table 2).

Table 2. Final model summary.

	Odds Ratio (95% CI)	Coefficient (SE)	95% CI	Z-Value ([a] *p*-Value)	Variable Importance
Echovariation main outcome model					
(Intercept)	7.77×10^{31} (111,740.12, 1.63×10^{73})	73.43 (SE = 38.61)	11.62, 168.57	0.057	
Echovariation	1.275 (1.1, 1.62)	0.24 (SE = 0.09)	0.09, 0.48	0.012 *	2.52
Dissimilarity	17.856 (2.61, 360)	2.88 (SE = 1.19)	0.96, 5.88	0.016 *	2.40
Entropy	<0.001 (0.001, 0.01)	-13.75 (SE = 6.31)	$-29.66, -3.98$	0.029 *	2.17
Gray-Level Uniformity	1 (0.99, 1)	0 (SE = 0)	$-0.001, 0$	0.154	1.42
Echointensity main outcome model					
(Intercept)	3.64×10^{20} (0, 5.00×10^{54})	47.34 (SE = 32.57)	$-8.6, 125.95$	0.146	
Echointensity	0.86 (0.74, 0.93)	-0.14 (SE = 0.05)	$-0.29, -0.06$	0.009 *	2.62
Dissimilarity	15.65 (2.33, 287.63)	2.75 (SE = 1.17)	0.84, 5.66	0.019 *	2.33
Entropy	0.001 (0, 5.02)	-6.69 (SE = 4.87)	$-18.43, 1.61$	0.170	1.37
Gray-Level Uniformity	1 (0.99, 1)	0 (SE = 0)	$-0.001, 0$	0.142	1.46

95% CI: 95% confidence interval; SE: Standard Error. [a] significant if *p* < 0.05 (marked with asterisk).

Both models showed high classification performance. The sensitivity of the EV and EI models was 90.48% in both cases, while the specificity rates were 86.96% and 95.65%, respectively. ROC curve analysis showed a significant AUC of 94.20% (95% CI: 87.39–100%) for the EV model and one of 95.45% (95% CI: 89.54–100%) for the EI model (Figure 1).

Regarding classification accuracy, the correct classification rate for EV was 22.73%, while that for EI was 84.09%. The classification rates for dissimilarity and entropy were 29.55% and 63.64%, respectively.
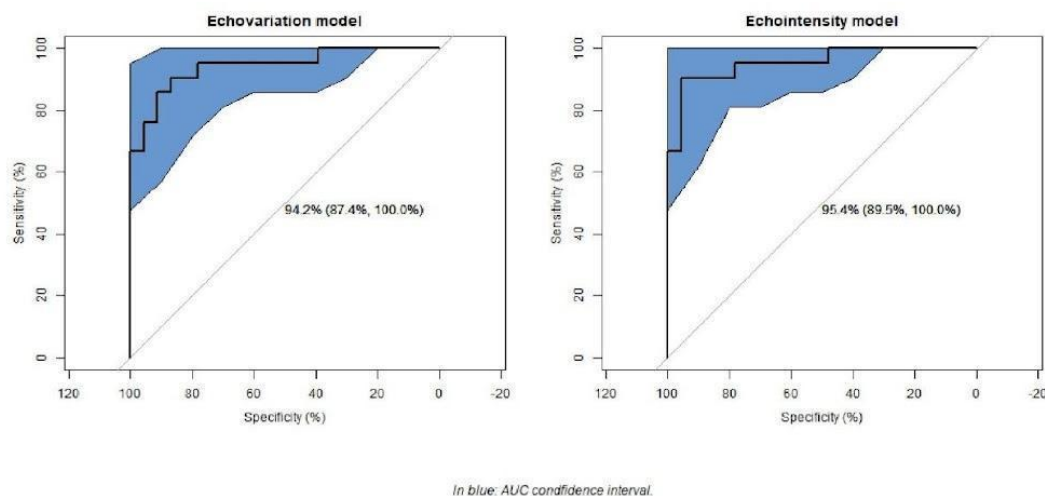
In blue: AUC condfidence interval.

Figure 1. Model receiver operating characteristic (ROC) curves.

4. Discussion

This secondary analysis builds on the methodological foundations established in the initial exploratory study [14] by incorporating advanced statistical validation and refining the dataset to improve its clinical applicability. The results demonstrate high inter-examiner reliability, reinforcing the robustness of the original classification (low–high impairment) developed from the previous study. Including a third independent examiner further reduced potential bias and strengthened the consistency of the original classification approach. In addition, by ensuring that only one US image per limb was selected from each patient, this study mitigated the potential over-representation of individual patients, which may have influenced the original study results.

The results of this secondary analysis align with those of the original study, confirming that echotexture features, particularly EV and EI, are valuable indicators of muscle tissue impairment in post-stroke individuals. Logistic regression models and ROC curve analyses provided a more rigorous assessment of the predictive power of these features, demonstrating high classification performance with excellent sensitivity and specificity. Importantly, this study also identified additional relevant features, such as dissimilarity, entropy, and GLU, which were not initially considered as key features in the exploratory analysis performed in the original study [14]. These results suggest that traditional expert-based assessment may not fully capture all relevant structural changes in muscle tissue. Although expert judgment remains essential, specific echotexture changes may not be visually apparent but can be objectively quantified by using statistical models and predictive analysis.

Our results confirm the importance of EI and EV first-order echotexture features in assessing muscle tissue quality in US images, as previously highlighted in the original research study [14]. Previous studies have also highlighted the importance of these parameters to classify different types of soleus muscle injuries [20], to differentiate individuals with patellar tendinopathy from healthy controls [21], and to assess gastrocnemius medialis and soleus muscle tissue in plantar fascia pathology [39]. Apart from this use in musculoskeletal conditions, EV has shown good accuracy for muscle tissue assessment in individuals with amyotrophic lateral sclerosis [16,40]. The association between high EI and increased muscle tissue impairment is well supported by the previous literature describing

histopathological changes such as disuse-induced atrophy and fibroadipose replacement of hypoechoic contractile elements [41,42]. In parallel, lower EV values observed in more impaired muscles may reflect the loss of structural complexity and tissue differentiation, as fibrous and adipose infiltration replace the heterogeneous architecture of healthy muscle tissue. However, while first-order features remain valuable, they may not be sufficient for more complex image processing tasks, where higher-order texture parameters, such as those derived from GLCM and GLRLM, offer superior diagnostic accuracy [9].

Building on this premise, our secondary analysis highlights that in addition to EI and EV, some GLCM (dissimilarity and entropy) and GLRLM (GLU) features may be key indicators of muscle tissue integrity in post-stroke populations, although the original research study did not identify them as primary indicators [14]. This is consistent with prior research demonstrating that GLCM and GLRLM features improve the accuracy of supraspinatus tendon rupture classification [43] and are also relevant in characterizing forearm flexor and quadriceps muscle tissue in individuals with amyotrophic lateral sclerosis [16]. Notably, the latter study in amyotrophic lateral sclerosis suggests that the integration of echotexture features with conventional muscle US variables, such as muscle thickness, may further improve diagnostic capabilities [16]. In light of these data, future research should explore comprehensive models that integrate first-order, GLCM, and GLRLM features alongside conventional US parameters to refine the accuracy and clinical applicability of muscle echotexture analysis.

A fundamental difference between this secondary analysis and the original study by Asadi et al. [14] is the image selection method. The original dataset included three US images per limb for each participant, which, while helpful in assessing measurement reliability, may have introduced redundancy and potential bias in statistical comparisons. In contrast, this secondary analysis refined the dataset by selecting only one representative image per limb for each patient, aligning with standard clinical practice and ensuring a more rigorous assessment of muscle tissue impairment.

This study also addresses one of the limitations identified in the original research work [14], which is inter-examiner reliability. By including additional examiners and using Cohen's and Light's kappa to assess agreement, the present study demonstrates strong reliability of echotexture analysis for assessing muscle tissue. However, some limitations remain, such as the relatively small sample size and the inability to conduct demographic subgroup analysis (e.g., sex, age, and time since stroke onset) due to this constraint, which could influence the results and limit their generalizability. In addition, although this study employed the rectangular ROI technique (also named the square technique) to select the amount of muscle tissue area for image analysis, as performed in previous studies [16,40], there are alternative approaches, such as the trace technique, in which the classifier delineates all visible muscle without artefacts. Given these differences, it is essential to emphasize that echotexture outcomes may not be interchangeable between the rectangular/square and trace techniques [44], mainly because the use of irregular or manually traced ROIs may introduce computational challenges by not conforming to standard matrix-based texture analysis frameworks.

These results further support the integration of echotexture analysis as a quantitative tool to assess muscle tissue quality in post-stroke individuals. In contrast to traditional qualitative assessments, echotexture features provide objective and reproducible metrics that could improve clinical decision making. However, future studies should validate these results in larger cohorts to confirm the reliability of echotexture features across various demographic groups and further explore their correlation with functional outcomes or patient-reported symptoms. Further studies are needed to determine their clinical relevance for monitoring treatment response and therapeutic progress, enabling necessary

adjustments to intervention. In addition, future research should explore the usefulness and predictive ability of echotexture analysis on long-term rehabilitation outcomes, as echotexture features may help clinicians to prevent the adverse effects of some treatments (such as botulinum toxin) and to tailor and personalize treatment for each patient [45], as well as the long-term prognostic value of echotexture features in predicting muscle tissue impairment post-stroke. Furthermore, further research into echotexture image locations is needed, as an existing study found significant differences in texture analysis between hamstring muscles and measurement locations [23], suggesting that the assessment of different muscle locations may influence echotexture values. This finding underscores the importance of standardizing image acquisition protocols for future research. Finally, it would be interesting for future studies to explore texture analysis approaches adapted to non-rectangular ROI selections.

5. Conclusions

This secondary analysis reinforces the validity of echotexture analysis for assessing muscle tissue quality in post-stroke individuals by integrating advanced statistical techniques and refining the methodological limitations present in an original exploratory study. The findings support the clinical utility of echotexture analysis as a quantitative assessment tool, confirming EV and EI as the most reliable indicators of muscle tissue impairment while also identifying other potential echotexture features from GLCM and GLRLM, such as dissimilarity, entropy, and GLU. However, further research is needed to establish standardized imaging protocols, validate these findings in larger cohorts, and investigate the potential of echotexture features to inform rehabilitation strategies and therapeutic interventions.

Supplementary Materials: The following supporting information can be downloaded at: https://www.mdpi.com/article/10.3390/jcm14092902/s1, Supplementary Material.docx contains five tables and two figures, which are as follows: Table S1: Features derived from first-order statistics, Table S2: Features derived from gray-level co-occurrence matrix, Table S3: Features derived from the gray-level run-length matrix, Table S4: Impairment-level agreement among examiners, Table S5: Impairment level vs. modified Heckmatt scale correlation, Figure S1: Plot diagnosis for impairment-level models for echovariation model, Figure S2: Plot diagnosis for impairment-level models for echointensity model.

Author Contributions: Conceptualization, B.A. and P.H.; methodology, B.A., J.N.C.-Z., P.H., and D.L.-H.; software, B.A. and J.N.C.-Z.; validation, P.H. and D.L.-H.; formal analysis, B.A. and J.N.C.-Z.; investigation, B.A., A.C.-O., and D.L.-H.; data curation, B.A.; writing—original draft, B.A., J.N.C.-Z., A.C.-O., P.H., and D.L.-H.; writing—review and editing, B.A., J.N.C.-Z., A.C.-O., P.H., and D.L.-H.; supervision, P.H.; project administration, P.H. and D.L.-H. All authors have read and agreed to the published version of the manuscript.

Institutional Review Board Statement: This study was conducted in accordance with the Declaration of Helsinki and was approved by the Aragon Ethics Committee (protocol code PI24/030 and date of 7 February 2024).

Informed Consent Statement: Informed consent was obtained from all the subjects involved in this study. Written informed consent was obtained from the patients to publish this paper.

Data Availability Statement: The data presented in this study are available from the corresponding author upon request, due to the fact that these data are part of a larger, ongoing project and may not yet be fully available for public sharing until the project is completed.

use of ChatGPT (GPT-3.5) and Grammarly, which helped us to improve the grammar and fluency of some parts of the text.

Conflicts of Interest: The authors declare no conflicts of interest.

References

1. Dougherty, G. *Medical Image Processing: Techniques and Applications*; Biological and Medical Physics, Biomedical Engineering; Springer: New York, NY, USA, 2011; ISBN 978-1-4419-9769-2.
2. Chowdhary, C.L.; Acharjya, D.P. Segmentation and Feature Extraction in Medical Imaging: A Systematic Review. *Procedia Comput. Sci.* **2020**, *167*, 26–36. [CrossRef]
3. Ker, J.; Wang, L.; Rao, J.; Lim, T. Deep Learning Applications in Medical Image Analysis. *IEEE Access* **2017**, *6*, 9375–9379. [CrossRef]
4. Hilbert, A.; Ramos, L.A.; van Os, H.J.A.; Olabarriaga, S.D.; Tolhuisen, M.L.; Wermer, M.J.H.; Barros, R.S.; van der Schaaf, I.; Dippel, D.; Roos, Y.B.W.E.M.; et al. Data-Efficient Deep Learning of Radiological Image Data for Outcome Prediction after Endovascular Treatment of Patients with Acute Ischemic Stroke. *Comput. Biol. Med.* **2019**, *115*, 103516. [CrossRef]
5. Kazerouni, A.S.; Gadde, M.; Gardner, A.; Hormuth, D.A.; Jarrett, A.M.; Johnson, K.E.; Lima, E.A.B.F.; Lorenzo, G.; Phillips, C.; Brock, A.; et al. Integrating Quantitative Assays with Biologically Based Mathematical Modeling for Predictive Oncology. *iScience* **2020**, *23*, 101807. [CrossRef]
6. Niederer, S.A.; Lumens, J.; Trayanova, N.A. Computational Models in Cardiology. *Nat. Rev. Cardiol.* **2019**, *16*, 100. [CrossRef]
7. Carlier, P.G.; Marty, B.; Scheidegger, O.; Loureiro De Sousa, P.; Baudin, P.Y.; Snezhko, E.; Vlodavets, D. Skeletal Muscle Quantitative Nuclear Magnetic Resonance Imaging and Spectroscopy as an Outcome Measure for Clinical Trials. *J. Neuromuscul. Dis.* **2016**, *3*, 1–28. [CrossRef]
8. Kamiya, N. Deep Learning Technique for Musculoskeletal Analysis. *Adv. Exp. Med. Biol.* **2020**, *1213*, 165–176. [CrossRef] [PubMed]
9. Paris, M.T.; Mourtzakis, M. Muscle Composition Analysis of Ultrasound Images: A Narrative Review of Texture Analysis. *Ultrasound Med. Biol.* **2021**, *47*, 880–895. [CrossRef]
10. Haralick, R.M.; Dinstein, I.; Shanmugam, K. Textural Features for Image Classification. *IEEE Trans. Syst. Man. Cybern.* **1973**, *SMC-3*, 610–621. [CrossRef]
11. Haralick, R.M. Statistical and Structural Approaches to Texture. *Proc. IEEE* **1979**, *67*, 786–804. [CrossRef]
12. Galloway, M.M. Texture Analysis Using Grey Level Run Lengths. *STIN* **1974**, *75*, 18555.
13. Correa-de-Araujo, R.; Harris-Love, M.O.; Miljkovic, I.; Fragala, M.S.; Anthony, B.W.; Manini, T.M. The Need for Standardized Assessment of Muscle Quality in Skeletal Muscle Function Deficit and Other Aging-Related Muscle Dysfunctions: A Symposium Report. *Front. Physiol.* **2017**, *8*, 87. [CrossRef] [PubMed]
14. Asadi, B.; Pujol-Fuentes, C.; Carcasona-Otal, A.; Calvo, S.; Herrero, P.; Lapuente-Hernández, D. Characterizing Muscle Tissue Quality Post-Stroke: Echovariation as a Clinical Indicator. *J. Clin. Med.* **2024**, *13*, 7800. [CrossRef] [PubMed]
15. Ríos-Díaz, J.; del Baño-Aledo, M.E.; Tembl-Ferrairó, J.I.; Chumillas, M.J.; Vázquez-Costa, J.F.; Martínez-Payá, J.J. Quantitative Neuromuscular Ultrasound Analysis as Biomarkers in Amyotrophic Lateral Sclerosis. *Eur. Radiol.* **2019**, *29*, 4266–4275. [CrossRef] [PubMed]
16. Martínez-Payá, J.J.; Ríos-Díaz, J.; Del Baño-Aledo, M.E.; Tembl-Ferrairó, J.I.; Vazquez-Costa, J.F.; Medina-Mirapeix, F. Quantitative Muscle Ultrasonography Using Textural Analysis in Amyotrophic Lateral Sclerosis. *Ultrason. Imaging* **2017**, *39*, 357–368. [CrossRef]
17. Behr, M.; Noseworthy, M.; Kumbhare, D. Feasibility of a Support Vector Machine Classifier for Myofascial Pain Syndrome: Diagnostic Case-Control Study. *J. Ultrasound Med.* **2019**, *38*, 2119–2132. [CrossRef]
18. Del-Canto-fernández, A.; Calleja-Martínez, P.; Descalzo-Hoyas, B.; Rodríguez-Posada, S.; Cuenca-Zaldívar, N.; Fernández-Carnero, S.; Naranjo-Cinto, F.; Gallego-Izquierdo, T. The Application of Image Texture Analysis Techniques on the Effects of Dry Needling versus Placebo in Low-Back Pain Patients: A Pilot-Study. *Appl. Sci.* **2022**, *12*, 5556. [CrossRef]
19. Escriche-Escuder, A.; Trinidad-Fernández, M.; Pajares, B.; Iglesias-Campos, M.; Alba, E.; García-Almeida, J.M.; Roldán-Jiménez, C.; Cuesta-Vargas, A.I. Responsiveness of the New Index Muscular Echotexture in Women with Metastatic Breast Cancer: An Exercise Intervention Study. *Sci. Rep.* **2022**, *12*, 15148. [CrossRef]
20. De-La-cruz-torres, B.; Romero-Morales, C. Muscular Echovariation as a New Biomarker for the Classification of Soleus Muscle Pathology: A Cross-Sectional Study. *Diagnostics* **2021**, *11*, 1884. [CrossRef]
21. Molina-Payá, F.J.; Ríos-Díaz, J.; Carrasco-Martínez, F.; Martínez-Payá, J.J. Infrared Thermography, Intratendon Vascular Resistance, and Echotexture in Athletes with Patellar Tendinopathy: A Cross-Sectional Study. *Ultrason. Imaging* **2023**, *45*, 47–61. [CrossRef]
22. Molinari, F.; Caresio, C.; Acharya, U.R.; Mookiah, M.R.K.; Minetto, M.A. Advances in Quantitative Muscle Ultrasonography Using Texture Analysis of Ultrasound Images. *Ultrasound Med. Biol.* **2015**, *41*, 2520–2532. [CrossRef]

23. Sahinis, C.; Kellis, E. Hamstring Muscle Quality Properties Using Texture Analysis of Ultrasound Images. *Ultrasound Med. Biol.* **2023**, *49*, 431–440. [CrossRef]
24. Serra, M.C. STROKE. *Innov. Aging* **2019**, *3*, S574. [CrossRef]
25. Ryan, A.S.; Dobrovolny, C.L.; Smith, G.V.; Silver, K.H.; Macko, R.F. Hemiparetic Muscle Atrophy and Increased Intramuscular Fat in Stroke Patients. *Arch. Phys. Med. Rehabil.* **2002**, *83*, 1703–1707. [CrossRef] [PubMed]
26. Tok, F.; Özçakar, L.; Safaz, I.; Alaca, R. Effects of Botulinum Toxin-A on the Muscle Architecture of Stroke Patients: The First Ultrasonographic Study. *J. Rehabil. Med.* **2011**, *43*, 1016–1019. [CrossRef] [PubMed]
27. Yang, Y.B.; Zhang, J.; Leng, Z.P.; Chen, X.; Song, W.Q. Evaluation of Spasticity after Stroke by Using Ultrasound to Measure the Muscle Architecture Parameters: A Clinical Study. *Int. J. Clin. Exp. Med.* **2014**, *7*, 2712. [PubMed]
28. Hadi, S.; Khadijeh, O.; Hadian, M.; Niloofar, A.Y.; Olyaei, G.; Hossein, B.; Calvo, S.; Herrero, P. The Effect of Dry Needling on Spasticity, Gait and Muscle Architecture in Patients with Chronic Stroke: A Case Series Study. *Top. Stroke Rehabil.* **2018**, *25*, 326–332. [CrossRef]
29. Picelli, A.; Tamburin, S.; Cavazza, S.; Scampoli, C.; Manca, M.; Cosma, M.; Berto, G.; Vallies, G.; Roncari, L.; Melotti, C.; et al. Relationship between Ultrasonographic, Electromyographic, and Clinical Parameters in Adult Stroke Patients with Spastic Equinus: An Observational Study. *Arch. Phys. Med. Rehabil.* **2014**, *95*, 1564–1570. [CrossRef]
30. Heckmatt, J.Z.; Leeman, S.; Dubowitz, V. Ultrasound Imaging in the Diagnosis of Muscle Disease. *J. Pediatr.* **1982**, *101*, 656–660. [CrossRef]
31. Vandenbroucke, J.P.; von Elm, E.; Altman, D.G.; Gøtzsche, P.C.; Mulrow, C.D.; Pocock, S.J.; Poole, C.; Schlesselman, J.J.; Egger, M.; Blettner, M.; et al. Strengthening the Reporting of Observational Studies in Epidemiology (STROBE): Explanation and Elaboration. *Int. J. Surg.* **2014**, *12*, 1500–1524. [CrossRef]
32. Shrestha, B.; Dunn, L. The Declaration of Helsinki on Medical Research Involving Human Subjects: A Review of Seventh Revision. *J. Nepal. Health Res. Counc.* **2020**, *17*, 548–552. [CrossRef]
33. Tsai, D.-M.; Hsiao, B. Automatic surface inspection using wavelet reconstruction. *Pattern Recognit.* **2001**, *34*, 1285–1305. [CrossRef]
34. Chu, A.; Sehgal, C.M.; Greenleaf, J.F. Use of gray value distribution of run lengths for texture analysis. *Pattern Recognit. Lett.* **1990**, *11*, 415–419. [CrossRef]
35. Amadasun, M.; King, R. Textural features corresponding to textural properties. *IEEE Trans. Syst. Man Cybern.* **1989**, *19*, 1264–1274. [CrossRef]
36. Moreta, M.C.; Fleet, A.; Reebye, R.; McKernan, G.; Berger, M.; Farag, J.; Munin, M.C. Reliability and Validity of the Modified Heckmatt Scale in Evaluating Muscle Changes With Ultrasound in Spasticity. *Arch. Rehabil. Res. Clin. Transl.* **2020**, *2*, 100071. [CrossRef] [PubMed]
37. Fleis, L.; Levin, B.; Paik, M.C. The Measurement of Interrater Agreement. In *Statistical Methods for Rates and Proportions*, 2nd ed.; John Wiley: New York, NY, USA, 1981.
38. Mavuto, M. Statistics Corner: A Guide to Appropriate Use of Correlation Coefficient in Medical Research. *Malawi Med. J.* **2012**, *24*, 69–71.
39. Canosa-Carro, L.; López-López, D.; García-Sanz, F.; Díaz-Meco-conde, R.; García-Bermejo, P.; De-La-cruz-torres, B.; Marszalek, J.; Romero-Morales, C. Features of Extrinsic Plantar Muscles in Patients with Plantar Fasciitis by Ultrasound Imaging: A Retrospective Case Control Research. *Diagnostics* **2022**, *12*, 897. [CrossRef]
40. Martínez-Payá, J.J.; del Baño-Aledo, M.E.; Ríos-Díaz, J.; Tembl-Ferrairó, J.I.; Vázquez-Costa, J.F.; Medina-Mirapeix, F. Muscular Echovariation: A New Biomarker in Amyotrophic Lateral Sclerosis. *Ultrasound Med. Biol.* **2017**, *43*, 1153–1162. [CrossRef]
41. Pillen, S.; Arts, I.M.P.; Zwarts, M.J. Muscle Ultrasound in Neuromuscular Disorders. *Muscle Nerve* **2008**, *37*, 679–693. [CrossRef]
42. Akazawa, N.; Harada, K.; Okawa, N.; Kishi, M.; Tamura, K.; Moriyama, H. Changes in Quadriceps Thickness and Echo Intensity in Chronic Stroke Survivors: A 3-Year Longitudinal Study. *J. Stroke Cerebrovasc. Dis.* **2021**, *30*, 105543. [CrossRef]
43. Park, B.E.; Jang, W.S.; Yoo, S.K. Texture Analysis of Supraspinatus Ultrasound Image for Computer Aided Diagnostic System. *Healthc. Inform. Res.* **2016**, *22*, 299–304. [CrossRef]
44. Sarwal, A.; Parry, S.M.; Berry, M.J.; Hsu, F.C.; Lewis, M.T.; Justus, N.W.; Morris, P.E.; Denehy, L.; Berney, S.; Dhar, S.; et al. Interobserver Reliability of Quantitative Muscle Sonographic Analysis in the Critically Ill Population. *J. Ultrasound Med.* **2015**, *34*, 1191–1200. [CrossRef] [PubMed]
45. Picelli, A.; Bonetti, P.; Fontana, C.; Barausse, M.; Dambruoso, F.; Gajofatto, F.; Girardi, P.; Manca, M.; Gimigliano, R.; Smania, N. Is Spastic Muscle Echo Intensity Related to the Response to Botulinum Toxin Type A in Patients with Stroke? A Cohort Study. *Arch. Phys. Med. Rehabil.* **2012**, *93*, 1253–1258. [CrossRef] [PubMed]

Study 5

Clinical case/ Case Series

A complementary patch-based histogram analysis for quantifying muscle tissue in ultrasound imaging

Borhan Asadi[1,2] ✉ ⊙ 0000-0001-7505-7958

Sarkout Abdi[3] ⊙ 0009-0005-2627-2113

Luis Pérez-Espallargas[1,2] ⊙ 0009-0007-7701-9884

Noureddin Nakhostin Ansari[4] ⊙ 0000-0003-2742-2273

Diego Lapuente-Hernández[1,2] ⊙ 0000-0002-6506-6081

[1] iHealthy Research Group, Instituto de Investigación Sanitaria (IIS) Aragon, University of Zaragoza, 50009 Zaragoza, Spain.
[2] Department of Physiatry and Nursing, Faculty of Health Sciences, University of Zaragoza, 50009 Zaragoza, Spain.
[3] Department of Mathematics, Rasht Branch, Islamic Azad University, Rasht, Iran.
[4] Department of Physiotherapy, School of Rehabilitation, Tehran University of Medical Sciences, Tehran, Iran.

ABSTRACT

Introduction: Ultrasound imaging is widely used for muscle assessment due to its non-invasive nature and real-time imaging capabilities. Histogram-based echotexture analysis has proven to be a valuable tool for quantifying muscle tissue composition using features such as echointensity (EI) and echovariation (EV), especially in neuromuscular and neurological disorders. However, variability in region of interest (ROI) selection and image processing methods can significantly affect the extracted echotexture features. This study presents a novel histogram-based analysis approach to investigate the effects of subdividing a single ROI into different patch sizes for muscle tissue assessment. By focusing on the EI and EV of the gastrocnemius medialis in a stroke patient, this research aims to refine quantitative ultrasound analysis to improve clinical applicability.

Case presentation: One stroke patient was randomly selected from a previously collected dataset to perform a complementary analysis. The initially selected grey-scale ROI was extracted and divided into patches of different sizes (10×10, 20×20, 30×30, 40×40 and 50×50 pixels). The EI and EV of each patch were calculated, and their distributions were analyzed using descriptive statistics and correlation methods.

Results: The EV values for patches of sizes 10×10, 20×20, 30×30, 40×40, and 50×50 were 26.48, 24.58, 20.44, 16.78, and 10.38, respectively, which deviated significantly from the original ROI value of 45.54. In contrast, the EI values remained around 81 across all patch sizes, indicating that varying patch sizes did not affect EI.

Conclusions: Patch-based histogram analysis offers a complementary method for assessing muscle texture in ultrasound. While EI appears to be robust to ROI subdivision, EV shows variability, raising concerns about its reliability when small patches are used. Standardized methods and future research with larger datasets are needed to optimize echotexture analysis and ensure reproducibility in clinical practice.

Keywords: Ultrasonography; Muscle tissue; Echotexture analysis; Histogram; Stroke.

1. Introduction

Ultrasound imaging is a non-invasive, safe, accessible, and cost-effective technique commonly used for assessing muscle structure and function. It is widely utilized across various medical fields, including sports medicine, rehabilitation, and the assessment of neuromuscular disorders[1-3]. One of its primary advantages is that it provides high-resolution, real-time imaging, enabling the visualization of muscle dynamics and tissue changes[4]. Additionally, ultrasound offers valuable quantitative and qualitative insights into muscle tissue, making it an essential tool for diagnosing and monitoring muscle diseases and alterations[5]. However, despite significant advances in ultrasound technology, the quantitative analysis of ultrasound images remains a major challenge in medical and clinical research.

Image texture is commonly defined as the spatial variation of pixel intensity, and in ultrasound imaging, this concept is referred to as echotexture[6,7]. This definition is widely accepted in image processing, where texture analysis techniques are employed for classification, segmentation, and synthesis[8]. Several computational approaches have been developed to facilitate the identification of complex tissue patterns from texture feature extraction from images, such as the gray-level co-occurrence matrix (GLCM), gray-level run-length matrix (GLRLM), Fast Fourier transform (FFT), and neural networks[9].

Among these approaches, histogram analysis has received considerable attention due to its simplicity and utility in the assessment of muscle composition, particularly in the evaluation of neuromuscular disorders[7, 10-12]. This technique examines the distribution of pixel intensities within ultrasound images, allowing the extraction of first-order statistical features such as mean, standard deviation, skewness, kurtosis, energy, or entropy[13]. Previous studies have shown that these statistical parameters derived from histogram analysis can characterize muscle tissue quality in different health conditions, demonstrating their potential for use in clinical settings[14-18]. The advantage of histogram-based (first-order) parameters over second-order parameters such as GLCM and GLRLM is that they can be directly computed from the original pixel values and the initial image matrix. In contrast, second-order parameters require the prior calculation of GLCM and GLRLM matrices before extracting the desired features. On the other hand, second-order parameters may provide additional texture information that cannot be captured by first-order parameters.

Among the key quantitative features extracted from muscle tissue in neuromuscular disorders and other neurological disorders such as stroke, echointensity (EI) and echovariation (EV) have proven to be particularly relevant and applicable to clinical practice[12,19-21]. On the one hand, EI determines the mean pixel intensity, while EV quantifies the variation of the EI. In particular, a study by Asadi et al.[20] analyzed ultrasound images of the gastrocnemius medialis in stroke individuals and found a strong inverse correlation between EV and the modified Heckmatt scale. However, this scale has notable limitations due to its subjective nature and its restricted four-grade grading system[22], so EV was proposed as a reliable quantitative approach to assess muscle tissue quality in individuals with stroke[20].

In the aforementioned study[20] the region of interest (ROI) for echotexture feature extraction was defined as the largest possible area of muscle tissue between the superficial and deep fascia.

However, there is considerable variability in the selection and size of ROIs among studies analyzing muscle echotexture[19,23-26]. In addition to this variability, when performing the histogram analysis on a selected ROI, it remains unclear to what extent the chosen methodology influences the extracted echotexture features. Some studies may simply select the entire ROI as a single unit, while others may segment the same image into multiple ROIs, or even divide each ROI into patches of different sizes. The previous histogram-based analyses often considered one ROI without accounting for spatial heterogeneity within the muscle[14-18]. This limitation may lead to an oversimplified representation of muscle echotexture, potentially missing localized pathological changes. The proposed patch-based analysis methodology could provide a more complete and reliable representation of the selected ROI, as it generates a distribution of values rather than a single value and may also enhance sensitivity to subtle tissue alterations. However, the impact of this approach on key muscle tissue analysis features, such as EI and EV, is unknown.

Therefore, the primary objective of this study was to perform a complementary analysis of EI and EV variations in a single stroke patient using a histogram-based analysis by dividing the original ROI into patches of different sizes. This study aims to investigate whether patch-based division influences histogram-derived muscle tissue analysis, specifically examining the impact of patch size on the assessment of echotexture in ultrasound images.

2. Description of the clinical case

2.1 Patient information

A single participant was selected from the study's dataset by Asadi et al[20]. This stroke patient was recruited from the Hospital Clínico Universitario Lozano Blesa in April 2024. Inclusion criteria required participants to be older than 18 years, have a confirmed diagnosis of stroke verified by computed tomography (CT) or magnetic resonance imaging (MRI), and be able to walk independently, with or without assistance. Exclusion criteria included the presence of other neurological disorders, history of lower extremity surgery, or any medical condition that could interfere with data collection. The study was approved by the Aragon Ethics Committee (PI24/030) and registered in ClinicalTrials.gov (NTC06411587). In addition, the study adhered to the ethical guidelines of the Declaration of Helsinki[27].

2.2 Data Collection

In the study by Asadi et al.[20], ultrasound images were acquired using the Butterfly iQ+ portable ultrasound system, following a standardized imaging protocol with a gain setting of 50% and a depth setting of 5-7 cm. A trained physiotherapist performed the scans while the patients were seated with knees flexed at 90°. The ultrasound probe was placed proximally at 30% of the distance between the medial condyle of the tibia and the medial malleolus, with an adjusted angle of approximately 35-45° to optimize image quality.

For this case study, a single image of the gastrocnemius medialis muscle was randomly selected from the data set collected by Asadi et al.[20] for detailed analysis. The method of muscle tissue extraction was identical to that used in the original study, and this extracted area was considered the main ROI, carefully chosen to include as much muscle tissue as possible while

excluding superficial and deep fascia[28]. The selected original ROI was then converted from color to grayscale using a Python-based program for further analysis.

2.3 Data Analysis

In this case study, the grayscale ultrasound ROI was divided into square patches of predefined sizes (10×10, 20×20, 30×30, 40×40, and 50×50 pixels). Each patch size is shown in Figures 1 to 5 of the supplementary material. For each patch, EI, defined as the mean intensity of the pixels within the ROI, and EV, defined as the ratio of the standard deviation to the mean intensity, were calculated. The corresponding formulae are as follows:

$$\frac{1}{N}\sum_{i=1}^{N} x_i \quad \text{for EI} \qquad \frac{\sum_{i=1}^{N}(x_i-\mu)^2}{\sum_{i=1}^{N} x_i} \quad \text{for EV}$$

Descriptive statistics were calculated to characterize the EI and EV value distribution, including mean, standard deviation, median, interquartile range (IQR), and skewness. Skewness was used to classify the shape of the distribution as normal, right-skewed, or left-skewed. Histograms of both features were generated to visualize their distributions, with annotations highlighting key statistical measures.

The normality of the EI and EV distributions was first assessed by inspecting the histograms. If the distribution appeared normal, the mean and standard deviation were used for further analysis; whereas if the distribution of EI or EV was skewed (right or left), the median and IQR were used instead. In both cases, the correlation between EI or EV and data dispersion was calculated using Kendall's tau coefficient, a rank-based method well suited for small data sets[29, 30].

The selected statistical measures were then compared with the original EI and EV values of the original ROI in a graphical representation to evaluate the observed changes and assess the dispersion of EV and EI depending on the patch size selected for the ROI. Additionally, to improve visualization and facilitate a clearer and more accurate comparison of variations, changes in EV were scored on the primary EV function for stroke patients derived from the study by Asadi et al.[20]. This function showed that higher EV values were associated with better muscle tissue quality, whereas lower EV values correspond to greater muscle impairment in stroke-affected muscles[20]. Therefore, the mean or median EV values extracted from the histograms were plotted on the function: $y = a^*e^{bx} + c^*e^{dx} + E$; using the parameters: $a = 37.13$, $b = -0.14$, $c = 132,052.16$, $d = -2^*10^{-6}$, and $E = -131,990.30$. There is no equivalent function for EI, which precludes applying the same approach to this feature.

3. Results

The distribution type, mean, standard deviation, median, and IQR were calculated for the original ROI with five different patch sizes: 10×10, 20×20, 30×30, 40×40, and 50×50 pixels. The results indicated that the histogram showed a normal distribution for the EI feature, whereas the EV feature showed a right-skewed distribution, suggesting that the EV data did not conform to normality. Figure 1 presents the histogram plots for EI, while Figure 2 shows the histogram plots for EV for each patch size.

a) 10*10 patches

b) 20*20 patches

c) 30*30 patches

d) 40*40 patches

e) 50*50 patches
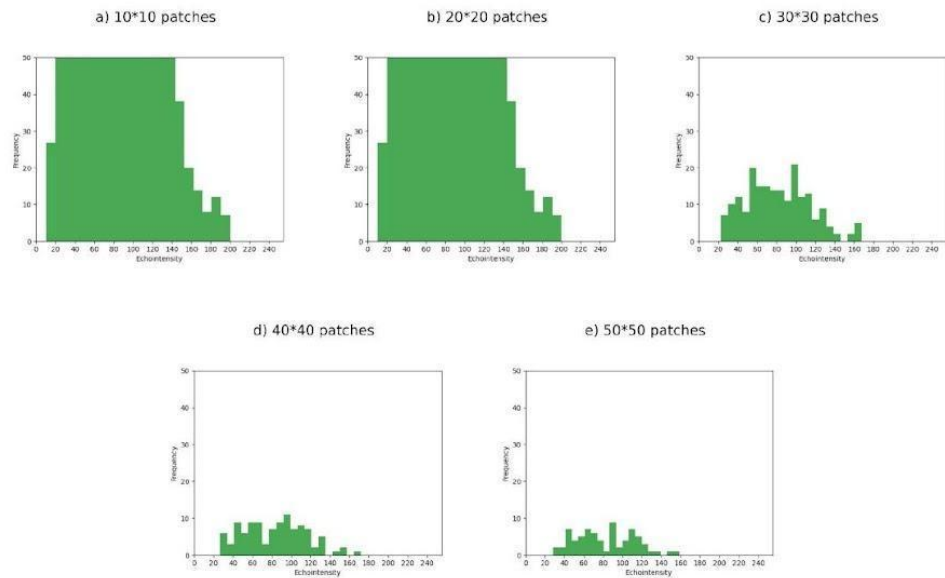
Figure 1. Echointensity histograms derived from the original ROI of the ultrasound image of the gastrocnemius medialis muscle. The x-axis represents the echointensity values, while the y-axis indicates the frequency of occurrence. (a) Histogram for 10×10 pixel patches, (b) 20×20 pixel patches, (c) 30×30 pixel patches, (d) 40×40 pixel patches and (e) 50×50 pixel patches.

a) 10*10 patches

b) 20*20 patches

c) 30*30 patches

d) 40*40 patches

e) 50*50 patches
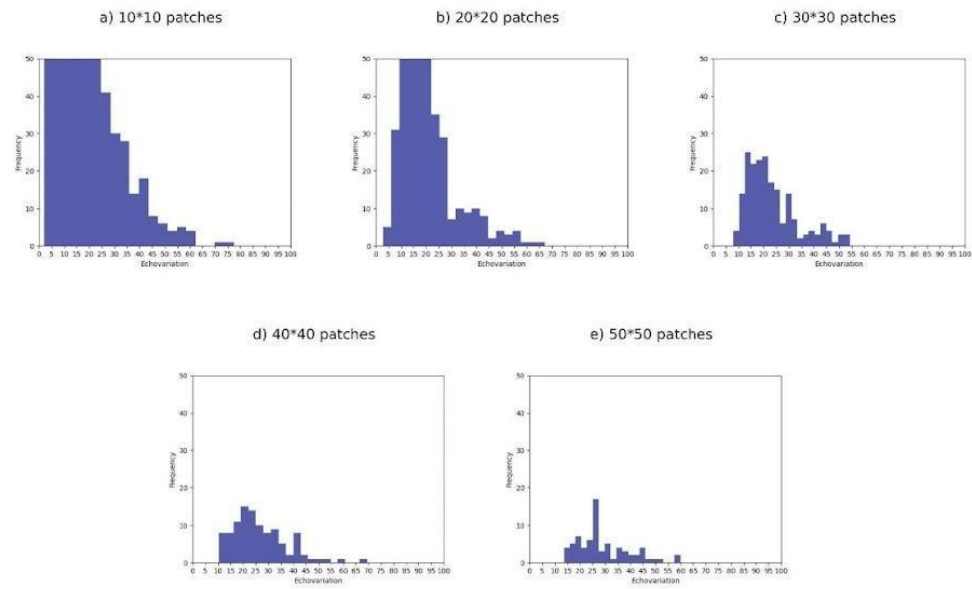
Figure 2. Echovariation histograms derived from the original ROI of the ultrasound image of the gastrocnemius medialis muscle. The x-axis represents the echovariation values, while the y-axis indicates the frequency of occurrence. (a) Histogram for 10×10 pixel patches, (b) 20×20 pixel patches, (c) 30×30 pixel patches, (d) 40×40 pixel patches and (e) 50×50 pixel patches.

On the one hand, since the EI values followed a normal distribution, the mean and standard deviation were used to describe the data. Kendall's correlation coefficient yielded a value of -0.4, indicating no significant correlation between the mean EI and its standard deviation. Figure 3 illustrates the EI and standard deviation variations for each patch size. Both parameters remained relatively stable across the different patches, with values approaching the 81.89 value of the EI of the original ROI.

Mean and Standard Deviation across Images
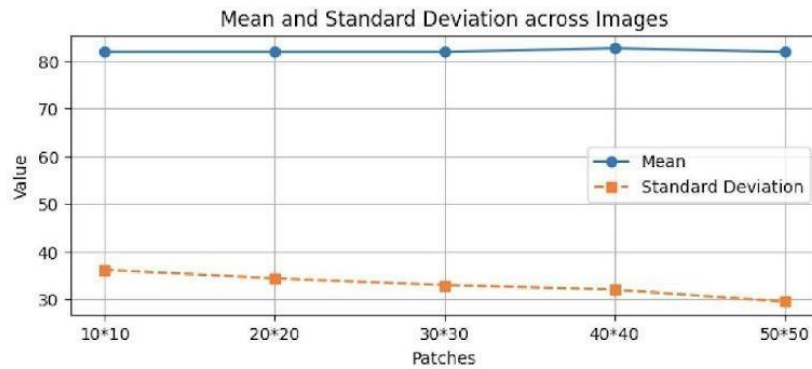
Figure 3. Line graph illustrating the mean and standard deviation values of echointensity for each patch size. The X-axis represents the patch sizes, while the Y-axis indicates the corresponding values of the mean and standard deviation of echointensity. The blue line represents the mean and the orange line the standard deviation.

On the other hand, the EV values followed a non-normal distribution, which made it necessary to use the median and IQR to summarize the data. In addition, Kendall's correlation coefficient yielded a value of 1, indicating a perfect correlation between median EV and IQR values. Figure 4 illustrates the variations of median EV and IQR in the histograms for the predefined patch sizes. The highest median EV value (26.48) was observed at the 50×50 patch size, which was still substantially lower than the EV value of 45.54 of the original ROI. In addition, the dispersion values indicate that smaller patch sizes showed the lowest IQR, while larger patch sizes showed an increasing IQR (Figure 4). Therefore, as the patch size increases, both the dispersion and the median EV increase, progressively approximating the EV value of the original ROI.

Median and IQR across Images
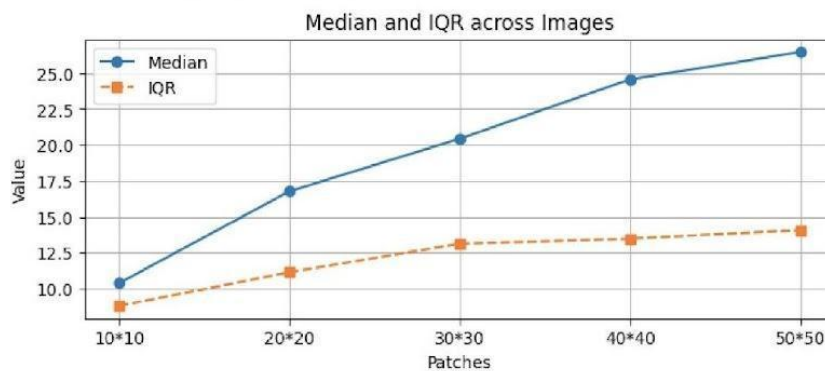
Figure 4. Line graph illustrating the median and Interquartile range (IQR) values of echovariation for each patch size. The X-axis represents the patch sizes, while the Y-axis indicates the corresponding values of the median and IQR of echovariation. The blue line represents the median and the orange line the IQR.

The median EV values extracted from the histograms were plotted on the function derived from the study by Asadi et al.[20] In our case study, the results revealed a clear trend: as patch size decreased, median EV shifted toward values characteristic of more affected regions; conversely, as patch size increased, median EV approached the EV value of the original ROI (Figure 5).
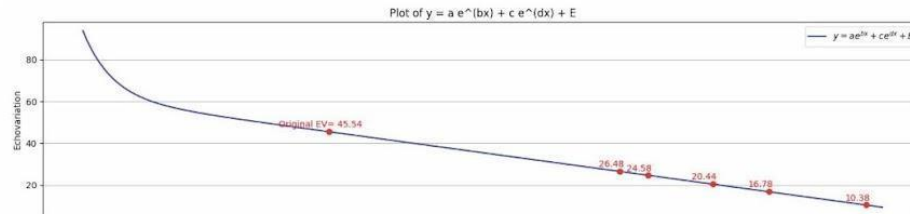
Figure 5. Visualization of the median values of echovariation (EV) extracted from the histograms for different patch sizes, represented in the function of the study by Asadi et al. (20). From left to right: 45.54 represents the original ROI, 26.48 corresponds to the 50×50 patch, 24.58 to the 40×40, 20.44 to the 30×30, 16.78 to the 20×20, and 10.38 to the 10×10 pixel.

4. Discussion

Numerous studies have employed histogram-based approaches to extract quantitative features from ultrasound images. Some researchers have refined this methodology by segmenting the image in different ROIs before applying histogram analysis to improve diagnostic accuracy and interpretability[31, 32]. This segmentation-based approach allows a localized assessment of tissue features, which is particularly valuable in medical imaging. To our knowledge, no previous studies have explored whether dividing the ROI into patches produces different results than analyzing the entire ROI, which remains the most commonly used method in histogram-based analysis. Furthermore, to our knowledge and our findings, no research has examined how patch size influences histogram-derived outcomes when applying a patch-based approach. The proposed methodology could provide a more representative characterization of muscle tissue and improve the reliability of comparisons between studies with similar objectives.

In this study, we integrate histogram-based analysis with a patch-based dividing strategy of the ROI, which included the maximal amount of muscle tissue in the gastrocnemius medialis. Our results indicate that mean EI values calculated from patches accurately reflect the EI of the original ROI. In contrast, the median EV values obtained from patches do not reliably represent the EV of the original ROI. This discrepancy is critical, as previous research has successfully classified muscle tissue characteristics in stroke patients based on EV values[20]. If the EV values of smaller patches deviate significantly from the actual EV of the original ROI, questions arise about the reliability of using the mean EV values of patches for clinical or diagnostic purposes. Our results suggest that relying on the median EV of smaller patches could lead to misinterpretations, as these values may not accurately reflect the severity of muscle impairment[20].

Regarding the standard deviation or IQR values, our analysis demonstrates that, for the EI feature, there are no differences in the standard deviation values extracted from the patched ROI compared to the original ROI. However, for the EV feature, there is a systematic increase in the IQR as the patch size increases. This finding is crucial, as it suggests that changes in patch size

influence the statistical representation and, consequently, the interpretation of EV on ultrasound images, which has been defined as a relevant ultrasonographic objective indicator in previous studies for different neurological populations[19, 20]. Consistent with our findings, several previous studies have explored how different methods of segmenting ROIs within the same ultrasound image may affect, for example, the performance of automated tumor selection algorithms[33] or luminal contour detection in intravascular ultrasound[34].

A limitation of our study is that the analysis was performed on a single ultrasound image and only analyzed in a ROI size, which included the maximal amount of muscle tissue. Although the results of this methodology suggest a clear pattern and indicate that the EI feature can be used reliably, unlike EV, further studies are needed to validate these findings. Future research should include comparisons using more images for each patch size and assess the impact of different ROI sizes within the same image. In addition, it is essential to investigate whether a standardized patch division strategy across an entire dataset could improve the classification of ultrasound images by correlating the results with validated tools such as the Heckmatt scale. A uniform approach could allow for more consistent feature extraction and improve differentiation between healthy and affected tissues. These studies are crucial to determine whether this methodological framework could improve the diagnostic value of echotexture analysis, particularly for the EV feature.

5. Conclusion

This study explored a complementary patch-based histogram analysis to assess muscle tissue characteristics in ultrasound images, focusing on EI and EV features. Our findings indicate that the EI values from divided patches closely align with the original ROI's, supporting their stability as a valuable muscle tissue characterization indicator. However, EV values from smaller patches deviate significantly from the original ROI, raising questions about its reliability for clinical applications, as the variations in ROI division influence its statistical representation. Although this study is limited to a single ultrasound image in a single ROI size, the results underscore the need for standardized methodologies in histogram-based analysis and further research to refine the use of EV in diagnostic applications of ultrasound imaging.

References

1. Whittaker JL, Stokes M. Ultrasound imaging and muscle function. J Orthop Sports Phys Ther. 2011;41(8):572–80. doi:10.2519/jospt.2011.3682

2. Chang KV, Wu WT, Özçakar L. Ultrasound imaging and rehabilitation of muscle disorders: part 1. Traumatic injuries. Am J Phys Med Rehabil. 2019;98(12):1133–41. doi:10.1097/PHM.0000000000001307

3. Hodges PW. Ultrasound imaging in rehabilitation: just a fad? J Orthop Sports Phys Ther. 2005;35(6):333–7. doi:10.2519/jospt.2005.0106

4. Stokes M, Hides J, Nassiri DK. Musculoskeletal ultrasound imaging: diagnostic and treatment aid in rehabilitation. Phys Ther Rev. 1997;2(2):73–92. doi: 10.1179/ptr.1997.2.2.73

5. Naruse M, Trappe S, Trappe TA. Human skeletal muscle size with ultrasound imaging: a comprehensive review. J Appl Physiol (1985). 2022;132(5):1267–79. doi:10.1152/japplphysiol.00041.2022

6. Materka A, Strzelecki M. Texture Analysis Methods - A Review. Technical University of Lodz, Institute of Electronics, COST B11 Report. 1998.

7. Paris MT, Mourtzakis M. Muscle composition analysis of ultrasound images: a narrative review of texture analysis. Ultrasound Med Biol. 2021;47(4):880–95. doi:10.1016/j.ultrasmedbio.2020.12.012

8. Nailon WH. Texture analysis methods for medical image characterisation. Biomed Imaging. 2010;75:100. doi:10.5772/8912

9. Lubner MG, Smith AD, Sandrasegaran K, Sahani DV, Pickhardt PJ. CT texture analysis: definitions, applications, biologic correlates, and challenges. Radiographics. 2017;37(5):1483–503. doi:10.1148/rg.2017170056

10. Mailloux GE, Bertrand M, Stampfler R, Ethier S. Local histogram information content of ultrasound B-mode echographic texture. Ultrasound Med Biol. 1985;11(5):743–50. doi:10.1016/0301-5629(85)90108-5

11. Pillen S, Van Alfen N. Muscle ultrasound from diagnostic tool to outcome measure—Quantification is the challenge. Muscle Nerve. 2015;52(3):319–20. doi:10.1002/mus.24613

12. Pillen S, Arts IM, Zwarts MJ. Muscle ultrasound in neuromuscular disorders. Muscle Nerve. 2008;37(6):679–93. doi:10.1002/mus.21015

13. Shannon CE. A mathematical theory of communication. ACM SIGMOBILE Mob Comput Commun Rev. 2001;5(1):3–55. doi:10.1145/584091.584093

14. Sogawa K, Nodera H, Takamatsu N, Mori A, Yamazaki H, Shimatani Y, et al. Neurogenic and myogenic diseases: quantitative texture analysis of muscle US data for differentiation. Radiology. 2017;283(2):492–8. doi:10.1148/radiol.2016160826

15. Ismail C, Zabal J, Hernandez HJ, Woletz P, Manning H, Teixeira C, et al. Diagnostic ultrasound estimates of muscle mass and muscle quality discriminate between women with and without sarcopenia. Front Physiol. 2015;6:302. doi:10.3389/fphys.2015.00302

16. Pagán-Conesa A, García-Ortiz MT, Salmerón-Martínez EJ, Moya-Martínez A, López-Prats F. Diagnostic ultrasound shows reversal of supraspinatus muscle atrophy following arthroscopic rotator cuff repair. Arthroscopy. 2021;37(10):3039–48. doi:10.1016/j.arthro.2021.04.039

17. Harris-Love MO, Gonzales TI, Wei Q, Ismail C, Zabal J, Woletz P, et al. Association between muscle strength and modeling estimates of muscle tissue heterogeneity in young and old adults. J Ultrasound Med. 2019;38(7):1757–68. doi:10.1002/jum.14864

18. Calvo-Lobo C, Useros-Olmo AI, Almazán-Polo J, Martín-Sevilla M, Romero-Morales C, Sanz-Corbalán I, et al. Quantitative ultrasound imaging pixel analysis of the intrinsic plantar muscle tissue between hemiparesis and contralateral feet in post-stroke patients. Int J Environ Res Public Health. 2018;15(11):2519. doi:10.3390/ijerph15112519

19. Martínez-Payá JJ, Ríos-Díaz J, Del Baño-Aledo ME, Tembl-Ferrairó JI, Vazquez-Costa JF, Medina-Mirapeix F. Quantitative muscle ultrasonography using textural analysis in amyotrophic lateral sclerosis. Ultrason Imaging. 2017;39(6):357–68. doi:10.1177/0161734617711370

20. Asadi B, Pujol-Fuentes C, Carcasona-Otal A, Calvo S, Herrero P, Lapuente-Hernández D. Characterizing muscle tissue quality post-stroke: echovariation as a clinical indicator. J Clin Med. 2024;13(24). doi:10.3390/jcm13247800

21. Akazawa N, Harada K, Okawa N, Kishi M, Tamura K, Moriyama H. Changes in quadriceps thickness and echo intensity in chronic stroke survivors: a 3-year longitudinal study. J Stroke Cerebrovasc Dis. 2021;30(3):105543. doi: 10.1016/j.jstrokecerebrovasdis.2020.105543

22. Heckmatt JZ, Leeman S, Dubowitz V. Ultrasound imaging in the diagnosis of muscle disease. J Pediatr. 1982;101(5):656–60. doi:10.1016/s0022-3476(82)80286-2

23. Molinari F, Caresio C, Acharya UR, Mookiah MR, Minetto MA. Advances in quantitative muscle ultrasonography using texture analysis of ultrasound images. Ultrasound Med Biol. 2015;41(9):2520–32. doi:10.1016/j.ultrasmedbio.2015.04.021

24. Sahinis C, Kellis E. Hamstring muscle quality properties using texture analysis of ultrasound images. Ultrasound Med Biol. 2023;49(2):431–40. doi:10.1016/j.ultrasmedbio.2022.09.011

25. Escriche-Escuder A, Trinidad-Fernández M, Pajares B, Iglesias-Campos M, Alba E, García-Almeida JM, et al. Responsiveness of the new index muscular echotexture in women with metastatic breast cancer: an exercise intervention study. Sci Rep. 2022;12(1):15148. doi:10.1038/s41598-022-19532-7

26. Del-Canto-Fernández A, Calleja-Martínez P, Descalzo-Hoyas B, Rodríguez-Posada S, Cuenca-Zaldívar N, Fernández-Carnero S, et al. The application of image texture analysis techniques on the effects of dry needling versus placebo in low-back pain patients: a pilot study. Appl Sci. 2022;12(11):5556. doi:10.3390/app12115556

27. Shrestha B, Dunn L. The declaration of Helsinki on medical research involving human subjects: a review of seventh revision. J Nepal Health Res Counc. 2020;17(4):548–52. doi:10.33314/jnhrc.v17i4.1042

28. Caresio C, Molinari F, Emanuel G, Minetto MA. Muscle echo intensity: reliability and conditioning factors. Clin Physiol Funct Imaging. 2015;35(5):393–403. doi:10.1111/cpf.12175

29. Bujang MA. An elaboration on sample size determination for correlations based on effect sizes and confidence interval width: a guide for researchers. Restor Dent Endod. 2024;49(2):e21. doi:10.5395/rde.2024.49.e21

30. Hunsberger S, Long L, Reese SE, Hong GH, Myles IA, Zerbe CS, et al. Rank correlation inferences for clustered data with small sample size. Stat Neerl. 2022;76(3):309–30. doi:10.1111/stan.12261

31. Kermani A, Ayatollahi A, Talebi M. Segmentation of medical ultrasound image based on local histogram range image. In: 3rd International Conference on Biomedical Engineering and Informatics; 2010. IEEE. doi:10.1109/BMEI.2010.5639996

32. Zhu Q. Ultrasonic image analysis of cardiac space-occupying diseases based on grey clustering algorithm. In: 2023 International Conference on Telecommunications, Electronics and Informatics (ICTEI); 2023. IEEE. doi:10.1109/ICTEI60496.2023.00173

33. Zhang D, Liu Y, Yang Y, Xu M, Yan Y, Qin Q. A region-based segmentation method for ultrasound images in HIFU therapy. Med Phys. 2016;43(6):2975–89. doi:10.1118/1.4950706

34. Dos Santos E, Yoshizawa M, Tanaka A, Saijo Y, Iwamoto T. Detection of luminal contour using fuzzy clustering and mathematical morphology in intravascular ultrasound images. Conf Proc IEEE Eng Med Biol Soc. 2005;2005:3471–4. doi:10.1109/iembs.2005.1617226
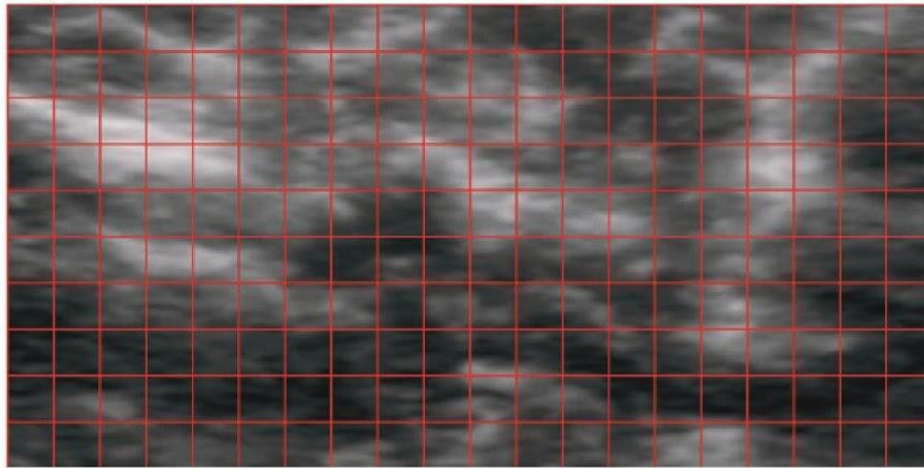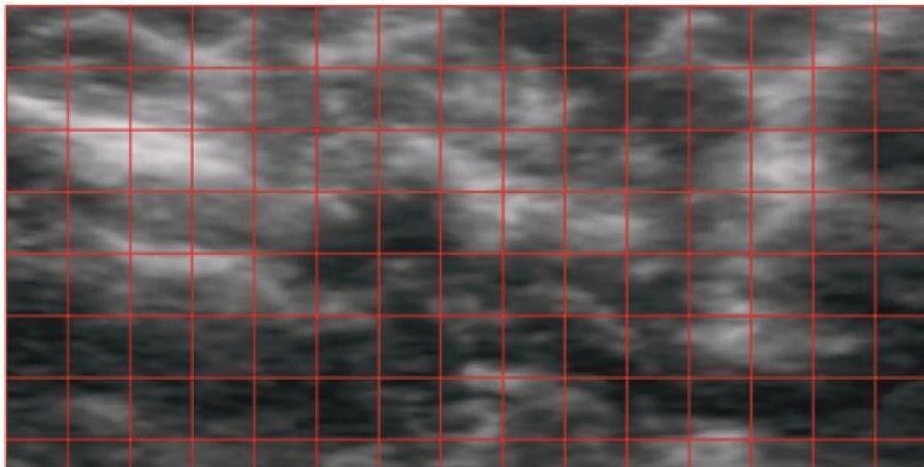
Supplementary material
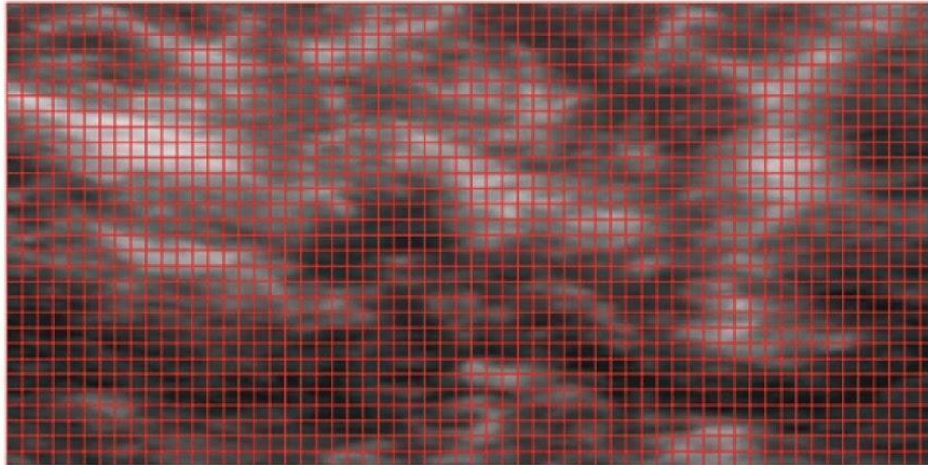
Figure S1. Original ROI of the whole muscle segmented into 10*10 pixel patches.
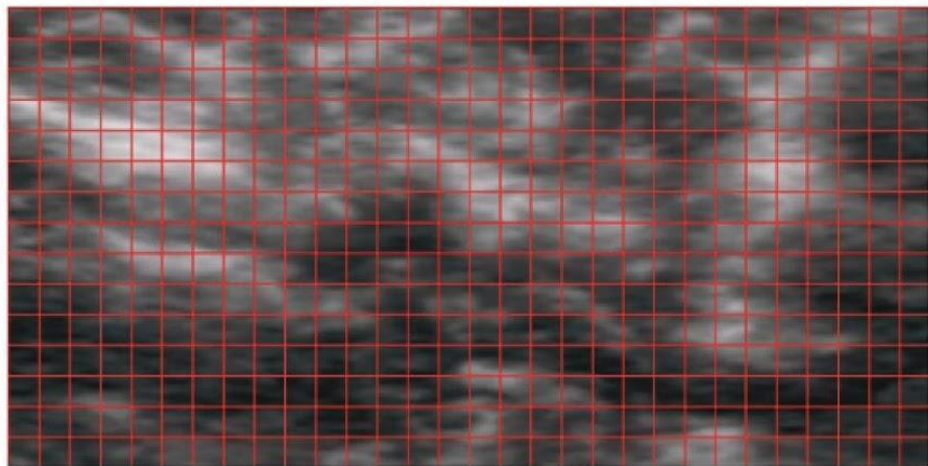
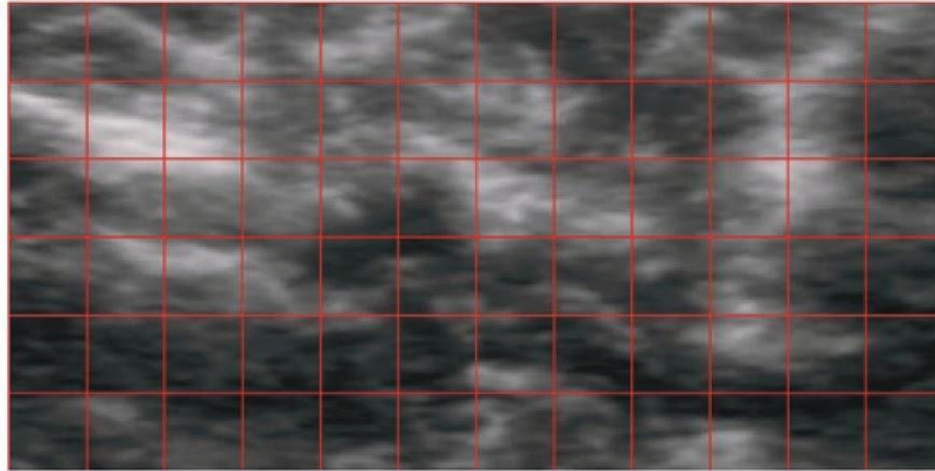**Figure S2.** Original ROI of the whole muscle segmented into 20*20 pixel patches.

Figure S3. Original ROI of the whole muscle segmented into 30*30 pixel patches.

Figure S4. Original ROI of the whole muscle segmented into 40*40 pixel patches.

Figure S5. Original ROI of the whole muscle segmented into 50*50 pixel patches.

Editorial information

✉ Correspondence

basadi@iisaragon.es

Author Contributions

Conceptualization, B.A. and D.L.-H; methodology, B.A. and D.L.-H..; software, B.A.; validation, D.L.-H.; formal analysis, B.A. and D.L.-H.; investigation, B.A. and D.L.-H..; data curation, B.A.; writing—original draft preparation, B.A. and D.L.-H.; writing—review and editing, B.A., S.A., L.P., NN.A. and D.L-H; visualization, B.A.; supervision, D.L.-H.; project administration, B.A. and D.L.-H.; All authors have read and agreed to the published version of the manuscript.

Patient's informed consent

Informed consent was obtained from all the subjects involved in this study. Written informed consent was obtained from the patients to publish this paper.

Data Availability Statement

The data presented in this study are available from the corresponding author upon request, due to the fact that these data are part of a larger, ongoing project and may not yet be fully available for public sharing until the project is completed.

Conflicts of Interest

The authors declare no conflicts of interest.

Suggested citation

Disclaimer/Publisher's Note

Copyright